**Ph.D. DISSERTATION**

# FACULTY OF WOOD ENGINEERING AND CREATIVE INDUSTRIES

**UNIVERSITY OF SOPRON**

***by***

**CHENAR A. TAHIR**

**SOPRON, HUNGARY**

**April 2024**

# Air-cathode ML-MFC reactor configuration using wood as container and separator to prevent deterioration and biofilm formation on cathode surface

**A DISSERTATION**

***submitted in partial fulfilment of the***

***requirements for the award of the degree of***

**DOCTOR OF PHILOSOPHY**

***by***

**CHENAR A. TAHIR**

***under the supervision of***

**PROF. DR. LEVENTE CSÓKA**

**DR. ZOLTÁN PÁSZTORY**


**FACULTY OF WOOD ENGINEERING AND CREATIVE INDUSTRIES**

**UNIVERSITY OF SOPRON**

**SOPRON, HUNGARY**

**April 2024**

**Air-cathode ML-MFC reactor configuration using wood as container and separator to prevent deterioration and biofilm formation on cathode surface**

Dissertation for doctoral (PhD) degree
University of Sopron József Cziráki Doctoral School
of Wood Sciences and Technologies,
P4 Fiber and nanotechnology programme

Written by:

***Chenar A. TAHIR***

Made in the framework of P4 Fiber and nanotechnology programme.

of the József Cziráki Doctoral School, University of Sopron

Supervisors: Prof. Dr. Csóka Levente DSc., Dr. Pásztory Zoltán
I recommend for acceptance (yes / no)

(signature)

The candidate reached …..... % at the complex exam,

Sopron, ..... .....
Chairman of the Examination Board

As assessor I recommend the dissertation for acceptance (yes/no)

First assessor (Dr. .....) yes/no

(signature)

Second assessor (Dr. .....) yes/no

(signature)

(Possible third assessor (Dr. .....) yes/no

(signature)

The candidate reached .....% in the public debate of the dissertation

Sopron,

.....
Chairman of the Assessor Committee

Qualification of the doctoral (PhD) degree ….....

.....
Chairman of the University Doctoral
and Habilitation Council (UDHC)

**UNIVERSITY OF SOPRON**

# DECLARATION

I undersigned **Chenar Ali Tahir** by signing this declaration declare that my PhD thesis entitled **"Air-cathode ML-MFC reactor configuration using wood as container and separator to prevent deterioration and biofilm formation on cathode surface"** was my own work; during the dissertation I complied with the regulations of Act LXXVI of 1999 on Copyright and the rules of the doctoral dissertation prescribed by the Cziráki József Doctoral School, especially regarding references and citations.[1]

Furthermore, I declare that during the preparation of the dissertation I did not mislead my supervisors or the programme leader with regard to the independent research work.

By signing this declaration, I acknowledge that if it can be proved that the dissertation is not self-made or the author of a copyright infringement is related to the dissertation, the University of Sopron is entitled to refuse the acceptance of the dissertation.

Refusing to accept a dissertation does not affect any other legal (civil law, misdemeanour law, criminal law) consequences of copyright infringement.

Sopron, 20/04/2024

……..

PhD candidate

[1] **Act LXXVI of 1999** Article 34 (1) Anyone is entitled to quote details of the work, to the extent justified by the nature and purpose of the recipient work, by designating the source and the author specified therein.

Article 36 (1) Details of publicly lectures and other similar works, as well as political speeches, may be freely used for the purpose of information to the extent justified by the purpose. For such use, the source, along with the name of the author, shall be indicated, unless this is impossible.

This work is dedicated to my parents, brothers and sisters, for always being there and supporting me...

## ACKNOWLEDGEMENTS

First and foremost, I want to express my most profound thankfulness to the Almighty God (Allah; the creator of all what is on earth and skies) for accepting my completion of this Ph.D. study. My mother, I am inexhaustibly, incessantly, and permanently grateful for the difficulties she faced and endured in raising me. The assistance she provided me was immeasurable. My father, my deepest heartfelt gratitude go out to him. May he have found peace. I ask God to grant him heaven. He is still alive in my heart with his wisdom.

I'd like to take this moment to express my genuine thanks to my first supervisor, ***Prof. Dr. Levente Csóka***, I completed this Ph.D. study with his tremendous help. I consider myself extremely fortunate to have worked under his expert supervision, and I appreciate him for guiding me in the proper direction. He has set an example with his meticulous eye, a strong sense of dignity, and ethics. I thank my next supervisor ***Dr. Zoltán Pásztory*** for his assistance during this research.

I want to give thanks to the faculty members at the University of Sopron, especially ***Dr. Tamás Hofmann*** and his team, and research staff ***Dr. Tibor Alpár, Dr. Faridul MK Hassan***, ***Dr. Charu Agarwal***, ***Dr. Zoltán Börcsök,*** for their gracious cooperation and help in carrying out this study. I express my gratitude to ***Dr. Barham Majeed*** for extending his hands constantly whenever I was in the urge for help. I want to convey my sincere gratitude to all my lab colleagues and friends- Fatima, Rami, Ilyas, Zehiroglu, Zsofi, G-Ossama, and others for their support, insight, and motivation toward my target. Also, I want to thank my brothers and sisters, all my family members, friends, and teachers, who contributed to this study in one way or another.

*Chenar A. Tahir*

# TABLE OF CONTENTS

## LIST OF FIGURES

## LIST OF TABLES

## LIST OF ABBREVIATIONS

| | |
|---|---|
| AEM | anion exchange membrane |
| BOD | biological oxygen demand |
| CE | coulombic efficiency |
| CEM | cationic exchange membrane |
| DMA | dynamic mechanical analysis |
| EDX | energy-dispersive X-ray spectroscopy |
| HMWG | heavy metal-containing wheat grain |
| MC | moisture content |
| MFC | microbial fuel cell |
| ML-MFC | membrane-less microbial fuel cell |
| MPD | maximum power density |
| OCV | open circuit voltage |
| OLR | organic loading rate |
| ORR | oxygen reduction reaction |
| PD | power density |
| PEM | proton exchange membrane |
| PTFE | polytetrafluoroethylene |
| SEM | scanning electron microscopy |
| SMFC | single chamber microbial fuel cell |
| SCE | Saturated calomel electrode |
| TMFC | two-chamber microbial fuel cell |
| WML-MFC | wooden membrane-less microbial fuel cell |
| XRD | X-ray diffraction |

## ABSTRACT

In this study, we introduce a novel application of wood as the construction material for Microbial Fuel Cell (MFC) containers, developing what we term the Wooden Membrane-less Microbial Fuel Cell (WML-MFC). This innovative approach leverages the natural properties of wood to enhance the sustainability and cost-effectiveness of MFCs. Employing three different types of wood—pine, oak, and black locust—the WML-MFC design incorporates a carbon felt anode inside the wooden container and a carbon cloth cathode wrapped externally. This configuration not only protects the cathode from biofouling but also utilizes the inherent moisture management capabilities of wood to maintain operational stability. The performance of these wooden MFCs was assessed in terms of electricity generation and water treatment efficacy. Pine and oak containers achieved maximum power densities (MPD) of 35 $mW/m^2$ and 4 $mW/m^2$, respectively, with corresponding maximum open-circuit voltages of 551 mV and 269 mV. Black locust showed the least effective bioelectricity generation. COD removal efficiency was observed between 18% and 48% for pine and 3% to 39% for oak over hydraulic retention times of 24-48 hours. Notable water loss due to moisture diffusion was recorded at 20%/d in pine and 6%/d in oak. Durability assessments through DMA and SEM analyses confirmed the suitability of wood as a container material, emphasizing the dual environmental and economic benefits of this WML-MFC design. Notably, 2 mm and 3 mm thick Scots pine and oak containers exhibited lower electricity production, reduced water treatment capacity, higher water loss with thinner walls, and increased voltage fluctuations compared to the 4 mm thick containers.

Briefly, This study demonstrates that the wooden membrane-less microbial fuel cell (WML-MFC) system offers a cost-effective, environmentally friendly, and sustainable approach. It effectively safeguards the cathode from biofilm formation, thus preventing its deterioration and showcasing its potential as an eco-friendly energy generation and water treatment technology.



Keywords: Membrane-less microbial fuel cell, cathode deterioration, biofilm, wooden container

# CHAPTER I-
# INTRODUCTION AND LITERATURE REVIEW

# 1. INTRODUCTION

## 1.1. Chapter synopsis

This chapter serves as a concise introduction and literature review focusing on various types of microbial fuel cells (MFCs). These MFC categories include MFCs with membranes, membrane-less MFCs (ML-MFCs), air-cathode MFCs, aqueous-cathode MFCs, and their variations with single or dual chamber designs. The subsequent sections delve deeper into membrane-less MFCs, examining recent research and developments using both traditional and contemporary testing techniques. Emphasis is placed on the applications in water treatment and electricity production. Additionally, this chapter provides an overview of the challenges and limitations within MFC technology, laying the foundation for the problem statement and study objectives. In conclusion, we offer an outline for the entire dissertation.

## 1.2. Problem statement and scope of the study

In recent decades, global concerns surrounding sustainability have driven the scientific community to seek innovative solutions for environmental issues (Nastro, 2014). Simultaneously, the depletion of crude oil resources has led to an increased focus on alternative energy sources. In this context, microbial fuel cells (MFCs) have gained international attention as a sustainable technology capable of generating electricity from organic matter in wastewater, while also aiding in wastewater treatment and environmental remediation (Feng et al., 2008). MFC technology holds the potential to contribute significantly to future energy needs (Logan, 2010). Moreover, it is cost-effective, self-sustaining, and, in some cases, does not require substantial capital investment.

Among MFC researchers, membrane-less microbial fuel cells (ML-MFCs) have shown superior performance compared to membrane-based MFCs. Air-cathode MFCs are preferred over aqueous-cathode counterparts due to their independence from an external air supply. However, cathode deterioration remains a common issue across all membrane-less air-cathode designs, primarily caused by biofilm formation on the cathode's surface due to contact with the anolyte. This problem leads to a gradual decline in cell efficiency over time, making MFCs economically unviable. Selecting appropriate designs and materials for constructing MFC units becomes crucial. Conventional ML-MFC unit construction is often labor-intensive, time-consuming, environmentally unfriendly, and costly. To address

these drawbacks, this study explores eco-friendly and readily available materials, such as wood, in ML-MFC unit construction. Wood exhibits numerous appealing properties, including biodegradability, porosity, accessibility, resistance to microbial attacks, and long lifespan.

### 1.3. Energy harvesting techniques

The world is experiencing a surge in electrical energy generation from primary environmental energy sources, including chemical (Rabaey and Verstraete, 2005), thermal sources such as geothermal and solar thermal (Kodama, 2003), vibrational energy (Ambrozkiewicz and Wolszczak, 2020), radio frequency (ElAnzeery et al., 2012), and mechanical energy sources such as water motion (Helseth and Guo, 2016). Additionally, modern technological devices consume less energy, especially small-sized devices and sensors. This makes microbial fuel cells a viable option for new biosensor applications and small devices that operate on battery power (Ivars-Barceló et al., 2018).

### 1.4. Background on Microbial fuel cell

The concept of microbial fuel cells (MFCs) was initially proposed by Michael Cressé Potter in 1912, utilizing Escherichia coli and Saccharomyces with platinum electrodes. However, low power output limited its early adoption (Yang et al., 2011). In the early 1990s, renewed interest in MFCs arose as advancements led to improved efficiency (Rahimnejad et al., 2015). In 1999, Kim et al. reported the first mediator-less MFC (Logan, 2008), paving the way for further developments and increased power density.

MFCs function by converting chemical energy from organic matter in wastewater directly into electrical energy with the assistance of electrogenic bacteria (Min and Logan, 2004) -Various microorganisms are capable of producing electrons through the metabolism of organic matter - (Cheng et al., 2006; Liu et al., 2004). An MFC typically consists of three components: the electrode system, a microorganism culture (either anaerobic or aerobic) fed with organic materials, and a container with a proton exchange membrane (PEM). MFCs come in different configurations, primarily single-chamber or dual-chamber designs (Khan et al., 2018), with most single-chamber MFCs incorporating a PEM to separate the anode and cathode compartments.

## 1.5. Background on membrane-less microbial fuel cell (ML-MFC)

Membranes in traditional MFCs introduce significant internal resistance, negatively impacting electrochemical performance and rendering them economically unviable (Logan, 2010). Efforts have been directed towards achieving higher output without membranes, leading to the emergence of membrane-less microbial fuel cells (ML-MFCs). These ML-MFCs offer several advantages, including energy self-sufficiency, operation at ambient temperatures, environmental friendliness by avoiding toxic by-products, reduced manufacturing costs, and extended operational lifespans (Fig. 1.2) (Yang et al., 2009).

ML-MFCs address the membrane-related disadvantages of traditional MFCs, where membranes impede functionality by increasing internal resistance (Jang et al., 2004). These devices hold the key to achieving higher efficiency by eliminating the membrane, thereby enhancing proton transfer and reducing internal resistance (Jang et al., 2004).

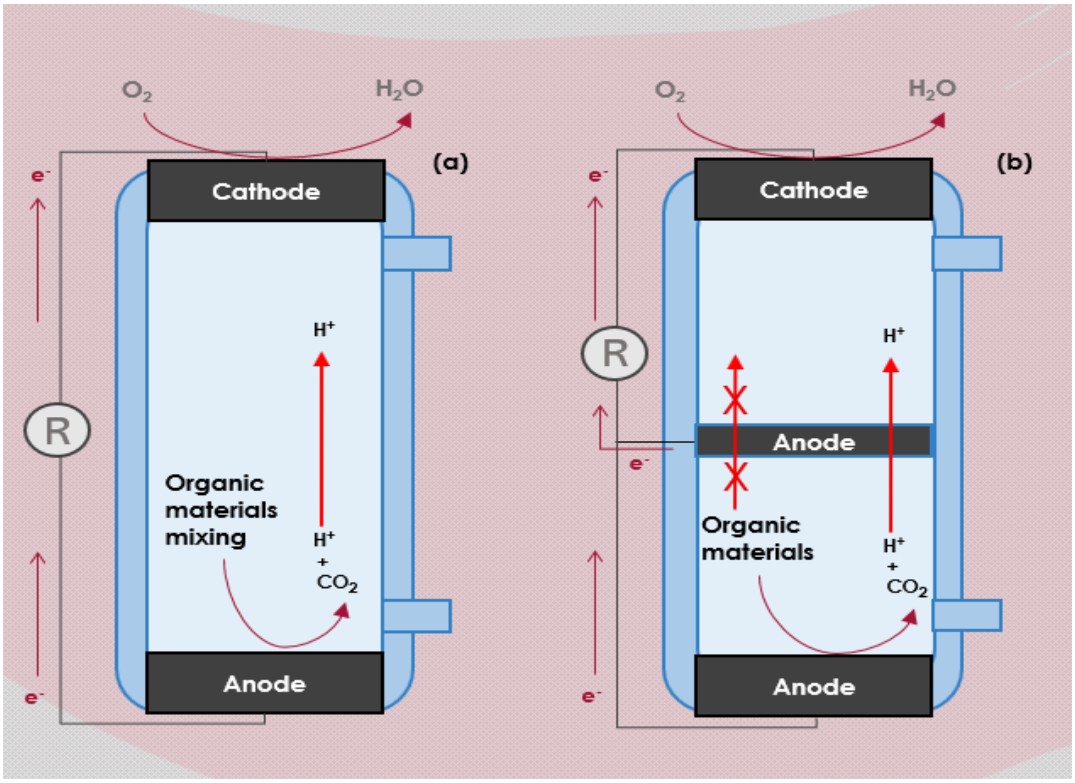


**Figure 1.1** Schematic representation of an ML-MFC (a) single-chamber unit, (b) dual-chamber unit. (Redrawn with modifications from Ref. (Kim et al., 2016)).

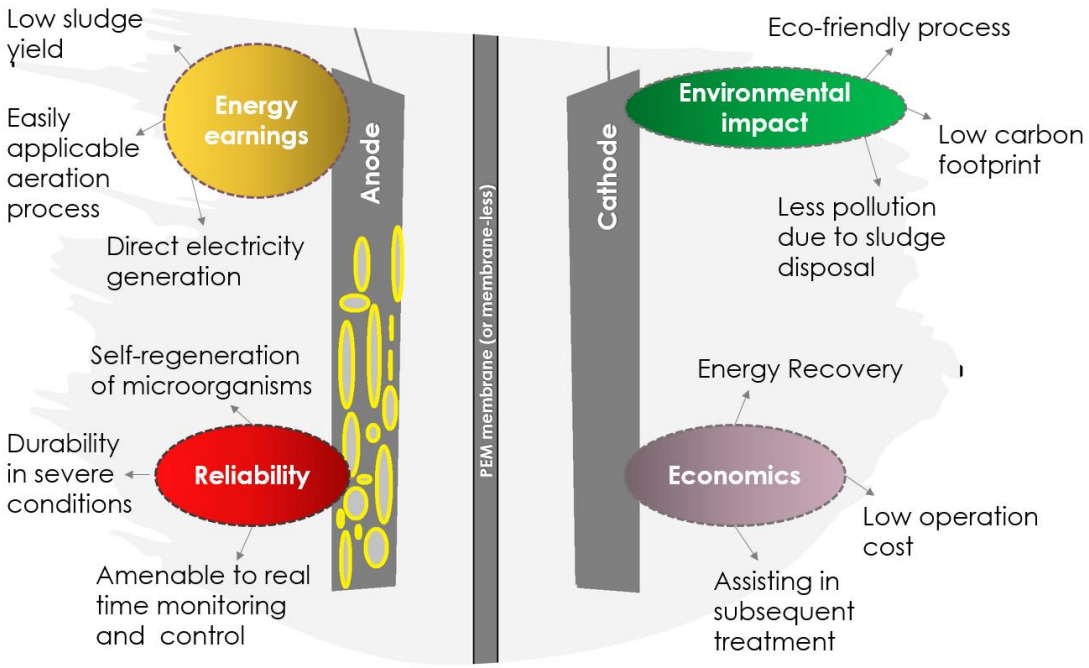


**Figure 1.2** Advantages of MFCs. (Redrawn with modifications from Ref. W. W. Li et al., (2014)).

## 1.6. The process of bio-electricity generation

The process of bio-electricity generation in MFCs is similar, where the substrate with microorganisms is located in the anode compartment (if the anode is partitioned from the cathode using a separator) of the MFC chamber (Lin et al., 2013). Microorganisms play the role of a catalyst in the process of energy generation, producing electrons and protons along with carbon dioxide ($CO_2$), and other inert gases. Over time, they create a biofilm on the anode surface, thus catalyzing the anaerobic bacterial oxidation (Z. Li et al., 2014; Waller and Trabold, 2013). The protons (hydrogen ions) ($H^+$) move from the anode towards the cathode, while the electrons transfer through an external electrical circuit connected to the cathode (Lin et al., 2013). Oxygen, which acts as the electron acceptor, is pumped from the air through the catholyte into the cathode compartment or is directly received if the cathode is in contact with the air (air-cathode) (Zhang and Ye, 2015). The basic chemical reactions taking place at the electrodes with the organic materials are depicted by Eq. (1.1). The specific reactions may vary in the anode compartment according to the type of substrate used; however, the products remain the same with altered stoichiometric coefficients (Khan et al., 2018). At the anode, the partition reaction in the case of glucose as substrate occurs as indicated by Eq. (1.1). The substrate, which functions as a fuel for the MFC unit, contains organic compounds that are degraded by the microorganisms during the process of

oxidation (Luo et al., 2007; Pauline and Boopathi, 2018). Agri-food industries produce a lot of waste easily broken down by bacteria and can be a good carbon source for MFCs. Other common substrates may include glucose, acetate, wastewaters from the domestic household, dairy, slaughterhouse, refinery, and dyeing industry (Jothinathan et al., 2018; Pallavi CK and Udayashankara TH, 2016; Savizi et al., 2012). In the cathode compartment, hydrogen ions and oxygen react with the help of electrons to form water or hydrogen peroxide (Eqs. 1.2 – 1.3) (Luo et al., 2017). The cathode electrode is generally coated with a catalyst such as platinum to assist in the reaction of hydrogen ions with oxygen or, in other words, to facilitate the oxygen reduction reaction (ORR) (Rahimnejad and Najafpour, 2011).

$$C_6H_{12}O_6 + 6H_2O \rightarrow 6CO_2 + 24H^+ + 24e^- \quad \textbf{Eq. 1.1}$$

At the cathode, the partition reaction occurs as indicated by Eqs. 1.1-1.2.

$$4H^+ + 4e^- + O_2 \rightarrow 2H_2O \quad \textbf{Eq. 1.2}$$

$$4H^+ + 4e^- + 2O_2 \rightarrow 2H_2O_2 \quad \textbf{Eq. 1.3}$$

Where, $〚\Delta G〛^{\wedge}o = -5792.2\ kJ/mol$

### 1.7. Influencing factors on MFC and ML-MFC

The performance of MFCs is influenced by a myriad of factors, encompassing chemical, physical, and biological elements that profoundly affect the overall efficiency of these units. Among the physical and chemical factors are reactor design (Jang et al., 2004; Liu and Logan, 2004; Luo et al., 2007; Ye et al., 2018), pH levels (Gil et al., 2003; Jadhav and Ghangrekar, 2009), temperature conditions (Feng et al., 2008; Jadhav and Ghangrekar, 2009) (Ahn and Logan, 2010), electrode surface area in conjunction with electrode spacing (Cheng and Logan, 2011; Ghangrekar and Shinde, 2007), pretreatment methods for influent (Ghangrekar and Shinde, 2008; Jadhav and Ghangrekar, 2009; Yang et al., 2013), as well as chemical treatments applied to the cathode and anode electrodes, and more.

Biological factors come into play as well, including the choice of microbial culture and the preparation of the substrate for these microorganisms (Hassan et al., 2014; Malvankar et al., 2012). Numerous studies have explored exogenous bacteria for their electron-producing capabilities (Cheng and Logan, 2007). A noteworthy challenge in ML-MFCs involves the mixing of the anolyte and catholyte, which can lead to a decrease

in cathode electrode efficiency due to biofouling. The primary objective of employing ML-MFCs is to mitigate internal resistance, optimize the conversion rate of organic materials within the substrate, reduce manufacturing costs, and enhance the efficiency of both anode and cathode electrodes (Rabaey and Verstraete, 2005).

Various methods exist for bacteria to transfer electrons to the anode, including electron transfer via a mediator, direct electron transfer, and electron transfer through bacterial nanowires (Khan et al., 2018). The thriving of bacterial cultures hinges on creating a conducive environment, with pH and temperature exerting significant influence on bacterial activity and, consequently, reactor performance. Multiple reviews have been published on MFCs, each emphasizing different aspects such as design features, substrates, microbial metabolism, performance, and associated challenges (Hindatu et al., 2017; Wei et al., 2011).

In this study, our focus centers on a physical factor that impacts the performance and efficiency of ML-MFCs, specifically the container or, more precisely, the wall of ML-MFCs. The use of wood as a container and separator has the potential to overcome cathode deterioration and the growth of microbial communities on the cathode while incorporating an air-cathode electrode.

### 1.8. Types of MFCs and ML-MFCs

Microbial Fuel Cells (MFCs) exhibit considerable diversity, and various classification schemes have been proposed in the literature. These classifications help us understand different aspects of MFCs, from their intended applications to their specific characteristics. In this section, we will explore classifications related to the presence or absence of membranes, the type of cathodes used, and their impact on bioelectric production and water treatment.

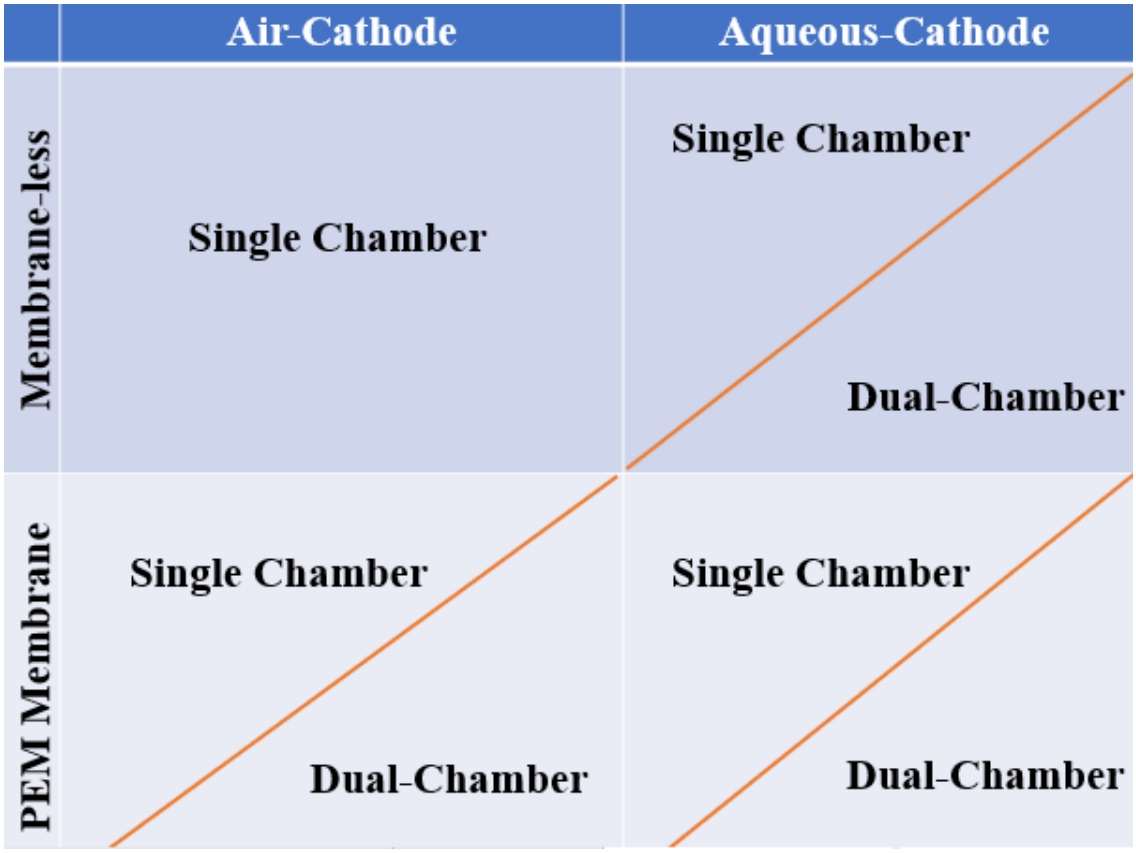


**Figure 1.3** MFC classification according to membrane absence and air-cathode and aqueous-cathode design.

### *1.8.1. MFC with PEM/AEM membrane*

One significant classification of MFCs involves the presence of Proton Exchange Membranes (PEM) or Anion Exchange Membranes (AEM). Numerous studies have delved into the comparison between MFCs with and without these membranes, revealing various advantages and disadvantages.

It is well-documented that membranes introduce increased internal resistance in MFCs (Liu and Logan, 2004; Tahir et al., 2022). Nevertheless, the benefits of using membranes in MFCs cannot be disregarded. These advantages include mitigating oxygen intrusion (Du et al., 2011), preventing cathode biofouling, and minimizing leakage issues (Yang et al., 2017).

Here, we will specifically discuss MFCs with membranes, categorizing them into two subtypes: air-cathode single-chamber and aqueous-cathode dual-chamber MFCs.

#### *1.8.1.1. Air-cathode MFC*

Researchers have explored various modifications of PEM/AEM membranes in air-cathode single-chamber MFCs. In one study, an MFC's cathode was equipped with a PEM (Nafion

117) membrane. This setup involved a single chamber with both the anode and cathode residing within it. The cathode, positioned between the substrate and the air, featured the Nafion membrane. The initial maximum voltage generation was lower compared to membrane-less units, but the MFC with the membrane exhibited a five-fold increase in voltage generation duration when compared to its membrane-less counterpart (Liu and Logan, 2004). This extended voltage output appeared to be influenced by glucose concentration.

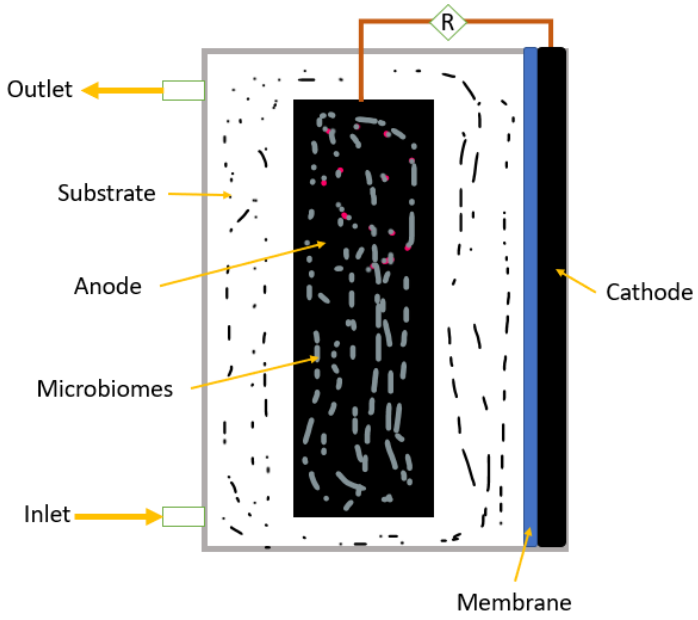


**Figure 1.4** Schematic diagram of an air-cathode MFC.

### *1.8.1.2. Aqueous-cathode MFC*

In another study, an aqueous-cathode dual-chamber MFC was constructed, with an anodic and cathodic chamber separated by a cationic exchange membrane (CEM) (CMI-7000) to assess different cathode types. In this configuration, the anode and cathode occupy separate chambers, interconnected by a channel containing the CEM. Remarkably, this study demonstrated the successful treatment of untreated wastewater, achieving a maximum power density of over 27 W/m³ (Zhang et al., 2013). A schematic representation of an aqueous-cathode MFC with a PEM membrane is shown in Figure 1.5, with the cathode chamber positioned next to the anode chamber. Notably, air pumping into the cathode compartment is essential in all cases of aqueous-cathode MFCs.

It is worth noting that the majority of MFC studies focus on lab-scale prototypes due to the high cost of membranes. This fact makes Membrane-Less Microbial Fuel Cells (ML-MFCs) a more attractive option compared to traditional MFCs. To provide you with

a clearer perspective, here are some examples of both lab-scale and pilot-scale experiments, as presented in Table 1.1.

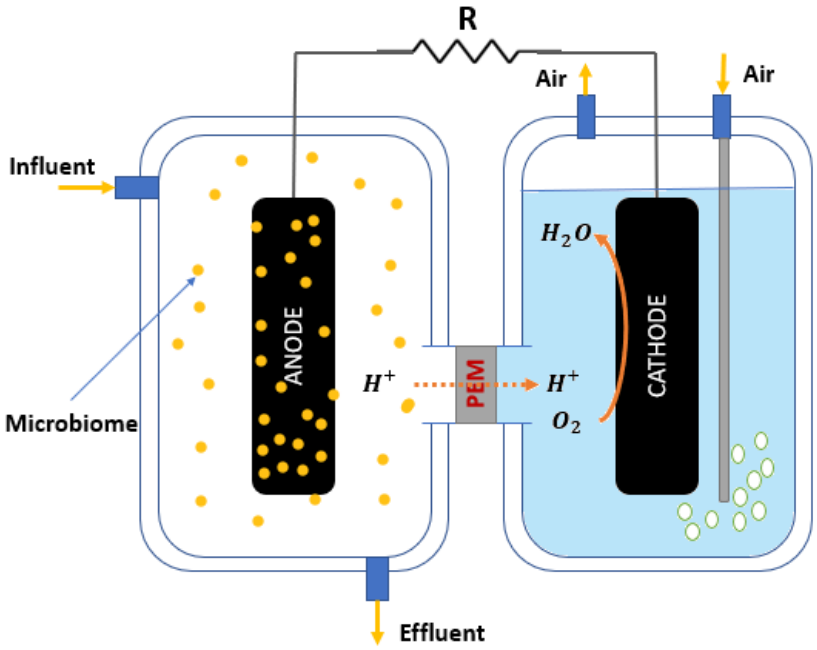


**Figure 1.5** Aqueous-cathode MFC with PEM membrane. Here, the cathode was placed next to the anode.

**Table 1.1** Some pilot-scale and lab-scale of MFC and ML-MFC experiments.

| **MFC design** | **Anode** | **Cathode** | **Substrate** | **Volume** | **Water treatment** | **Bioelectric productivity** | **Reference** |
|---|---|---|---|---|---|---|---|
| **Single chamber, air-cathode, ML** | Graphite rod | Cu-$MnO_2$<br>Co-$MnO_2$ | sodium acetate | 20 L | 80% of contaminant reduced, | 465 mW/m$^2$<br>500 mW/m$^2$ | (Jiang et al., 2011) |
| **Single Chamber, ML, aqueous-cathode** | Carbon Felt | Carbon plate | sodium acetate | 6.9 L | | 734 ± 54 mV | (Thung et al., 2019) |

| | | | | | | | |
|---|---|---|---|---|---|---|---|
| **Single-chamber, aqueous-cathode** | carbon fabric | graphite felt | River sediment and municipal wastewater | 1200 L | COD reduced rates 41.6 ± 3.5 mg/L/day | 25.6 ± 2.2 $mA/m^2$ | (Mohamed et al., 2021) |
| **Nafion membrane, dual-chamber** | carbon cloth | graphite rods | septic wastewater | 243.2 $cm^3$ | COD reduced 85% | 856 mV, 1750 $mA/m^2$, 602 $mW/m^2$ | (Khalili et al., 2017) |

### *1.8.2. ML-MFC of single/dual chamber with/without separator with affecting factors*

In this comprehensive study, our primary focus has been the development of ML-Microbial Fuel Cells (ML-MFCs). The overarching goal of this research endeavor is twofold: firstly, to mitigate cathode biofouling, and secondly, to reduce the overall maintenance costs associated with ML-MFCs. The core of ML-MFC technology revolves around two pivotal aspects: electricity generation and water treatment capabilities. It is essential to strike a harmonious balance between these factors while ensuring the efficient production and transfer of electricity. Various influential factors come into play when optimizing the harnessing of energy and expediting the oxygen reduction reaction (ORR) in ML-MFCs. These factors include the choice of different substrates, substrate pretreatment methods, anode electrode performance, cathode ORR proficiency, and reactor design, among others. Notably, the design of the MFC itself is the most critical factor affecting electricity production, water treatment capacity, and the overall cost-efficiency of the process (Pant et al., 2010).

One of the most significant components that can be eliminated through thoughtful design considerations is the membrane. The presence of a membrane has a substantial impact on MFC productivity and costs. For instance, Song and his research team dedicated their efforts to enhancing cathodic ORR without the use of precious metals. They employed a carbon cathode as a replacement for platinum, given its exorbitant cost. In their comparative study, they examined a single-chamber MFC (SMFC) with an air-cathode and no membrane against a two-chamber MFC (TMFC) equipped with a proton

exchange membrane (PEM). The results were unequivocal, with the ML-MFC exhibiting the highest power output and ORR activity. The substantial internal resistance imposed by the ion-exchange membrane is evident, as reflected in the resistance values of 45 Ω and 80 Ω for SMFC and TMFC, respectively (Song et al., 2020). Another investigation demonstrated that an ML-MFC outperformed an MFC equipped with a ceramic separator and salt-bridge connection between chambers, yielding a 140% higher power output of 520–570 μW and greater stability (You et al., 2020).

Likewise, studies comparing MFC configurations employing a metal anode with a carbonaceous cathode have consistently favored ML-MFCs with membranes, primarily due to their superior performance in terms of maximum power density (MPD) (Yamashita et al., 2016). This underscores the direct correlation between the use of salt bridges, membranes, or separators and the escalation of internal resistance within the reactor—a detrimental factor hindering higher power output and overall efficiency (Min et al., 2005). As a result, it is not surprising that single-chamber ML-MFCs are now favored over their membrane-equipped counterparts, prompting recent research efforts to enhance their performance and facilitate their commercial viability (Logan, 2010).

As mentioned earlier, ML-MFC performance is influenced by an array of factors, and the final reactor output is a culmination of their synergistic interaction. This complexity makes direct comparisons of the individual factors across various studies challenging. Most research endeavors dedicated to ML-MFCs have systematically explored the effects of these diverse variables. Therefore, any evaluations and comparisons must be grounded in reasoned analysis, research outcomes, and established theories and facts. Now, let us delve into an exploration of the factors that have had a significant impact on ML-MFCs and the measures taken to expand their limitations and boost production efficiency.

#### *1.8.2.1. Effect of Anode and Cathode Electrodes modification*

Microbial Fuel Cells (MFCs) have emerged as a sustainable solution for electricity generation, offering a promising response to global environmental concerns (Palanisamy et al., 2019). Within the realm of MFC design, the choice of electrodes assumes a central role, posing both a critical challenge and an opportunity for achieving optimal performance. Efforts to enhance anodes have focused on fostering bacterial adhesion and enhancing the capacity for electron collection and transfer from both bacteria and the surrounding medium (Hindatu et al., 2017). On the other hand, for cathodes, performance

in terms of the oxygen reduction reaction (ORR) significantly influences the coulombic efficiency (CE) of the MFC. It also plays a pivotal role in boosting the flow of electricity, ensuring durability, and maintaining long-term stability (Santoro et al., 2013) (Jiménez González et al., 2020).

The positioning of the cathode within the ML-MFC configuration is of paramount importance. Different designs come with their own sets of limitations. For instance, if the ML-MFC incorporates an air-cathode, it encounters challenges such as water loss, ORR activity, oxygen infiltration, cathode degradation, biofilm formation on the substrate-facing side, and anode performance and bacterial culture support. Over the past two decades, numerous studies have diligently addressed these issues and proposed innovative solutions. Despite notable progress in addressing cathode performance issues, certain challenges persist, rendering MFC technology nonviable for large-scale applications (Zhou et al., 2012).

Researchers have explored various materials for developing electrode materials in MFCs, with carbonaceous materials (such as carbon cloth, carbon felt, and graphite) and metallic materials (including copper, zinc, and stainless steel) being among the most widely utilized (see Figure 1.6) (Santoro et al., 2017). Carbon, in particular, has garnered significant attention due to its abundance in nature and its exceptional properties, including its ability to interact with electroactive biofilms, high conductivity, and durability in harsh environments. As such, carbonaceous materials find extensive application as electrodes in MFCs (Santoro et al., 2017).

Various analytical techniques, including scanning electron microscopy (SEM), transmission electron microscopy (TEM), and X-ray diffraction (XRD), have been commonly employed to characterize electrode material structures. Most studies have evaluated electrodes' electrochemical performance, particularly in the context of ORR, using techniques such as cyclic voltammetry and electrochemical impedance spectroscopy. Some studies have expanded their focus to investigate oxygen diffusion through cathodes, MPD, CE, and chemical oxygen demand (COD).

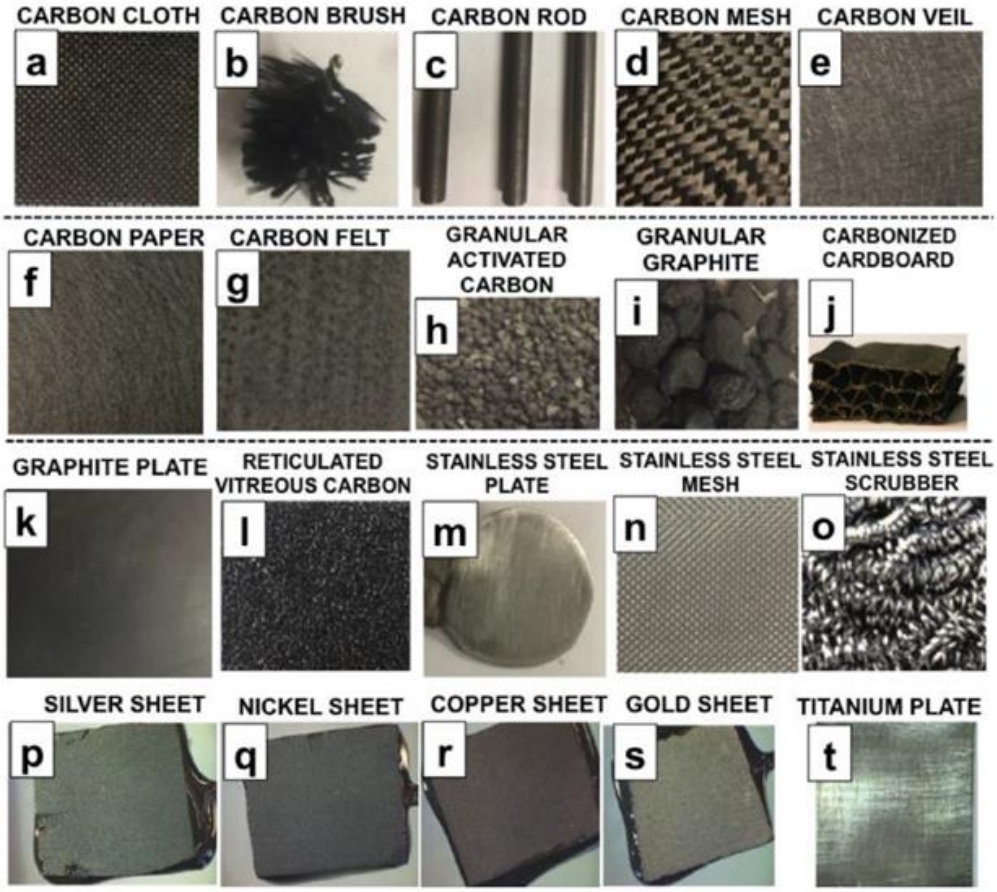


**Figure 1.6** Several carbonaceous and metallic materials are used for anode and cathode electrodes. (Published from Ref. Santoro et al., (2017) under CC BY 4.0 license).

#### *1.8.2.1.1. Cathode Electrode*

As mentioned, carbonaceous materials have unique properties such as electrical conductivity (Saba et al., 2017), corrosion resistivity (Slate et al., 2019), mechanical strength (Jia et al., 2018), high surface area (Yang et al., 2018), biocompatibility (Zhao et al., 2018), chemical stability (Cai et al., 2020b), environmental safety, and low cost (Liu et al., 2020). In a study, a carbon cathode was prepared from mixed carbon powder (Vulcan XC-72) and 30 wt% polytetrafluoroethylene (PTFE) solution, coated with different numbers of diffusion layers (DLs) from the airside. The optimum performance was obtained with four DLs, which significantly improved the Columbic Efficiency from 19.1% to 32%, while the MPD increased by 42% compared to an uncoated carbon cathode. Also, the open-circuit potential analyses revealed that the maximum potential difference between the cathode having four DLs and the uncoated cathode was 117 mV at 0.6 mA/cm2. The oxygen permeability and water loss from the cathode decreased with an increasing number of DLs (Cheng et al., 2006). Any attempt to seal the cathode further led to higher internal resistivity, like in the case of the MFC with PEM. A spun-bonded olefin sheet was used in

a study instead of a PTFE coating to seal the cathode to have lower resistivity. At the beginning (on day 5), this cathode produced an MPD of 750 mW/m$^2$, a current density of 2.0 A/m$^2$ (32 A/m$^3$), a CE of 55%, low resistance of about 4 Ω, and total internal resistance of 103 Ω. However, the total internal resistance increased to 247 Ω after 50 days, while the current density was less than 1.0 A/m$^2$ (16 A/m$^3$) with a CE less than 35% (Oh et al., 2012).

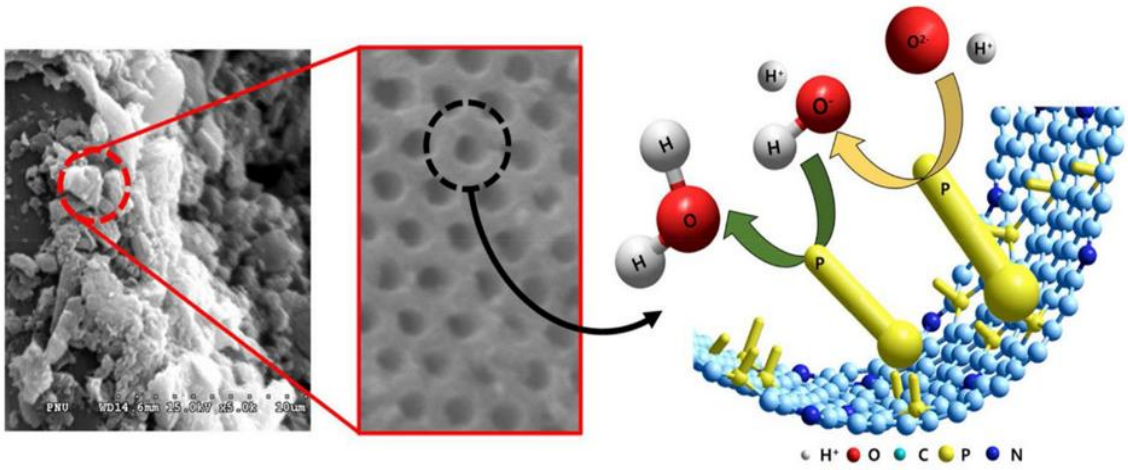


**Figure 1.7** Surface morphology of nitrogen- and phosphorus-doped ordered mesoporous carbon (NOPMC) illustrating the mechanism of the oxygen reduction reaction. (Reproduced with permission from Ref. Song et al., (2020) © 2020 Elsevier publisher).

With efforts to achieve high ORR activity at a reasonable cost. Recently, in a research conducted by Song et al., nitrogen- and phosphorus-doped mesoporous carbon (NPOMC) was used as a catalyst replacing platinum (Song et al., 2020). As elucidated in Fig. 1.7, the active phosphate sites on the mesoporous carbon surface are a doping centre for the ORR, where the nano porous structure of the catalyst helps intensify the ORR activity, and the nitrogen-doping sites cause a change in the charge distribution. The NPOMC in the ML-MFC gave only 30% of the ORR activity of Pt/C (154.0 mW/m$^2$) with 30–40% lower MPD. Moreover, the gradual formation of biofilm on the surface of the catalyst (biofouling) blocked the nano-structured active sites of the NPOMC and drastically affected its performance and stability. The electrochemical performance showed a current of 1.33 mA and internal resistance of 286 Ω after 30 days of operation (Song et al., 2020).

In another work, canvas cloth was used for the fabrication of electrodes. The non-conductive material was made to conduct electricity by coating it with one nickel or graphite and manganese dioxide ($MnO_2$) as the catalyst. The nickel-coated canvas produced a better result than the graphite-coated canvas, with an MPD of 86.03 mW/m$^2$, a COD reduction of 95%, and a CE of 30.2% (Zhuang et al., 2009). Yet, in another study, bamboo

charcoal coated with platinum was used as a cathode in an ML-MFC, giving maximum power and voltage of 1.16 mW and 0.50 V, respectively (Yang et al., 2009). Feng et al. employed stainless steel coated with polypyrrole/anthraquinone-2-sulfonate film as a cathode. It produced an MPD of 575 $mW/m^2$, and the cathode remarkably reduced oxygen and inhibited water leakage (Feng et al., 2011). Iron-based catalysts such as ricobendazole and niclosamide could be a possible alternative for platinum on the cathode electrode, as they have shown 20–25% higher efficiency than that platinum (Santoro et al., 2016).

Similarly, the ability of pristine graphene to enhance extracellular electron transfer has been exploited for platinum-free electrodes, producing a volumetric power of 3.51 $W/m^3$ (Call et al., 2017). Thus, it can be concluded that sealing the air-cathode electrode, choice of electrode material, and cathode coating catalyst are crucial considerations for achieving a high ORR activity. Still, there is immense scope for improvement of the MFC with many undiscovered possibilities for the cathode, the main challenges being long lifetime, stable performance, and cost of the electrodes.

#### *1.8.2.1.2. Anode Electrode*

The anode material and its arrangement play a vital role in the attachment of the bacteria, enrichment of the biofilm, oxidation of the substrate, as well as the transfer of electrons between the bacteria and the electrode, which in turn affect the final output. Several methods of modification such as surface treatment, ammonia gas treatment (Cheng and Logan, 2007), heat treatment (Feng et al., 2010), acid treatment, electrochemical oxidation, surface modification with nanomaterials, and surface coating with conductive polymers (Hindatu et al., 2017) have been used with anode electrode to improve the overall performance of an ML-MFC. The anode electrode should be bio-compatible with the bacteria, in addition to the other primary factors used for evaluating the cathode electrode. (Kumar et al., 2013). Here, trying to discuss some research of how modifying the anode electrode impacted ML-MFC efficiency.

A study used an anode made of carbon cloth treated with ammonia, while the cathode was carbon cloth with a platinum catalyst. This combination substantially improved CE by 20% compared to the untreated anode and an MPD increment from 1640 to 1970 $mW/m^2$. The power attained was 7.5 times higher than the untreated electrode, and the start-up time was reduced by 50% (Cheng and Logan, 2007). In another study, a carbon fibre brush treated with acid and heat was used as the anode produced an MPD of 1370

$mW/m^2$, which was greater by 34% and 7% than that achieved by using an untreated electrode and only a heat-treated electrode, respectively (Feng et al. 2010). Likewise, the anode was modified using nitric acid (CM-N) and ammonium nitrate (CM-A). CM-N performed better than CM-A giving an MPD of 792 $mW/m^2$ and CE of 24%, which were greater than that achieved with using an untreated anode by 43% and 71%, respectively. Also, the modified anodes showed deep cracks and rough surface that improved electron transfer (Zhou et al., 2012). An MPD of 1788 $mW/m^3$ was achieved in a similar study by treating the anode surface with nitric acid and ammonia (Yang et al., 2014).

Lin et al. worked as electrodes with different materials (stainless steel, copper, gold, and graphite carbon cloth). Copper anode showed erosion, while hindered electron transfer was observed in the case of stainless steel. On the other hand, the gold electrode showed very high performance. In terms of open-circuit voltage, the best result was obtained with a gold anode and a carbon cloth cathode, measuring in at 0.49 V (Lin et al., 2013). Another study used an anode of graphite felt coated with iron oxide ($Fe_2O_3$) and ferric oxyhydroxide (FeOOH) giving an MPD of 18 $W/m^3$ (Wang et al., 2013). A voltage of 573 mV and an MPD of 884 $mW/m^2$ were obtained when polyaniline was used with a graphene-modified carbon cloth as an anode (Huang et al., 2016). A flame-oxidized stainless-steel anode resulted in an MPD of 1063 $mW/m^2$, which was 24% higher than the untreated anode. Furthermore, it was appreciably higher by 323% than the same MFC configuration with membrane (Yamashita et al., 2016).

Peng et al. added 5% of nickel-iron oxide ($NiFe_2O_4$) to the anode to achieve an MPD of 806.4 $mW/m^2$, reducing the internal resistance by 39% compared to the untreated anode (Peng et al., 2017). Using indium tin oxide coated glass as an anode produced the voltage and power output of 471 mV and 418.8 $mW/m^2$, respectively. However, its COD reduced efficiency was lower than the carbon brush (Jiang et al., 2018). Another study found that using carbonized cotton textile modified with molybdenum carbide nanoparticles as an anode delivered an MPD of 1.12 $W/m^2$. This material offered a super performance in conductivity, high biocompatibility, electrochemical activity, and cost-effectiveness (Zeng et al., 2018). Graphene coated with iron sulfide ($FeS_2$) nanoparticles was employed as an anode on different substrates, achieving an MPD of 3220 $mW/m^2$ and an outstanding current density of 3.06 $A/m^2$ with COD reduction of 1319 mg/l (Wang et al., 2018). Many studies have shown tremendous progress by improving the anode with different materials, nanoparticles and composites to give a superior electrochemical

performance. It is of prime significance to check the compatibility of the treated anode with bacteria, its conductivity and durability to ensure optimum efficiency.

#### *1.8.2.2. Effect of operating temperature*

Literature has shown that temperature greatly impacts the performance of ML-MFC by affecting the growth and survival of microbial communities, the conductivity of the substrate solution, internal resistance, and start-up time (Gadkari et al., 2020). A study on a single-chamber, air-cathode ML-MFC compared two operating temperatures (20 and 30 ℃) and found a stable power density of 187±8 $mW/m^2$ and CE of 10% at 30 ℃. When the reactor was adjusted to 20 ℃, MPD and CE decreased to 155 $mW/m^2$ and 8.9%, respectively. Moreover, as the temperature decreased from 30 to 20 ℃, the cathode potential dropped drastically (cathode potential MPD was reduced by 315% (from 20 to −43 mV, versus saturated calomel electrode (SCE) reference electrode)), while the anode electrode potential lessened by 21% (Feng et al., 2008). Another work examined ML-MFC under different temperature ranges, i.e., 20-35 and 8-22 ℃. The higher working temperature range resulted in higher COD reduction of 90%, lower current of 0.7 mA, and CE of 1.5%. On the contrary, at a lower temperature range, the COD reduced to 59%, the current rose to 1.4 mA, and CE increased to 5%. Thus, the lower temperature range favoured the current and coulombic efficiency, while higher temperatures worked better for COD reduction (Jadhav and Ghangrekar, 2009). However, a different trend was observed in a continuous flow ML-MFC operating at 30 ℃, which showed a power density of 422 $mW/m^2$ (12.8 $W/m^3$), COD reduction of 26%, and CE of 1.7%. At ambient temperature (23 ℃), the power density reduced to 345 $mW/m^2$ (10.5 $W/m^3$), COD reduced to 19%, while CE dropped to a mere 0.7% (Ahn and Logan, 2010). Another study analysed the effects of varying temperatures in the range 15–35 ℃ and found the best results at 35 ℃, showing MPD, current and CE of 74 $mW/m^3$, 2.51 mA, and 10%, respectively (Tee et al., 2018).

The start-up temperature must be considered for maintaining longer power stability in batch and continuous mode ML-MFCs. Generally, the microbial community's sensitivity towards temperature decides the maximum operating temperature, beyond which the bacterial activity degenerates. In most studies, the observed optimum temperature ranges from 20 to 32 C favoured the growth of methanogenic bacteria and demonstrated a linear

rise in the power output. The highest operating temperature limit is usually 35 ℃, above which the reactor efficiency begins to decline.

#### *1.8.2.3. Effect of pH*

The bioactivity of the microbial community is considerably dependent on the pH of the substrate (Marashi and Kariminia, 2015). In a study, an increase of the pH value above 8.5 led to the precipitation of carbonates on the cathode surface in the batch mode of ML-MFC reactors. The deposition of the carbonate layer acted as a barrier and decreased the electrochemically active area, similar to the PTFE effect on cathode activity (Guerrini et al., 2015). Another work tested the effect of pH in the range of 5.5–7.5 and found that the internal resistance decreased as the pH difference between the anode and cathode solutions increased. The highest current was generated within an optimum pH range of 6.0–7.0, indicating lower microbial activity at sub-optimal pH compared to the optimal pH (Jadhav and Ghangrekar, 2009). Similar observations were found in yet another study that concluded the optimal pH of an ML-MFC as 7 (Gil et al., 2003). The effect of three different pH conditions (5.5, 7.0, and 8.5) was assessed on an ML-MFC. The highest power density was observed at pH 8.5, which was greater by 40% and 66% than the power densities observed at pH values of 7.0 and 5.4, respectively. This was evident as even though acidogenic and methanogenic bacteria are inactive in alkaline conditions, electrogenic bacteria are active (Marashi and Kariminia, 2015). When the pH of the anodic solution increased from 5.4 to 9.0 due to the hydrolysis of the urea, it caused a decrease in the anodic performance, implying that the anode can take a limited pH working range (Santoro et al., 2013). The acidogenic bacteria are active at pH 5.5, where hydrogen production dominates, overcoming the pollutants' degradation and decreasing COD removal, as compared to neutral or alkaline conditions (Marashi and Kariminia, 2015). In contrast, an alkaline environment is favorable for the electrogenic bacteria leading to a higher power generation (Yuan et al., 2011)

#### *1.8.2.4. Effect of substrate pre-treatment*

The quality of the substrate fed to the reactor is a crucial factor influencing the performance of the ML-MFC. The organic molecules need to be decomposed and dissolved in the substrate for the bacteria to be able to consume them. In a study, sludge was kept in the anode chamber for 15 days, followed by heat treatment at 100 ℃ and cooling to room

temperature. It was then re-inoculated, while no inoculation was done for the cathode. As a result, the COD reduced efficiency reached 91.4% at an organic loading rate (OLR) of 2.65 kg COD/$m^3$.d, giving a maximum power density of 6.73 mW/$m^2$ and a current density of 70.74 mA/$m^2$ (Ghangrekar and Shinde, 2008).

Similarly, a power density of 0.32±0.01 W/$m^2$ was obtained with a sludge fermented for nine days at 30 ℃ before dilution with the primary effluent, whereas the untreated primary effluent gave a power density of 0.24±0.03 W/$m^2$. The fermentation caused a reduction in the total suspended solids from 26.1 to 16.5 g/l and the pH from 5.7 to 4.5. Additionally, it increased the conductivity from 2.4 mS/cm to 4.7 mS/cm (Yang et al., 2013).

#### *1.8.2.5. Effect of reactor design and different separators*

The design of the ML-MFC reactor is the cornerstone for deciding the type of cathode material and assembly suitable for the reactor. The cathode can either be entirely submerged in the substrate or placed as an air-cathode electrode, where one half has contact with the substrate and the other half is exposed to the air. For the air-cathode, the ORR reaction occurs with the oxygen in the air; for the submerged cathode, the air is supplied through a compressor.

In a study, an ML-MFC was designed with a cylindrical shape having a diameter of 10 cm and a height of 100 cm. Graphite felt was used as the anode (surface area of 465 $cm^2$) and placed at the bottom of the reactor; with glass wool (4 cm depth) and glass bead (4 cm depth) set above the anode, as shown in Fig. 1.8. The cathode, made of graphite felt (surface area of 89 $cm^2$), was placed at the top of the reactor and the compartment was aerated. The electrode spacing was varied between 10 cm and 30 cm. The inlet of wastewater was from the bottom, and after passing through the layers, it was discharged from the top. The set-up yielded a power density of 1.3 mW/$m^2$ at a current density of 6-9 mA/$m^2$ (Jang et al., 2004). A similar design by Ghangrekar and Shinde gave the maximum voltage of 358 mV, power density of 10.9 mW/$m^2$, COD reduction of 88%, and BOD reduction of 87% (Ghangrekar and Shinde, 2007). A two-chambered cylindrical ML-MFC of Plexiglas was designed with a diameter of 75 mm and a height of 100 mm. A carbon paper separated the two chambers, and the electrodes too were made of carbon paper. The cathode electrode was coated with platinum and dipped into the cathode chamber. After a 400 h long run, the maximum voltage output of 551 mV and power density of 121 mW/$m^2$

were attained (Luo et al., 2007). In another work, the cathode and anode compartments were placed at different levels. The cathode chamber was located above the anode chamber so that the outlet of the anode was connected to the inlet of the cathode through a valve. The substrate was driven by gravity into the anode from the storage container placed at a higher level than the cathode. The air was pumped into the cathode chamber, and the influent entered from the anode and went through the connection to the cathode. The reactor assembly resulted in a maximum voltage of 160.7 mV, an MPD of 24.33 mW/m$^3$, COD reduced efficiency of 90.45% (Du et al., 2011).

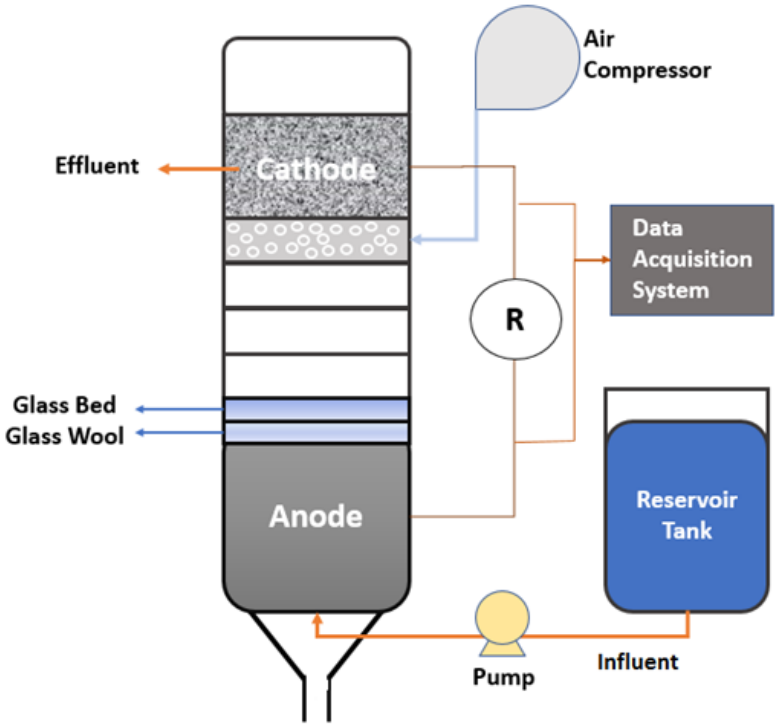


**Figure 1.8** Cylindrical ML-MFC with anode and cathode placed inside the reactor. (Redrawn with modifications from Ref. Jang et al., (2004)).

The cylindrical reactors have the advantage of capturing the maximum number of protons escaping from the anode, where the influent enters from the bottom of the reactor and leaves from the top. The influent comes in contact with the cathode as it emerges out of the reactor, accelerating the movement of hydrogen from the anode to the cathode. Moreover, the speed of the fluid flow affects the electricity production and the treatment of influent. Despite many advantages of the cylindrical reactor, some drawbacks are associated with these designs. Firstly, the spacing between the two electrodes affects the reactor output and needs to be optimized. Secondly, there is a requirement for external air pumping into the cathode compartment. Thirdly, when the cathode is completely immersed in the substrate, it leads to the biofilm's rapid formation, resulting in biofouling, thus

lowering the performance of the cathode. Finally, the cathode area may not be enough for the reactor; the literature shows that the optimal ratio of the cathode size to the anode size must be 2:1 or higher (Cheng and Logan, 2011). Another variation in the reactor design could be wherein the cathode is placed outside the reactor. In a study, a cylinder-shaped reactor made of Plexiglass was designed having 3 cm diameter, 13 cm height, and evenly drilled holes on the wall, as shown in Fig. 1.9. The cathode was a cylinder wrapped with a flexible carbon cloth coated with C/Pt, as an air-cathode. Carbon granules were used as the anode with a surface area of 31 $cm^2$. The inlet was from the bottom, while the effluent exited from the top. The reactor displayed a voltage of 0.384 V with a maximum volumetric power of 50.2 $W/m^3$ at a current density of 216 $A/m^3$ (with an internal resistance of 27 Ω) (You et al., 2007).

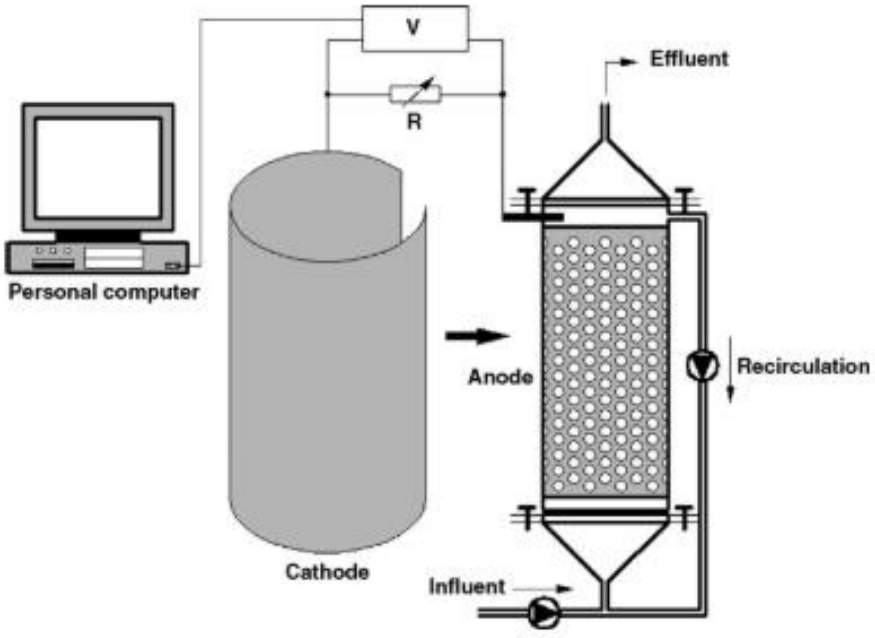


**Figure 1.9** Cylindrical ML-MFC with anode inside and cathode placed outside the reactor. (Reproduced with permission from Ref. You et al., (2007) © 2007 Elsevier publisher).

Furthermore, this design helped to have a longer lifespan and higher cathode performance, simultaneously decreasing the overall internal resistance by minimizing the distance between the cathode and the anode. A modified ML-MFC configuration was developed to solve the issue of space between the cathode and anode. The design consisted of a twin cylindrical compartment with a volume of 1.85 l, an air-cathode made of carbon cloth coated with platinum from the air-facing side, and a brush-type anode made of carbon cloth connected with titanium wires. The anode and cathode were placed on each end of the compartment, with the cathode being at a distance of 1 cm from the anode. The design

resulted in an MPD of 39–53 mW/m$^2$ from the cattle manure solid waste (Lee and Nirmalakhandan, 2011). Liu and Logan used a Plexiglass cylindrical container open from both sides with 4 cm length and 3 cm diameter, as shown in Fig. 1.10. The anode and cathode electrodes were placed on opposite sides of the cylinder. The anode was made of carbon paper, and the cathode was made of carbon cloth coated with platinum on the air-facing side. The inner side of the cathode was examined with and without PEM. The MFC, in the absence of PEM, could achieve an MPD of 146 mW/m$^2$ with 20% CE using domestic wastewater as the substrate; while in the presence of PEM, it produced an MPD of 28 mW/m$^2$ at 28% CE (Liu and Logan, 2004). A similar reactor was built with a glass tube placed on top of the reactor (4 cm long and 1.4 cm inner diameter) with a perforated cap to help the aerobic bacteria access to air. The anode was made of carbon fiber brush, and the cathode was made of carbon cloth coated with platinum. The results showed an MPD of 268.5 mW/m$^2$, COD reduction of 67%, phosphorus reduction of 97%, and ammonia reduction of 99% (Jiang, 2017). It implies that the productivity of small-sized reactors is generally higher than that of big-sized reactors due to the lower internal resistance of the former. However, a disadvantage of these designs is that mixing cathodic and anodic compartments is inevitable, thus creating biofouling on the inner side of the cathode.

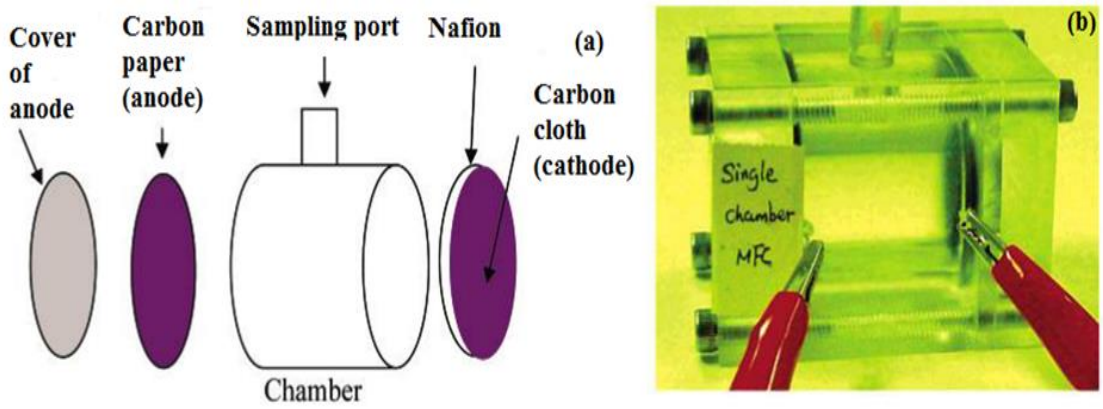


**Figure 1.10** Design of a lab-scale single-chamber ML-MFC. (Reproduced with permission from Ref. Liu and Logan, (2004) © 2004 ACS publisher).

In a different work, a micro-sized ML-MFC was designed with dimensions of 15 × 5 mm, a thickness of 0.37 mm with a volume of 83 µl, and the anode and cathode were made of carbon cloth (Fig. 1.11). Glass fiber was placed between the electrodes to alleviate the mixing of the fluids from the two compartments and for assisting in hydrogen transfer. The electrons were transferred through the titanium foils connected to each electrode. The

electrodes were held with the help of acrylic cover plates. The cell was sealed with a silicone pad stacked vertically, resulting in an MPD of 3.2 $mW/cm^3$ (Ye et al., 2018).

Many efforts have been made to utilize biochar as an electrode to develop economical and environmentally-friendly MFCs without compromising on their performance; parallel to this goal, a new design has emerged for MFCs. A study fabricated a cathode using a bamboo tube by carbonizing it at 900 ℃ in a nitrogen atmosphere followed by heat treatment at 350 ℃ to increase porosity (Fig. 1.12). The cathode was also brushed with polytetrafluoroethylene solution on the external side to make it waterproof. A carbon fiber brush was used as the anode. The cell produced an MPD of 40.4 $W/m^3$ and a CE of 55% (Yang et al., 2017). Biomass materials can be an excellent replacement for expensive electrode materials for ML-MFCs due to their renewability, wide availability, and low cost. One of the approaches to better design with a low price is preventing the mixing of anolyte with catholyte, minimizing oxygen intrusion, avoiding biofilm formation, and alleviating cathode deterioration. This can be achieved by putting a separator or an additional anode in the container to create a two-chamber ML-MFC (Kim et al., 2016). Recently, Nawaz and his team assembled a conical dual-chambered ML-MFC fabricated from graphite-based materials, as shown in Fig. 1.13. The cathode chamber was concentrically placed inside the anode chamber with 4 mm space between them. The anode was sealed from the top with an acrylic lid, and the air was pumped into the cathode. This design accomplished a treatment efficiency of 84.4% and MPD of 15.03 $W/m^3$ (Nawaz et al., 2020).

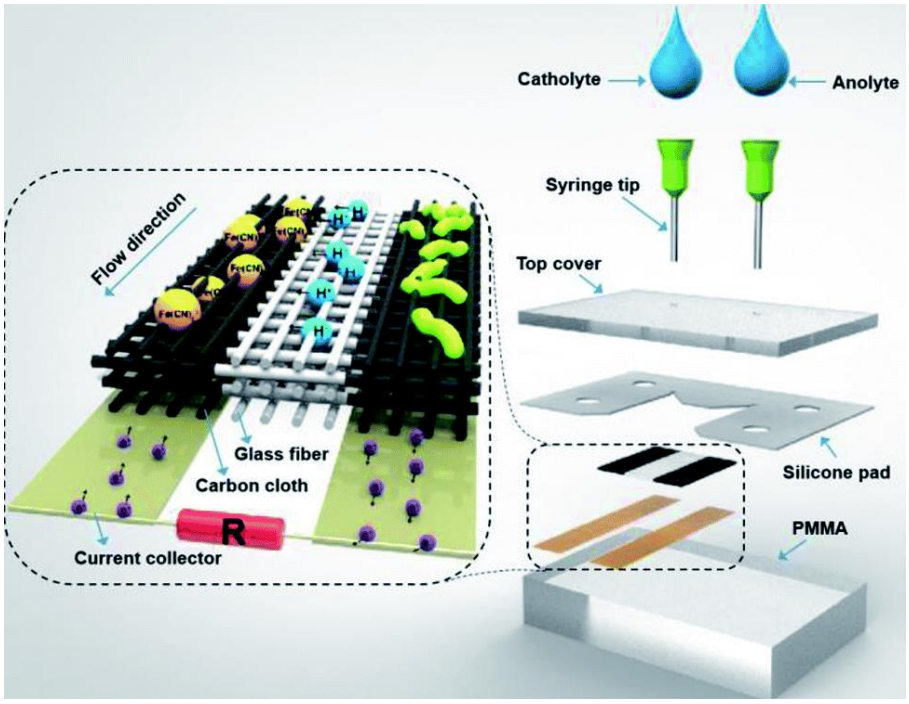


**Figure 1.11** Design of a millimetre scaled ML-MFC. (Published from Ref. Ye et al., (2018) under CC BY-NC 3.0 license).

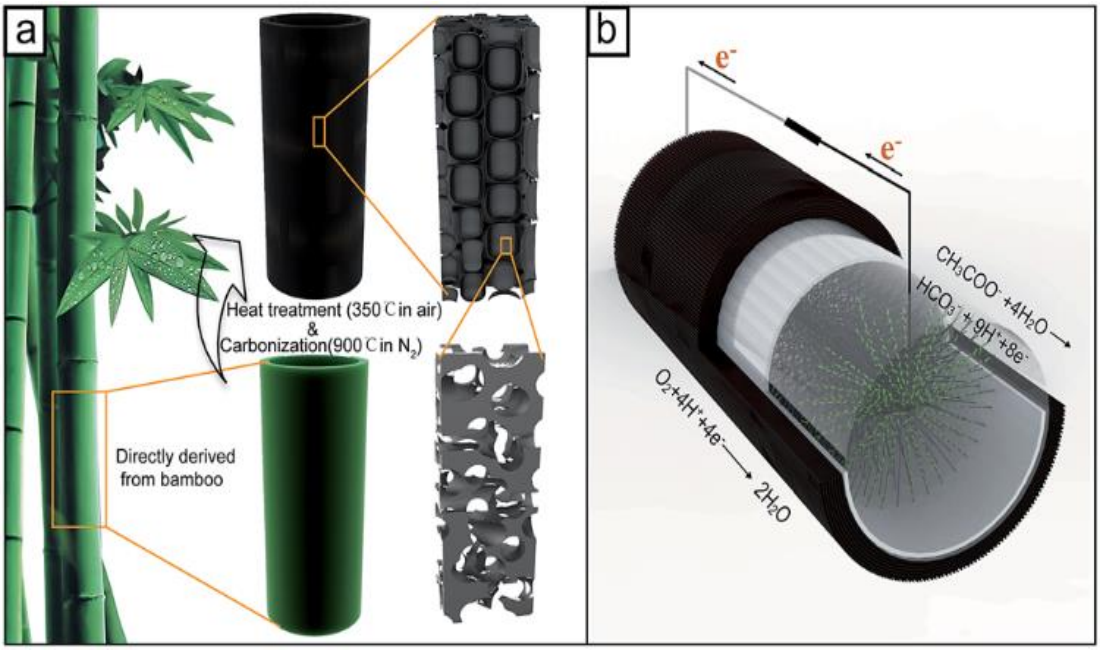


**Figure 1.12** (a) Fabrication process of the cathode from a bamboo tube; (b) MFC with a cathode made from the bamboo tube. (Published from Ref. Yang et al., (2017) under CC BY 3.0 license).

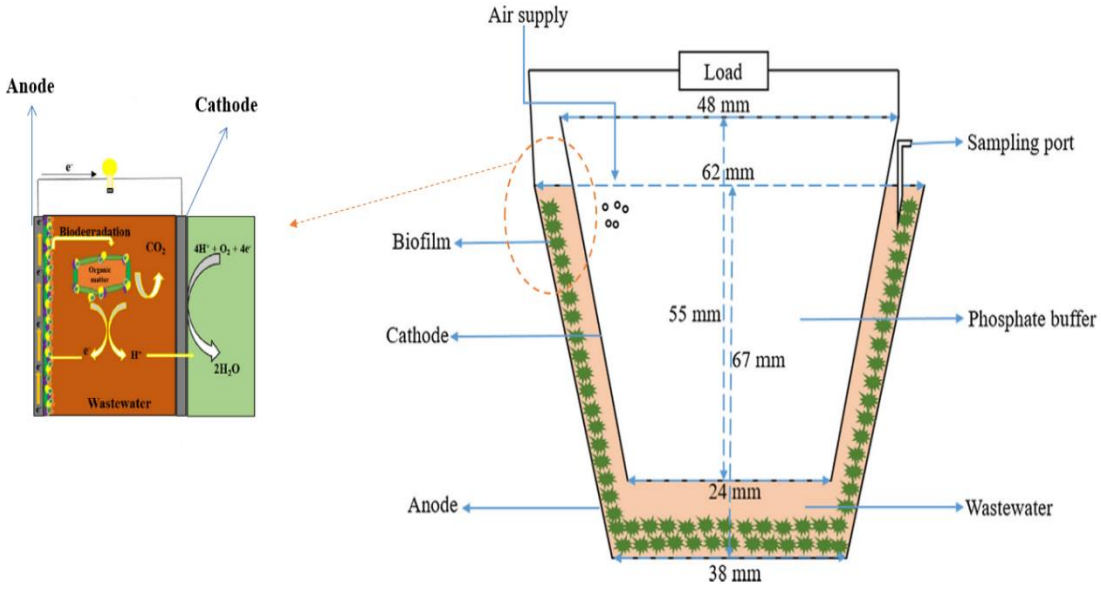


**Figure 1.13** Schematic representation of an ML-MFC with two containers concentrically placed inside one another. (Reproduced with permission from Ref. Nawaz et al., (2020b) # 2020 Elsevier publisher).

### *1.8.2.6. Effect of electrode surface area and electrode spacing*

The surface area of electrodes and the spacing between them are crucial factors to be taken into account for optimum performance of the ML-MFCs; it has to be chosen carefully where and in what anode/cathode ratio you will design the MFC container. A study investigated the effects of varying the electrode spacing (20, 24, and 28 cm) and anode area. It was found that more MPD could be achieved when the electrodes were placed close to each other. The maximum voltage of 358 mV was obtained at a distance of 20 cm. The power densities of 4.66, 6.45, and 10.13 mW/$m^2$ were achieved at anode surface areas of 210.64, 140.43, and 70.21 $cm^{2,}$ respectively. It shows that the power density decreases with the increased surface area of the anode (Ghangrekar and Shinde, 2007). The trials for scale-up of ML-MFC showed that doubling the cathode surface area increased the power output by 62%, and doubling the anode surface area increased the power output by 12% (Cheng and Logan, 2011). In an experiment with a three-column MFC connected in series, an enhancement in the anode surface area from 360 to 1080 $cm^2$ in each column increased the maximum power output by 264% for column 1, 118% for column 2, and 151% for column 3. Also, the COD and BOD reduction efficiencies were increased by 137% for column 1, 279% for column 2, 182% for column 3, and 63% for column 1, 161% for column 2 and 159% for column 3, respectively (Gálvez et al., 2009).

### *1.8.2.7. Effect of Substrate Conductivity*

The substrate's conductivity is another factor that profoundly influences the output performance of the ML-MFCs. One way to enhance the conductivity is by adding metal ions to the substrate. However, adding metal ions creates a toxic environment for the microorganisms. So MFCs are limited by the requirement to compromise between the toxicity issue and the conductivity of the substrate (Dong et al., 2015). It has been found that when the ions are added, the MPD increases linearly with rising electrolyte conductivity; the MPD escalated from 0.11 $W/m^2$ at a conductivity of 1e4 Sm1 to 1.02 $W/m^2$ at a conductivity of 1e2 Sm1. Further increase in conductivity beyond 2e1 Sm1 showed no more improvement in MPD (Gadkari et al., 2020).

In a trial, phosphate buffer was added to the substrate solution to increase its conductivity, which increased the power density from 1330 to 1640 $mW/m^2$ (Cheng and Logan, 2007). The MPD rose from 438 to 528 $mW/m^2$ when the phosphate buffer concentration was increased from 50 to 200 mM in a comparable experiment (Feng et al., 2008). The total power density was increased to 400 $mW/m^2$ by adding sodium acetate solution to the substrate (Jiang and Li, 2009). Likewise, putting as little as 0.5% of NaCl and $Na_2SO_4$ (1:1 ratio) changed the power density from 34 to 43 $mW/m^2$ and augmented the phenol removal rate by 4%. Increasing the amount of salt to 1% raised the MFC power density to 45 $mW/m^2$, whereas 2% salt resulted in an inhibitory effect on power generation (Du et al., 2015; Mousavi et al., 2016). Thus, inorganic salts can significantly improve the conductivity and decrease the resistance in the solution, thus boosting the efficiency of ML-MFCs.

Most research agreed on that one of the factors of power production from ML-MFCs is the result of increased conductivity, which in turn suggests greater ionic conduction and decreased ohmic loss. However, the substrate solution can only tolerate so much salt before it becomes unusable. As bacteria cannot tolerate high levels of salt in their environment, it is critical that the solution's high salinity does not negatively affect the bacterial colonies (Aaron et al., 2010; Mousavi et al., 2016). Therefore, it is important to carefully assess the bacterial response to external stimuli with respect to the compounds added to enhance the substrate's ionic strength.

## 1.9. ML-MFC applications in Water Treatment (Substrate)

The substrate plays a pivotal role in determining the efficacy of ML-MFCs in energy generation since it serves as the primary source of nutrients for the bacteria (Yang et al., 2009). ML-MFCs are designed to accommodate a wide range of substrates, which can consist of mixtures of various organic materials, wastewater, or lignocellulosic biomass (Pant et al., 2010). In contrast to traditional wastewater treatment methods, such as the energy-intensive aerobic-activated sludge process that necessitates significant air or oxygen supply to aeration tanks (Capodaglio and Olsson, 2020), ML-MFCs present a more sustainable approach. This work explores the potential of ML-MFCs in wastewater treatment by targeting the removal of organic compounds, inorganic substances, and heavy metals. Various researchers have evaluated ML-MFC performance using measurable parameters like current (or current density in $mA/cm^2$ or $mA/m^3$), voltage (open circuit or closed circuit), COD/BOD reduction, MPD, and CE, as well as inorganic or heavy metal reduction to assess substrate efficiency.

Numerous studies have focused on maximizing the efficiency of ML-MFCs for the treatment of wastewater containing organic matter while also generating electrical power. For instance, in a study, ML-MFCs fueled with glucose and wastewater achieved an MPD of 494 $mW/m^2$ and 146 $mW/m^2$, respectively, with corresponding CE values of 9–12% and 20%. The glucose-fed unit demonstrated an impressive glucose removal efficiency of 98%. Interestingly, when a proton exchange membrane (PEM) was employed in the same study, the MPD decreased to 262 $mW/m^2$ and 28 $mW/m^2$, with CE values of 40–55% and 28%, respectively (Liu and Logan, 2004). This observation suggests that the absence of a PEM led to an increase in MPD but a decrease in CE due to substantial oxygen diffusion into the anode. Furthermore, the glucose concentration was found to influence power output, with higher glucose concentrations resulting in improved MPD. Similar findings were reported in another study using acetate and butyrate as substrates, achieving MPDs of 506 $mW/m^2$ and 305 $mW/m^2$, respectively, which were 54% and 57% higher, respectively, compared to using a PEM (Liu et al., 2005). Feng et al. reported MPD values of 205 $mW/m^2$ for beer brewery wastewater, 494 mW/m2 for glucose (0.6 g/l), and 146 $mW/m^2$ for domestic wastewater, demonstrating an

increased COD reduction efficiency from 54% to 98% as the strength of brewery wastewater increased from 84 to 1600 mg/l.

Utilizing coal-tar refinery wastewater as a substrate yielded an MPD of 4.5 $mW/m^2$ at a voltage of 543 mV, along with an 88% COD reduction, 57% sulfate elimination, and 41% sulfur removal. Moreover, the ML-MFC efficiently removed over 90% of phenol and 2-methyl phenol (Park et al., 2012). When human urine was passed through an ML-MFC, it generated a current of 0.18–0.23 mA, reducing the initial COD of 10.9 g/l to 3.6 g/l after a 4-day retention period in the batch mode MFC unit. Another study investigating phenol concentrations in the range of 25–200 mg/l observed an increase in phenol removal from 80% to 97% as the phenol concentration increased from 25 to 100 mg/l. This setup achieved an MPD of 49.8 $mW/m^2$ and a current density of 292.8 $mA/m^2$ (Buitrón and Moreno-Andrade, 2014). Using rice straw pre-treated with acid (to degrade cellulose) as a substrate, an ML-MFC unit generated an MPD of 137.6 $mW/m^2$ and achieved a COD reduction efficiency of 79% with an initial COD of 400 mg/l (Wang et al., 2014). Similarly, purified terephthalic acid wastewater produced an MPD of 65.6 $mW/m^2$ at a COD concentration of 8000 mg/l (Marashi and Kariminia, 2015).

Wastewaters from dairy, leather, and sewage industries, rich in organic materials, generated maximum power outputs of 1.98 mW, 1.95 mW, and 1.28 mW, respectively, accompanied by COD reduction rates of 85.4%, 80%, and 65% (T. Aswin et al., 2017). Other lignocellulosic materials used as substrates resulted in an MPD of 29 $mW/m^3$ (Adekunle et al., 2016). When dye processing wastewater was tested at several organic loadings, it achieved an MPD of 515 $mW/m^2$, CE of 56%, and COD reduction of 85% at an organic loading of 1.0 g/l COD (Karuppiah et al., 2018). Additionally, a study involving petroleum refinery wastewater showed a treatment efficiency of 45.06% and a power density of 28.27 $W/m^3$, while whey wastewater treatment resulted in 72.76% treatment efficiency and 23.23 W/m3 power density (Mohanakrishna et al., 2018). Wood, rich in organic matter, also displayed potential as a fuel for MFCs, with poplar wood achieving an MPD of 8555 $mW/m^2$ (Erensoy and Çek, 2018). Another investigation used

tomato waste as a substrate and produced an MPD of 60.041 mW/$m^2$, a current density of 99.174 mA/$m^2$, and a voltage of 0.701 V (Kamau et al., 2018).

Recently, several studies have focused on heavy metal (sulfur, copper, mercury) removal using ML-MFCs, given the extreme toxicity and carcinogenicity associated with these pollutants. Various heavy metals are released in the effluents from tanning, cement, electroplating, and dye industries. In one study, a substrate made from hydrolyzed heavy metal-containing wheat grain (HMWG) produced an MPD of 381 mW/$m^2$, CE of 15.7%, and COD reduction of 83.4% (Yuan et al., 2018). However, increasing the concentration of HMWG hydrolysate resulted in a slowdown of reactor electricity production. In another study, Cu (II) was used as an electron acceptor to investigate the mechanism of metal treatment in an ML-MFC. A low Cu (II) ratio achieved an 87.56% reduction in heavy metals, while an increasing Cu (II) ratio led to a drop in heavy metal reduction efficiency to 36.98%. This change also caused the voltage to decrease from 71 to 11.1 mV (Chan et al., 2020).

### 1.10. Research rationale & objectives

- ✓ The discovery of various types of microbial fuel cells (MFCs) has opened up new avenues for applications in bioelectric harvesting, water treatment, hydrogen generation, desalination, and the removal of hazardous compounds from wastewater. In the construction of traditional ML-MFCs, plexiglass, glass, or plastic containers have typically been used in conjunction with different cathode and anode electrodes. However, these conventional ML-MFC designs utilizing these materials often suffer from cathode biofouling and cathode deterioration, which inevitably lead to reduced efficiency over time, rendering ML-MFCs commercially less viable.
- ✓
- ✓ To address the limitations associated with cathode biofouling and deterioration, this research explores the utilization of wood as both a container material and separator, offering a sustainable and eco-friendly alternative. The primary objective of this study is to manufacture an ML-MFC using wood and to design the container in a manner that prevents direct contact between the cathode electrode and the substrate.

This innovative approach aims to investigate the potential utility of untreated wood as a solution for mitigating cathode deterioration and biofouling issues.

- ✓ In light of these objectives, the following research goals have been formulated:
- ✓ Preparation of wooden ML-MFC containers under varying experimental conditions.
- ✓ Evaluation of the prototype's performance by assessing key response parameters, including open circuit voltage, current density, power density, and COD reduction.
- ✓ Modification of the wooden ML-MFC by altering the wall thickness to optimize its performance.
- ✓ Assessment of the wooden ML-MFC's capability for water treatment by measuring carbohydrate content in the substrate, including COD reduction, pH, conductivity, and sugar content.
- ✓ Characterization of the wood plates before and after utilization using advanced analytical techniques such as SEM and DMA.

## 1.7. Dissertation outline

This dissertation has been structured into four chapters as follows:

*i.* ***Chapter I***

This chapter sets the stage by introducing energy harvesting techniques and provides an overview of microbial fuel cells (MFCs) in general. It delves into the mechanisms of electric production and water treatment with MFCs and categorizes MFCs based on the presence or absence of membranes, air-cathodes, and aqueous-cathodes. Additionally, it briefly reviews various types of MFCs and focuses on ML-MFCs, highlighting the factors influencing electric production and water treatment quality. Finally, the chapter explores the diverse applications of ML-MFCs in wastewater treatment.

*ii.* ***Chapter II***

This chapter details the experimental procedures employed for constructing wooden ML-MFCs and preparing the substrate. It provides a comprehensive description of the necessary tests conducted to evaluate the novel prototype's performance in terms of electric production and water treatment capabilities. Additionally, advanced analytical techniques are employed to characterize the wood plates before and after their use.

*iii.* ***Chapter III***

In this chapter, the results and their subsequent discussion are presented. Key parameters related to electric production, water treatment capability, pH, conductivity, and water loss are analyzed and discussed, with a focus on the influence of different wood plate thicknesses in the fabrication of wooden ML-MFCs. Mechanical properties, EDX (Energy Dispersive X-ray), and SEM (Scanning Electron Microscopy) analyses of the wood plates are also included.

*iv.* ***Chapter IV***

The final chapter presents the innovative outcomes achieved throughout the study. Additionally, recommendations for future research directions are provided, offering insights into potential avenues for further exploration and development in the field of wooden ML-MFCs and their applications.

# CHAPTER II-
# MATERIALS & METHODS

## 2. Materials and Methods

### 2.1. Air-cathode WML-MFC fabrication

#### *2.1.1. Preparation of electrodes*

The anode electrode was prepared from carbon felt (PXFT-540, Zoltek Corporation, Bridgeton, USA), having a 114 $cm^2$ surface area -with 6 mm thickness- (assumed as a smooth surface). The cathode electrode was prepared from carbon cloth with a 162 $cm^2$ surface area. Both the electrodes were washed with deionized water and dried at 80 °C for 24 h. They soaked in 1M HCl for 24 h to remove the impurities on the surface of the electrodes. Finally, the electrodes were washed with deionized water and dried at 80 °C for 24 h. Four pieces of carbon felt as an anode electrode were connected with a copper wire and placed inside each WML-MFC container, as appears in Fig. 2.1. The anode occupies a total volume of 24 $cm^3$ inside the containers. The cathode electrode was placed outside the container, covering it from all sides; as shown in Fig. 2.2, it was tightened to the container with a fabric thread. The cathode electrode is connected with a copper wire. In this design, no catalyst was loaded on the cathode, nor was any pre-treatment done on the anode and the wood plates (Fig. 2.3). From each WML-MFC container, the extended anode and cathode wires were connected to a data logger through a breadboard. Before the current and power measurements, different external resistors between 400 Ω – 1 MΩ were tested to determine the optimal external resistor for WML-MFC.

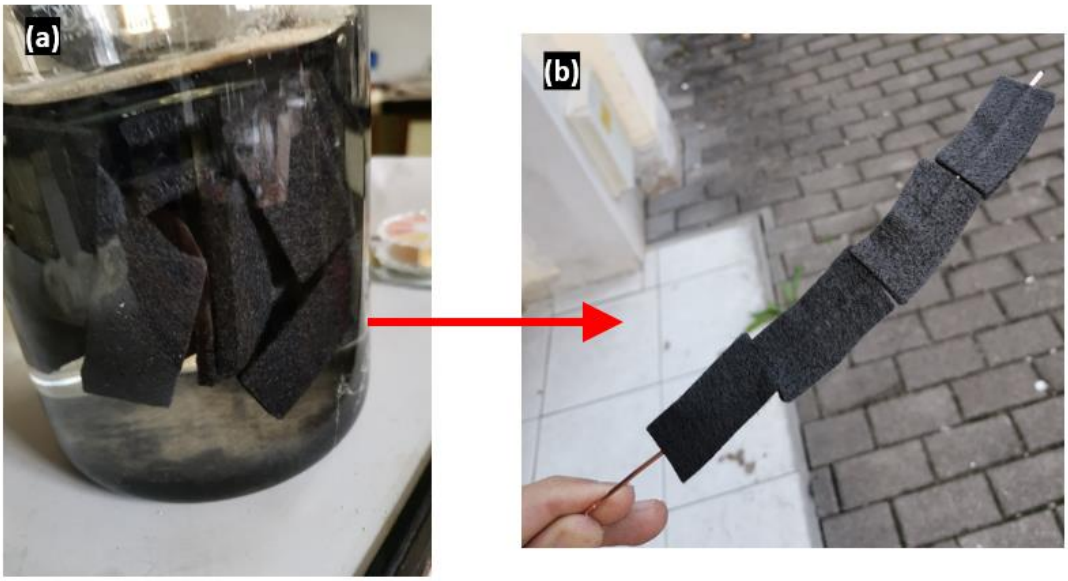


**Figure 2.1** The anode electrode preparation. (a) the carbon felt cut and immersed in HCl. (b) four sliced pieces of carbon felt joined through a copper wire.

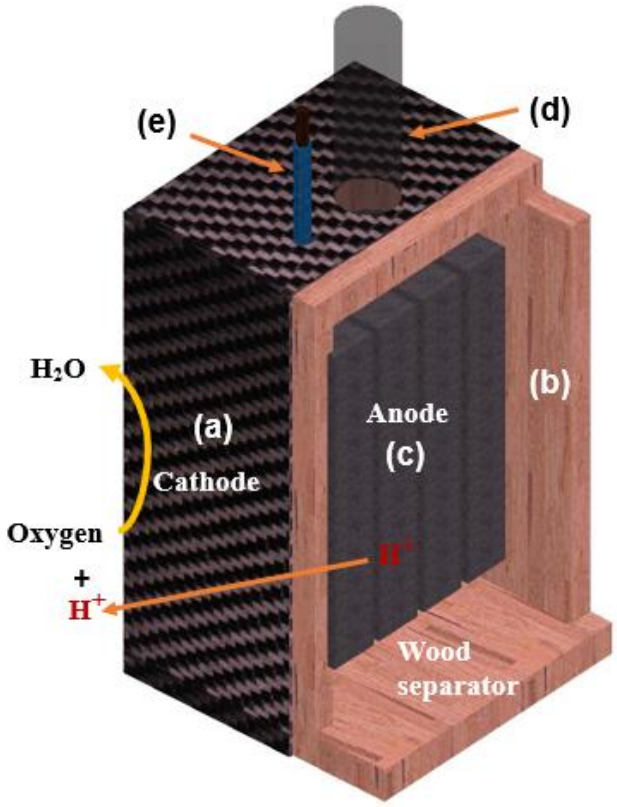


**Figure 2.2** Cross-sectional view of the WML-MFC designed in this study. (a) cathode electrode (b) wooden container (c) anode electrode (d) inlet/outlet for the substrate (e) copper wire extended from anode electrode.

### *2.1.2. Fabrication of the WML-MFC container using wood*

When deciding the wood species to use in the fabrication of WML-MFCs, it is vital to consider factors such as cost, wood-water relation, and availability. For this study, the untreated wooden plates were obtained from three common tree species, viz., oak (*Quercus robur*), Scots pine (*Pinus silvestris*) and black locust (*Robinia pseudoacacia*). The wood plates were collected from different places which therefore the wood plates considered as to be from different trees, and all were the heartwood part of the tree. They were cut into plates with 2 mm, 3 mm, and 4 mm thicknesses with the required dimensions by a wood cutting machine and assembled with the help of silicone adhesive (Fig. 2.3). The container's dimensions were 37 × 37 × 59 mm (±1 mm). The inner volume of each container was 55 ± 5 ml. After placing the anode inside the container, the internal volume was reduced to 25 ± 5 ml. Two holes were drilled on each box, one hole (9 mm diameter) for feeding of influent and discharging of effluent, and the other hole (2 mm diameter) for the copper wire extended from the anode electrode to pass through the container (Fig. 2.2). Three containers

of the same size were prepared from each of the three wooden species. The containers were used as such (with native wood) without any treated chemically or bleached, all used as their natural form. The experimental containers of WML-MFC have listed and annotated in Table 2.1.

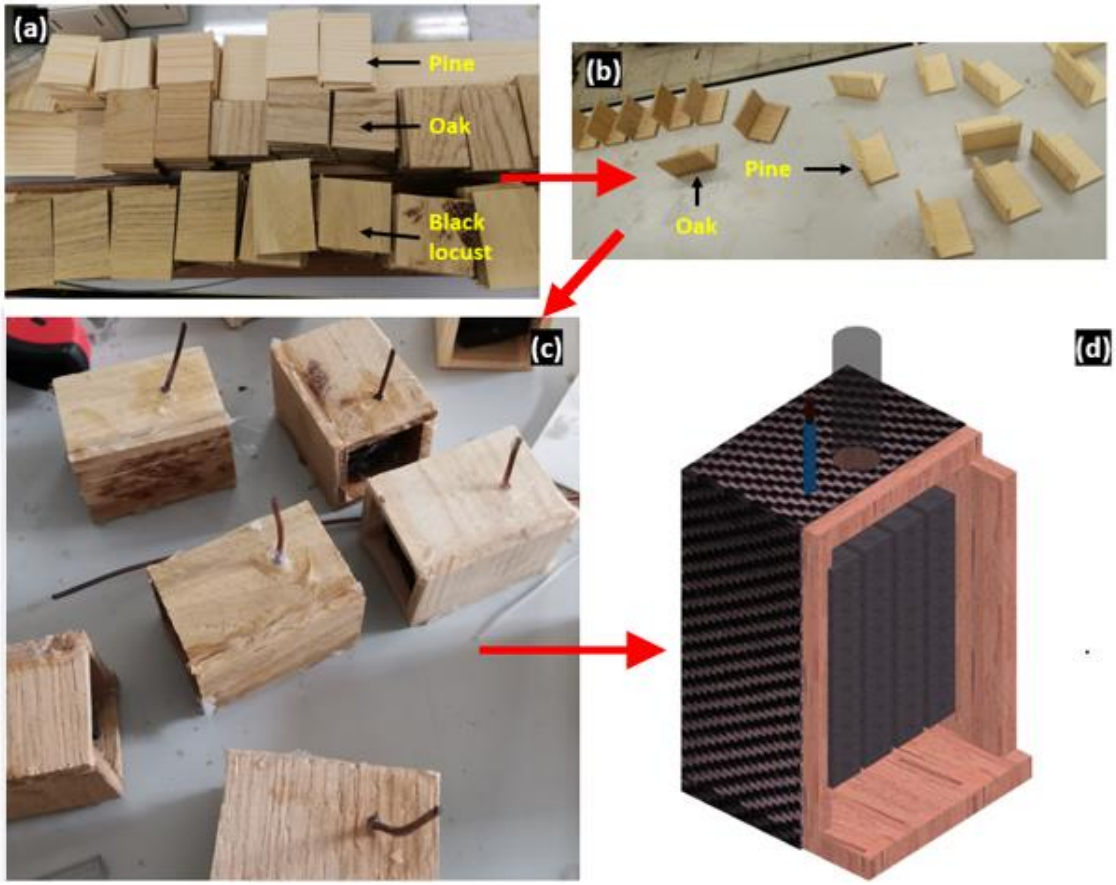


**Figure 2.3** Step-by-step preparation of WML-MFC. (a) Wood plates after they have been sliced using a wood cutting machine. (b) Wood plates glued together with silicone adhesive. (c) The anode electrode was inserted within the wood containers, and the sides were sealed. (d) The final appearance of the WML-MFC prototype after wrapping the WML-MFC with the carbon cloth cathode electrode.

**Table 2.1** Description of all experimental containers.

| Container description | Denoted as |
|---|---|
| Wooden Black locust (4 mm) – MFC – container no. 1 | WB4-MFC-1 |
| Wooden Black locust (4 mm) – MFC – container no. 2 | WB4-MFC-2 |
| Wooden Black locust (4 mm) – MFC – container no. 3 | WB4-MFC-3 |
| Wooden Oak (4 mm) – MFC – container no. 1 | WO4-MFC-1 |
| Wooden Oak (4 mm) – MFC – container no. 2 | WO4-MFC-2 |

| | |
|---|---|
| Wooden Oak (4 mm) – MFC – container no. 3 | WO4-MFC-3 |
| Wooden Pine (4 mm) – MFC – container no. 1 | WP4-MFC-1 |
| Wooden Pine (4 mm) – MFC – container no. 2 | WP4-MFC-2 |
| Wooden Pine (4 mm) – MFC – container no. 3 | WP4-MFC-3 |
| Wooden Oak (3 mm) – MFC – container no. 1 | WO3-MFC-1 |
| Wooden Oak (3 mm) – MFC – container no. 2 | WO3-MFC-2 |
| Wooden Oak (3 mm) – MFC – container no. 3 | WO3-MFC-3 |
| Wooden Pine (3 mm) – MFC – container no. 1 | WP3-MFC-1 |
| Wooden Pine (3 mm) – MFC – container no. 2 | WP3-MFC-2 |
| Wooden Pine (3 mm) – MFC – container no. 3 | WP3-MFC-3 |
| Wooden Oak (2 mm) – MFC – container no. 1 | WO2-MFC-1 |
| Wooden Oak (2 mm) – MFC – container no. 2 | WO2-MFC-2 |
| Wooden Oak (2 mm) – MFC – container no. 3 | WO2-MFC-3 |
| Wooden Pine (2 mm) – MFC – container no. 1 | WP2-MFC-1 |
| Wooden Pine (2 mm) – MFC – container no. 2 | WP2-MFC-2 |
| Wooden Pine (2 mm) – MFC – container no. 3 | WP2-MFC-3 |

## 2.2. Methodology for operating WML-MFC and analysis

### *2.2.1. Inoculation and operation of WML-MFC*

The inoculation of each Wood-based Microbial Fuel Cell (WML-MFC) was carried out with a 20 ± 5 mL substrate blend. This blend was composed of 200 mL anaerobic digestion sludge sourced from a municipal wastewater treatment plant in Sopron, Hungary, 300 mL distilled water, outdoor mud, and sucrose as a carbon source. Prior to introduction into the WML-MFC, the substrate was allowed to settle for one hour to separate the mud. The experiments were performed in a batch mode with varying Hydraulic Retention Times (HRTs). Initially, each WML-MFC was loaded with 25 mL of substrate and operated for a week under open circuit (OC) conditions. This phase was critical for stabilizing the voltage and establishing a robust microbial community in the anode compartment, as reported by An et al. (2014). During the microbial growth phase, the substrate was refreshed every three days in WML-MFCs with 4 mm wall thickness. In contrast, WML-MFCs with 3 mm and 2 mm wall thickness required daily substrate renewal.

Upon transitioning to a closed circuit (CC), HRTs were adjusted between 20 to 120 hours. Each refill involved either replacing the effluent with a new substrate or using the remaining substrate from the previous day(s). Due to the high moisture diffusion through the wooden walls, daily substrate addition was necessary to maintain adequate submersion of the anode electrode. No chemical adjustments were made to influent pH or salinity. The oxygen required for the Oxygen Reduction Reaction (ORR) in these air-cathode ML-MFCs was drawn from the atmosphere. All experiments were conducted at ambient room temperatures, ranging from 15 to 25 degrees Celsius.

### *2.2.2. Data acquisition and analysis with portable data logger TDS-302*

The TDS-302 portable data logger, equipped with a 10-channel switching box, was employed for measuring DC voltage and other parameters. The logger's operation was programmable to record data at specified intervals (Fig. 2.4).

During initial testing, voltage readings for each WML-MFC unit were manually recorded every 2 hours using a Tektronix MDO3104 oscilloscope. This process involved 15 containers representing three species, with five models each. Based on these preliminary results, bioelectrically productive containers were selected for further study. Continuous voltage monitoring was then conducted using the TDS-302 logger, programmed to record every 30 minutes. The optimal external load for power output was determined by varying the load from 400 Ω to 1 MΩ and monitoring the voltage stabilization for each load.


**Figure 2.4** TML portable TDS-302 analog data logger for measuring voltage.

The performance of the WML-MFCs was primarily evaluated based on their power output. The current (I) and power output (P) were calculated using Equations 2.1 and 2.2, respectively. Current density (j) and power density (Pd) were determined as a function of the anodic surface area (114 $cm^2$) using Equations 2.3 and 2.4. The equations are.

$$I = V/R \qquad \textbf{Eq. 2.1}$$

$$P = V \times I \qquad \textbf{Eq. 2.2}$$

$$j = V/(R \times A) \qquad \textbf{Eq. 2.3}$$

$$P_d = (I \times V)/A \qquad \textbf{Eq. 2.4}$$

Here, V represents voltage (mV), R the external load (Ω), and A the anode electrode surface area ($m^2$).

Chemical oxygen demand (COD), pH, and conductivity of the influent and effluent were analyzed. Additionally, daily water loss through moisture diffusion from each container was recorded and used as a standard measurement.

### *2.2.3. Morphological analysis through scanning electron microscopy (SEM)*

SEM, a method that scans materials with an electron beam to produce magnified images, was used for microanalysis and failure analysis of solid inorganic materials. In this study, SEM (S-4800, Hitachi) was employed to examine the inner wall of the wood containers and the cathode for bacterial growth and moisture diffusion effects on wood surface morphology and biofilm development on the cathode (Fig. 2.5).

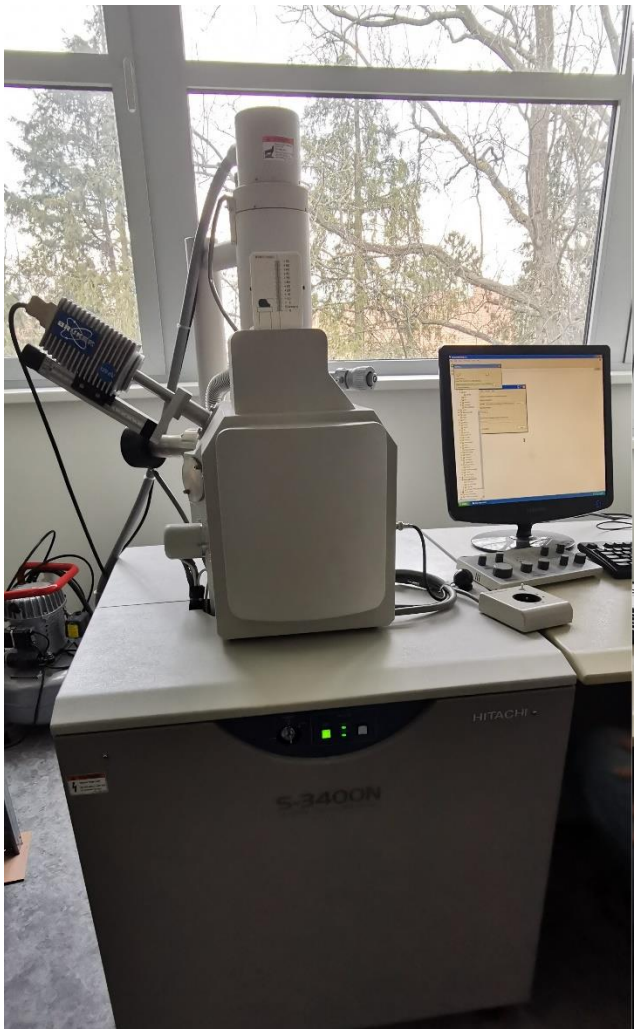


**Figure 2.5** Hitachi S-3400N scanning electron microscopy.

### *2.2.4. Viscoelastic behavior analysis through dynamic mechanical analysis (DMA)*

Dynamic Mechanical Analysis (DMA) is a sophisticated technique that applies sinusoidal stress to a material and measures its phase lagging deformation, offering insights into the material's viscoelastic properties. This method, as detailed by Schlesing et al. (2004) and Sun et al. (2007), is instrumental in analyzing the physical characteristics of solids and polymer melts. It provides comprehensive data on modulus, damping, and can be tailored to measure various parameters such as force, stress, strain, frequency, and temperature effects. Significantly, DMA is invaluable for assessing the viscoelastic behavior of materials across a broad frequency spectrum.

In this study, the DMA (METRAVIB DMA 50), as shown in Figure 2.6, was employed to evaluate the average elastic modulus of oak and Scots pine wood samples, both pre- and post-experimentation. The DMA tests involved subjecting the wood samples to sinusoidal deformation at a constant temperature of 25 °C and a consistent moisture content of 12 ± 2%. These tests were conducted over a frequency range of 1–100 Hz. The wood samples, with dimensions of 4 mm × 45 mm × 8.7 mm, were tested under a 3-point bending mode. For each frequency setting, ten readings of the storage modulus were recorded, and their average values were plotted against the respective frequencies, providing a comprehensive analysis of the wood's viscoelastic behavior.

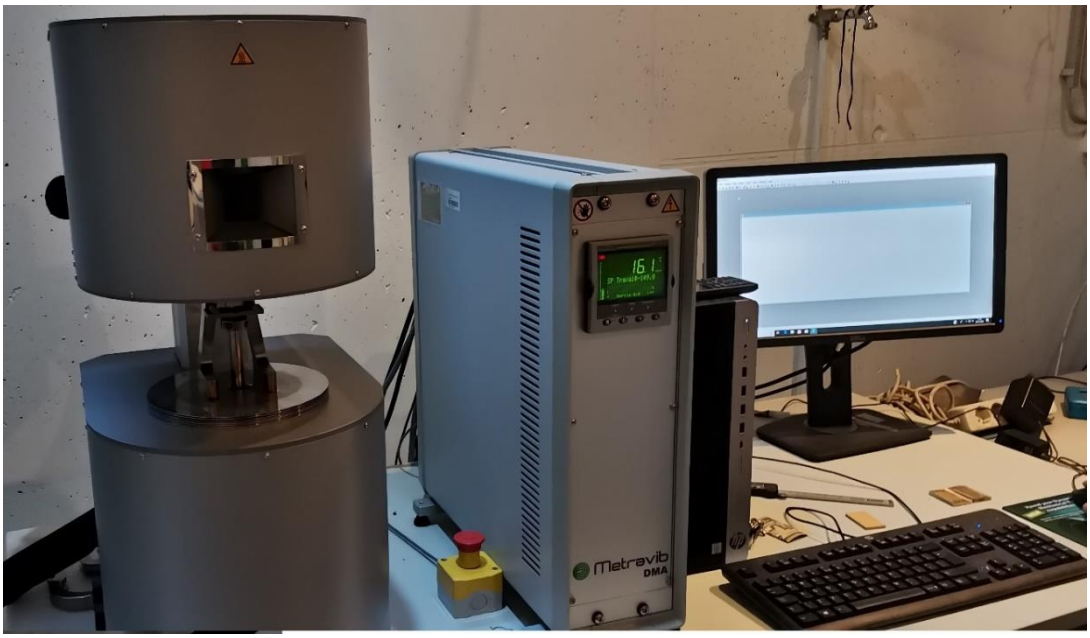


**Figure 2.6** Dynamic mechanical analysis machine of METRAVIB DMA 50.

### *2.2.5. Energy-dispersive X-ray spectroscopy (EDX)*

Energy-Dispersive X-Ray Spectroscopy (EDX), often paired with electron microscopy, is a powerful analytical technique used for elemental analysis and chemical composition determination of samples. This method, which generates distinctive X-ray emissions to identify sample components, is widely integrated with scanning electron microscopy for enhanced analysis (Torres-Rivero et al., 2021).

In this research, EDX analysis was performed using the S-4800 Hitachi model (depicted in Figure 2.5) on the inner walls of the wood containers. The primary objective was to investigate the effects of the influent on the wood surface. To ensure accuracy and minimize potential errors, EDX analysis was conducted on at least two different sections of each wood sample. This approach was critical for identifying the chemical composition of the wood species used and measuring the elements absorbed by the wood after exposure to wastewater. This analysis provided valuable insights into the interaction between the wastewater influent and the wood material, contributing to a deeper understanding of the material's suitability and performance in the experimental setup.

# CHAPTER III-
# RESULTS AND DISCUSSION

# 3. RESULTS AND DISCUSSION

## 3.1. Chapter Synopsis

This chapter provides a detailed analysis of the test results for Wood-based Microbial Fuel Cells (WML-MFC) using different wood types and thicknesses. We start by presenting preliminary findings, followed by a series of experiments focusing on Oak and Scots Pine wood at thicknesses of 2 mm, 3 mm, and 4 mm. These experiments aim to evaluate the effectiveness of using wood in WML-MFCs. Key performance indicators such as Open Circuit Voltage (OCV), Power Density (PD), Current Density (CD), and moisture-induced water loss are discussed, along with changes in Chemical Oxygen Demand (COD), pH, and conductivity in the influent and effluent. Additionally, the impact of wastewater on the wood and the cathode electrode surface is examined through Scanning Electron Microscopy/Energy Dispersive X-ray Analysis (SEM/EDX). Dynamic Mechanical Analysis (DMA) is employed to explore the viscoelastic properties of the wood samples.

## 3.2. Preliminary assessment of the 4 mm wall thickness WML-MFC

The feasibility of wooden microbial fuel cells was initially tested using 4 mm thick WML-MFC containers made from untreated European Oak, Scots Pine, and Black Locust wood. For each species, five sample containers were prepared. The Open Circuit Voltage (OCV) was the primary metric for assessing the concept's viability, recorded over 90 days at 2-hour intervals, manually with an oscilloscope. However, this section focuses on the final 210 hours of OCV data (refer to Figures 3.1, 3.2, and 3.3).

The preliminary tests showed that Black Locust exhibited significantly lower OCVs compared to Scots Pine and Oak. Specifically, Black Locust reached a maximum OCV of around 50 ± 20 mV upon fresh substrate addition, displaying brief stability before a rapid decline to as low as 1 mV at 22 ± 4 °C (Figure 3.1). In contrast, the maximum OCVs for Scots Pine and Oak were approximately 100 – 200% higher than those for Black Locust. These species also maintained electrical output stability 15 to 23 times longer after each substrate refresh (Figures 3.2 and 3.3). Oak showed greater stability, albeit with a lower maximum voltage than Scots Pine. Additionally, COD reduction efficiency was lowest in Black Locust. Consequently, due to its low electrical output, instability, natural bending when absorbing water, and minimal effect on COD reduction, Black Locust was excluded from further tests, focusing on Scots Pine and Oak.

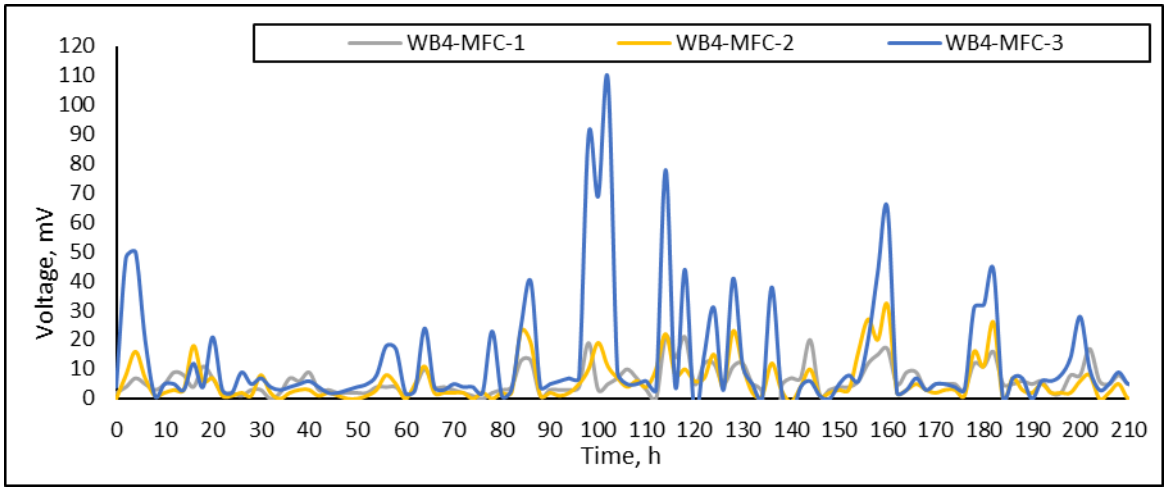


**Figure 3.1** Voltage of black locust containers during the last 210 h after 90 days of operating with open circuit condition.

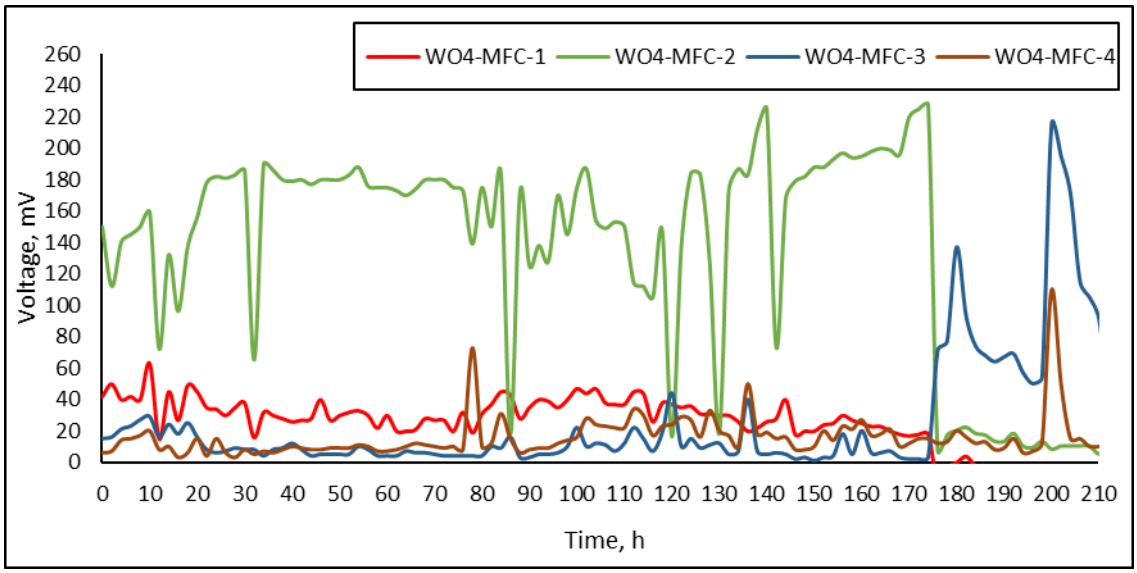


**Figure 3.2** Voltage of oak containers during the last 210 h after 90 days of operating with open circuit condition.

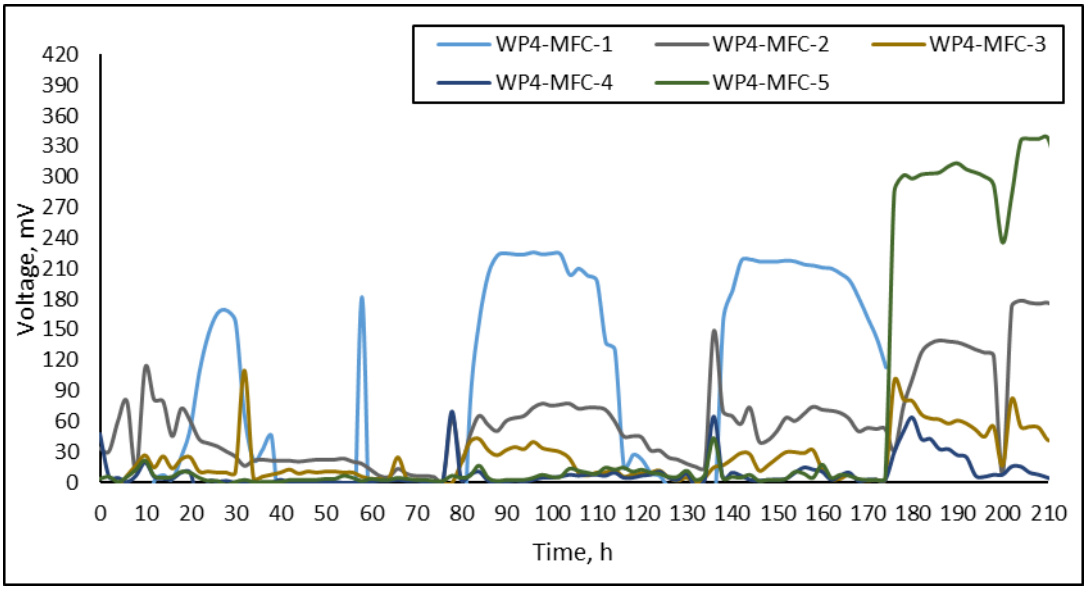


**Figure 3.3** Voltage of Scots pine containers of last 210 h after 90 days of operating with open circuit condition.

### 3.3. The WML-MFC with different wall thickness

Initial trials with Oak and Scots Pine were successful. Determining a preference between Scots Pine and Oak required testing both species at multiple thicknesses. WML-MFCs were constructed with wall thicknesses of 2 mm, 3 mm, and 4 mm for both species to identify the optimal thickness. The experiment commenced with 4 mm thick WML-MFCs.

A consistent experimental setup was employed for all container variants to facilitate a fair comparison across different thicknesses. The OCV, CD, and PD were measured under batch mode operation, with Hydraulic Retention Times (HRTs) ranging from 24 to 72 hours. Containers were manually filled with substrate using a pipette. During each substrate cycle, the lid was opened, effluent was extracted, and new influent was introduced. All necessary precautions were observed during these substrate replacement processes.

#### *3.3.1. Cell voltage with open-circuit and start-up progress to acclimation time*

##### *3.3.1.1. The WML-MFC with 4 mm wall thicknesses*

In this section, we delve into the performance of Wood-based Microbial Fuel Cells (WML-MFC) with a specific focus on 4 mm wall thicknesses. The experiment, conducted under uniform temperature and influent conditions for all samples, evaluated Open Circuit Voltage (OCV), Current Density (CD), and Power Density (PD) across different wood species. It commenced with an open circuit, reaching a peak OCV after 351 hours,

albeit with some fluctuations. Among 4 mm thick prototypes, WP4-MFC-1 showcased the highest OCV at 0.551 V (see Fig. 3.4) and a notable COD reduction efficiency of 42%.

Subsequently, additional containers of oak and Scots pine with 4 mm thickness were connected to data loggers. Upon influent addition, a gradual voltage increase was observed, with notable surges upon each substrate replacement (Fig. 3.4), indicative of biofilm growth on the anode. WP4-MFC-1 attained an OCV of 551 mV after 280 hours, marked as the acclimation point. Comparatively, WP4-MFC-3 and WP4-MFC-2 reached 321 mV and 269 mV respectively, over longer durations. Among the oak containers, WO4-MFC-2 performed best, achieving an OCV of 141 mV within 343 hours.

This performance is noteworthy when compared with similar studies. For instance, Logroño et al. (2017) reported a maximum OCV of 577 mV using carbon felt electrodes and anaerobic sludge, while Wang and Su (2013) observed a maximum OCV of 102 - 246 mV in microfluidic ML-MFCs with different influents. A soil-based ML-MFC study by Simeon et al. (2019) yielded a maximum OCV of 729 mV under similar electrode conditions. These comparisons suggest that wood is a viable biomaterial for MFC or ML-MFC fabrication.

The difference in electrical production between oak and Scots pine was significant, with Scots pine generating 78-81% higher OCV than oak. This discrepancy could be due to two factors. Firstly, wood density varies among species, affecting hydrogen permeability (Sándor and Mihály, 2006). Secondly, the presence of anti-bacterial compounds in wood, which differ across species, impacts microbial growth (Prida et al., 2006; Sanz et al., 2011).

Voltage spikes were observed after effluent replacement, peaking within 25-30 hours before stabilizing. These fluctuations were quicker than reported in other studies (Nayak et al., 2018), possibly due to substrate conductivity, galvanic corrosion, oxygen intrusion, and moisture diffusion through the wood. Differences in anodic microorganism cultures and untreated electrodes may also contribute.

Voltage disparities among containers of the same wood species were attributed to the concentration of anti-bacterial compounds, wood anisotropy, and physical properties. Scots pine and oak's differing densities (330-520 kg/m³ and 697 kg/m³, respectively) influence their bioelectrical production (Sándor and Mihály, 2006).

Additionally, during biofilm development, voltage increases were noted, particularly in WP4-MFC-2 and WP4-MFC-3 (Fig. 3.4). These were influenced by daily temperature variations, as observed in previous studies (Ahn and Logan, 2010; Jadhav and Ghangrekar, 2009; Feng et al., 2008). Ambient temperature changes affect substrate temperature, impacting microbial activity, especially in softwoods like Scots pine.

Oxygen diffusion into the anodic chamber, a critical factor for microbial activity, differed between night and day (Liu and Logan, 2004; Fan et al., 2007; Lepage et al., 2012; Venkata Mohan et al., 2008). This variation was more pronounced in Scots pine due to its higher oxygen diffusion coefficient compared to oak (Gartner et al., 2004; Sorz and Hietz, 2006). At night, lower oxygen levels led to a slight voltage increase, which did not affect oak as much.

Overall, the findings emphasize the potential of using wood as an efficient and cost-effective separator and container for enhancing cathode performance and durability in WML-MFCs, promising for sustainable bioelectricity generation.

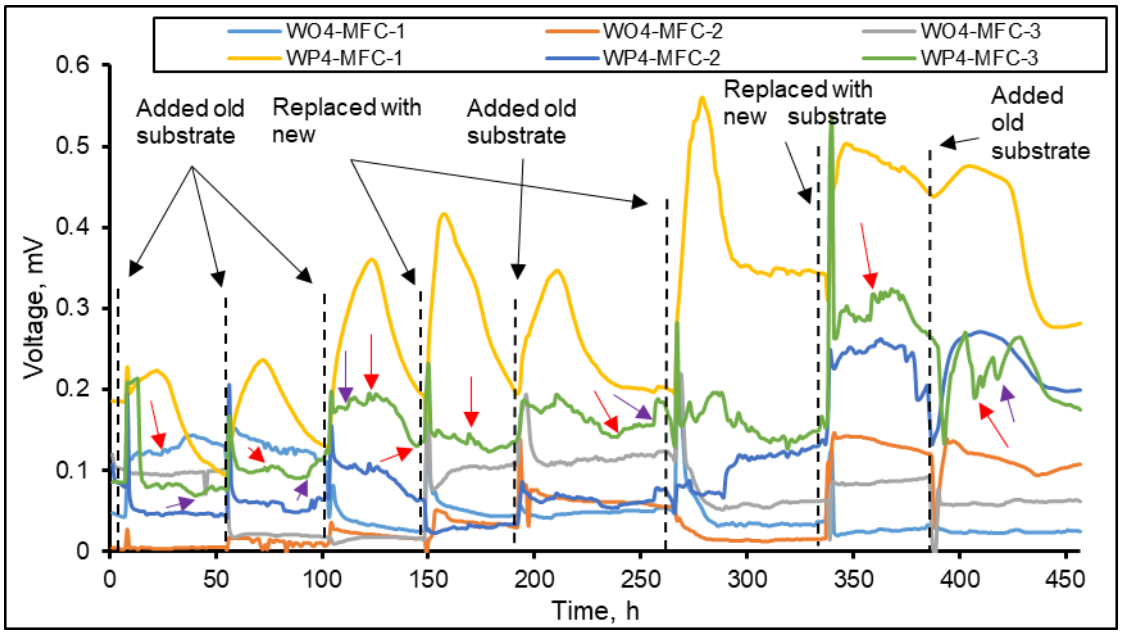


**Figure 3.4** Voltage during the start-up of 4 mm wall thickness oak and pine WML-MFCs with open circuit condition for 457 h until acclimation (red arrows indicate daytime, and purple arrows indicate nighttime).

#### *3.3.1.2. WML-MFC with 2 mm and 3 mm wall thickness*

This section focuses on the evaluation of Wood-based Microbial Fuel Cells (WML-MFC) with reduced wall thicknesses of 2 mm and 3 mm. The experiment aimed to understand how these variations in thickness influence the Open Circuit Voltage (OCV), Current Density (CD), and Power Density (PD) of the cells. Data were collected using a data logger, allowing for a detailed analysis of each container's voltage output potential.

The experimental procedure began in an open-circuit condition and was conducted over approximately 700 hours. Among the tested prototypes, WP3-MFC-2 and WP3-MFC-1 showed the highest OCVs at 0.147 V and 0.139 V, respectively (refer to Fig. 3.5). These values are notably lower than those observed for 4 mm thick WML-MFCs, indicating a potential correlation between wall thickness and voltage output.

A significant challenge encountered during data collection was the high level of noise (fluctuations) in the voltage recordings, potentially due to external electrical interference or data logger anomalies. Despite applying Data Analysis Exponential Smoothing to mitigate these fluctuations, clear night-and-day variations remained indiscernible. Nonetheless, a general trend was observed where WML-MFCs recorded slightly higher voltages during the day and at elevated room temperatures, with a slight decrease at night.

In comparing the performance based on wood thickness and type, it was noted that Scots pine with a 3 mm thickness generated higher voltages than its oak counterpart. Conversely, 2 mm thick oak containers outperformed those made from Scots pine. This observation suggests that both wood type and oxygen intrusion play crucial roles in voltage generation. Arranging the containers by wood density (from high to low) and maximum OCV (from low to high), a pattern emerges, indicating the significance of wood type in containers with a thickness of 3 mm or more. In contrast, for thicknesses less than 3 mm, wood density appears to be a more influential factor, affecting oxygen intrusion and water loss through diffusion.

Additionally, the ease with which hydrogen can reach the cathode layer is affected by the wood's density, particularly in thinner containers. This highlights the need for a cathode layer with high Oxygen Reduction Reaction (ORR) capabilities. Previous studies have shown that thicker polymer separators in MFCs reduce oxygen intrusion but are limited in power output due to increased resistance (Kondaveeti et al., 2017). Moreover,

the development of microbial biofilms or fungi on the wood surface can impact oxygen penetration and wood degradation (Mohamed et al., 2021).

Intriguingly, with 2 mm thick Scots pine (WP2-MFC), a negative voltage was recorded (Fig. 3.8), a phenomenon not observed in 2 mm thick oak containers (WO2-MFC) (Fig. 3.7). This suggests that below a 3 mm thickness, excess oxygen intrusion interferes with the hydrogen in the anode chamber, causing ORR to occur within the container itself before hydrogen can reach the cathode. This observation opens up new avenues for exploring combinations of thin-wall Scots pine MFCs with membranes and cathodes optimized for high ORR, potentially enhancing the overall efficiency and performance of these innovative bio-electrical systems.

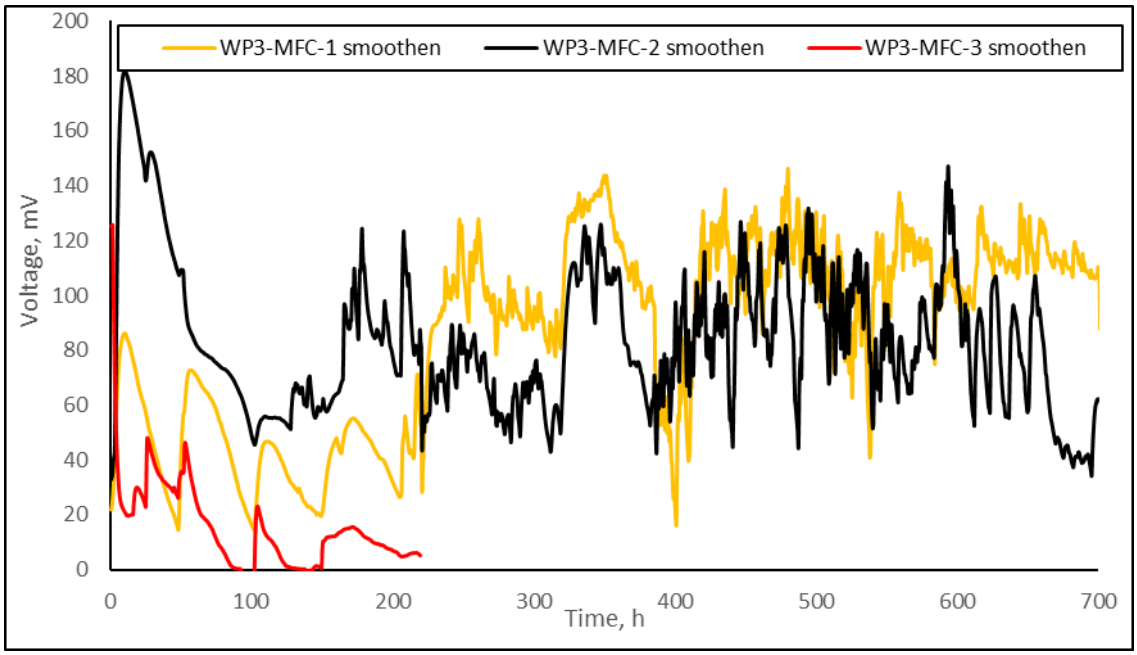


**Figure 3.5** Voltage of 3 mm wall thickness Scots pine WML-MFCs with open circuit condition from the start-up until 700 h.

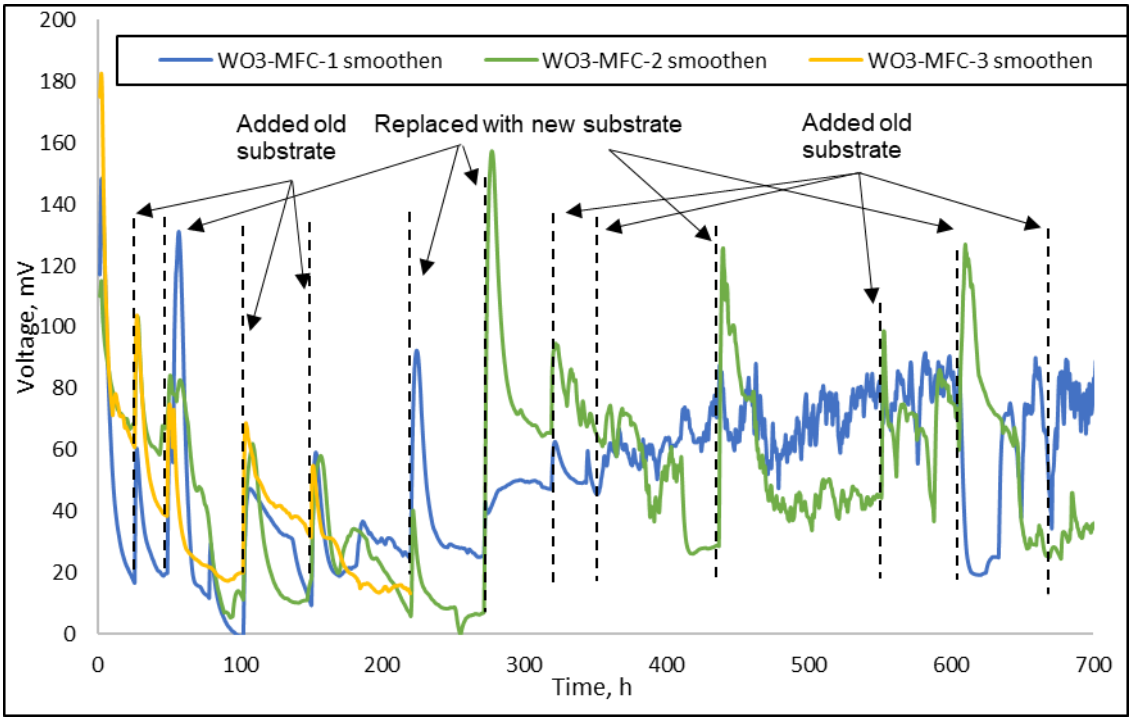


**Figure 3.6** Voltage of 3 mm wall thickness Oak WML-MFCs with open circuit condition from the start-up until 700 h.

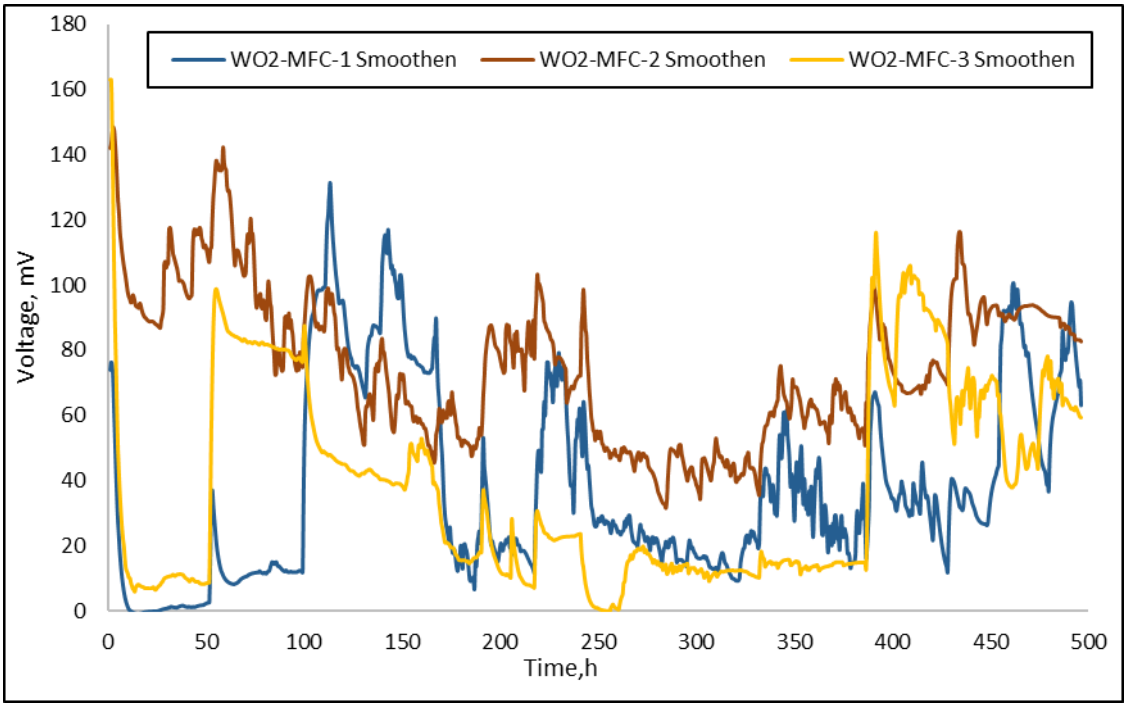


**Figure 3.7** Voltage of 2 mm wall thickness Oak WML-MFCs with open circuit condition from the start-up until 500 h.

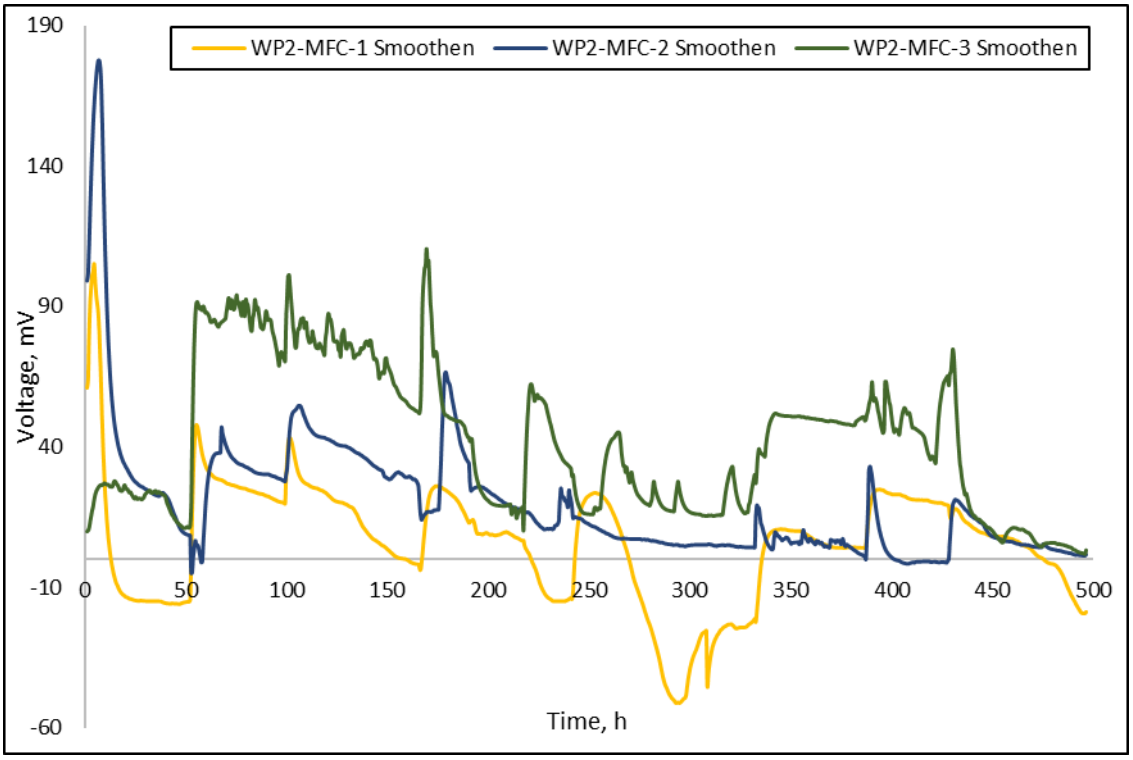


**Figure 3.8** Voltage of 2 mm wall thickness Scots pine WML-MFCs with open circuit condition from the start-up until 500 h.

### *3.3.2. External resistor selection*

The selection of the external resistor was crucial for optimizing the power output of the Wood-based Microbial Fuel Cells (WML-MFC). A range of resistors from 400 Ω to 1 MΩ were tested to determine the most suitable one for each cell type. The testing involved WP4-MFC-1, WO3-MFC-2, WP3-MFC-1, WO2-MFC-2, and WP2-MFC-3, using a breadboard setup. For each resistor, voltage was recorded after a 5-10 minute interval to assess its impact on power density. Consequently, the Maximum Power Density (MPD) for each cell type was achieved with specific resistances: 330 kΩ for WP4-MFC, 51 kΩ for WO3-MFC, 20 kΩ for WP3-MFC, 820 kΩ for WO2-MFC, and 81 kΩ for WP2-MFC, as illustrated in Figure 3.9. Subsequent measurements of power and current were conducted using these optimal resistances for the respective cell types, revealing that the 3 mm wall thickness WML-MFCs demonstrated superior performance in terms of MPD.

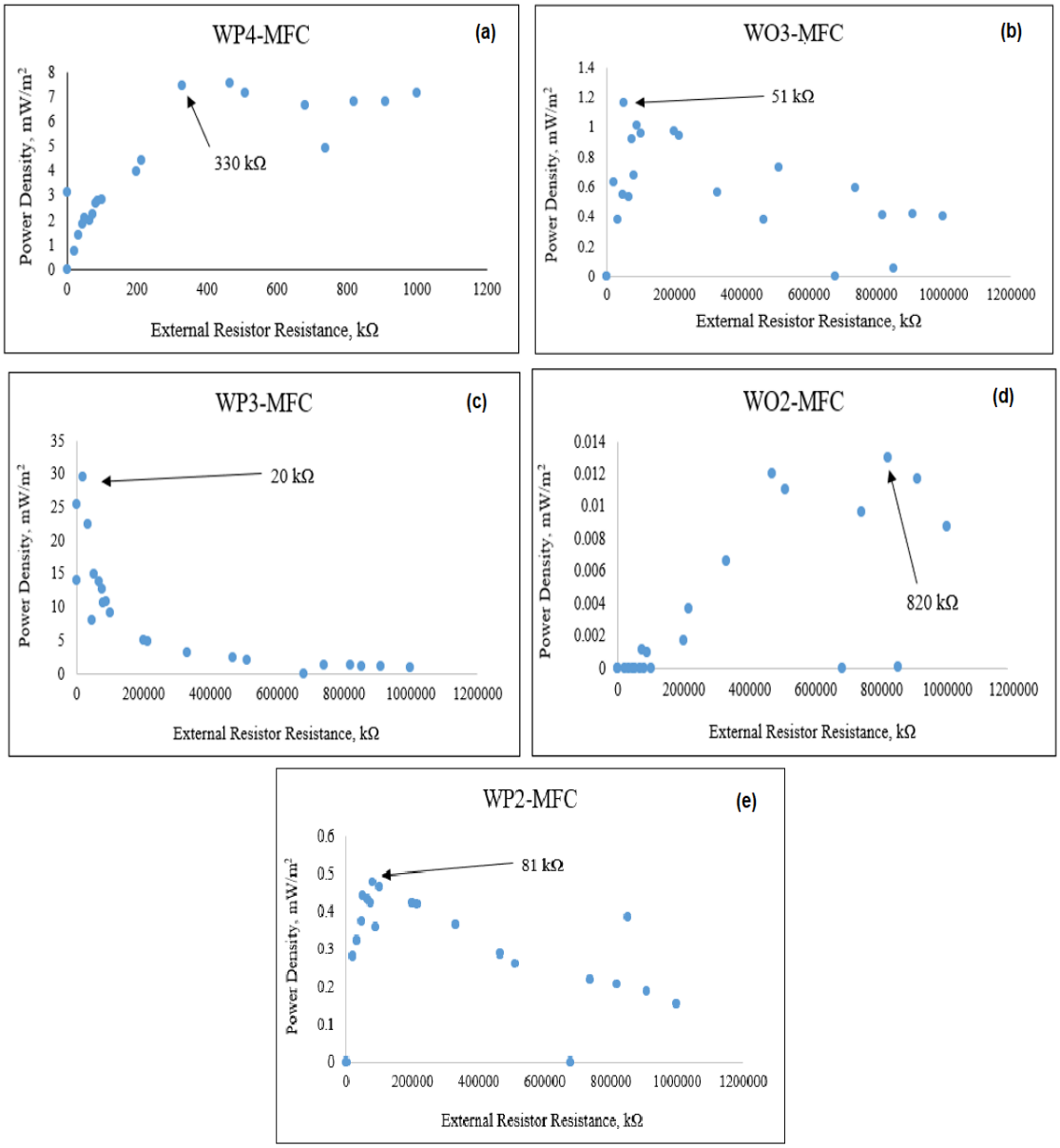


**Figure 3.9** Resistor selection assessment based on power density for; (a) WP4-MFC, (b) WO3-MFC, (c) WP3-MFC, (d) WO2-MFC, and (e) WP2-MFC.

### *3.3.3. Bioelectricity generation of WML-MFC as a closed circuit*

#### *3.3.3.1. The WML-MFC with 4 mm wall thickness*

Upon switching from Open Circuit (OC) to Closed Circuit (CC) with selected resistors (330 kΩ for 4 mm wall thickness), WP4-MFC-3 exhibited the highest Maximum Power Density (MPD) and Maximum Current Density (MCD) of 35 mW/m$^2$ and 0.09 mA/m$^2$, respectively, after 397 hours. Comparatively, WO4-MFC-2 reached an MPD of 4 mW/m$^2$ and an MCD of 0.03 mA/m$^2$ after 404 hours (refer to Figures 3.10 and 3.11). The CC phase spanned 420 hours, involving five cycles of substrate replacement, necessitated by water loss through moisture diffusion.

The observed bioelectricity production and water treatment efficacy were modest, aligning with findings from previous studies which indicated limitations under low conductivity and untreated electrode conditions (Khater et al., 2022; Liu et al., 2022; Wang et al., 2022). Studies using plain carbon felt as electrodes reported lower voltage and MPD compared to treated carbon (Harshiny et al., 2017; Vicari et al., 2016). In contrast, a ceramic separator MFC achieved a higher MPD of 3.2 $W/m^3$ even in low conductivity conditions (Santoro et al., 2018), suggesting the potential of wood as a feasible material for MFCs, warranting further optimization.

The experiment revealed significant current fluctuations due to varied substrates and Hydraulic Retention Times (HRTs). Initially, fresh influent was used in all containers, with WP4-MFC-2 showing an initial high PD of 24 $mW/m^2$, which then dropped to 2 $mW/m^2$ after 26 hours. Subsequent fillings with older substrates led to lower bioelectricity production. A notable cessation of current growth occurred when containers were fed with distilled water, indicating the washout of microorganisms from the anode. However, replenishing with freshly seeded substrate led to a gradual increase in CD, suggesting the re-establishment of biofilms on the anode.

The bioelectricity generation showed a marked increase in the final cycle, especially in WP4-MFC-3, which outperformed WP4-MFC-2 in the last two cycles. Oak containers, however, exhibited sluggish performance throughout. The experiment underscores the importance of inoculating the anode with a vibrant microbial culture and maintaining optimal HRTs for efficient bioelectricity generation. Ambient temperature fluctuations also impacted CD, as indicated by the rise in early morning (red arrow in Figure 3.11) and the decrease after sunset (purple arrow), emphasizing the sensitivity of WML-MFC performance to environmental conditions.

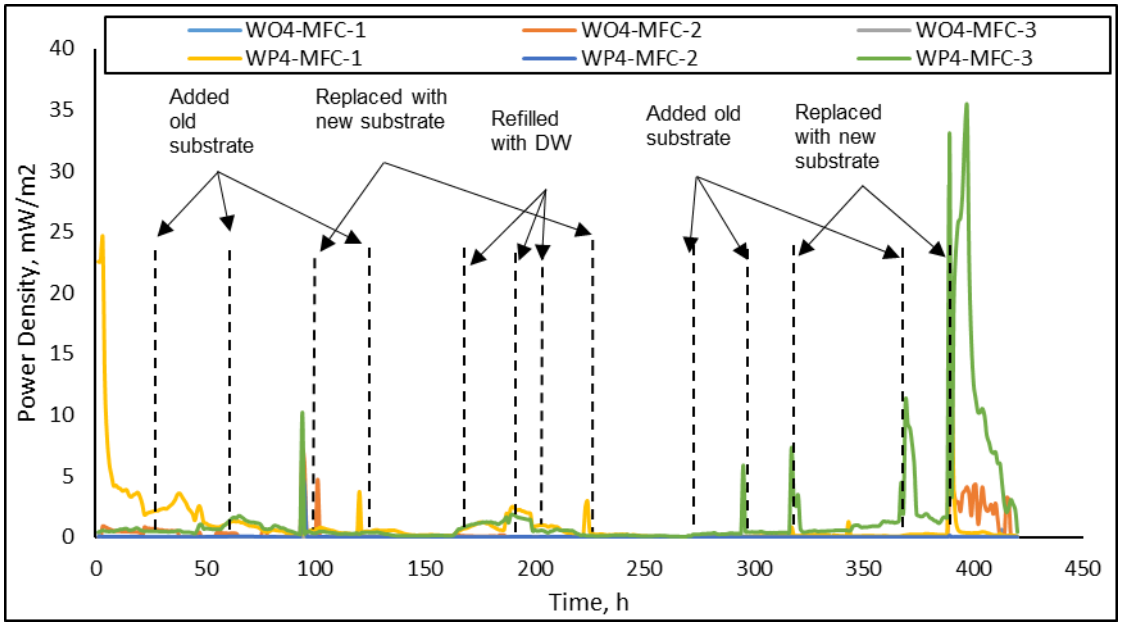


**Figure 3.10** Power density of 4 mm wall thickness oak and Scots pine containers according to the surface area of the anode.

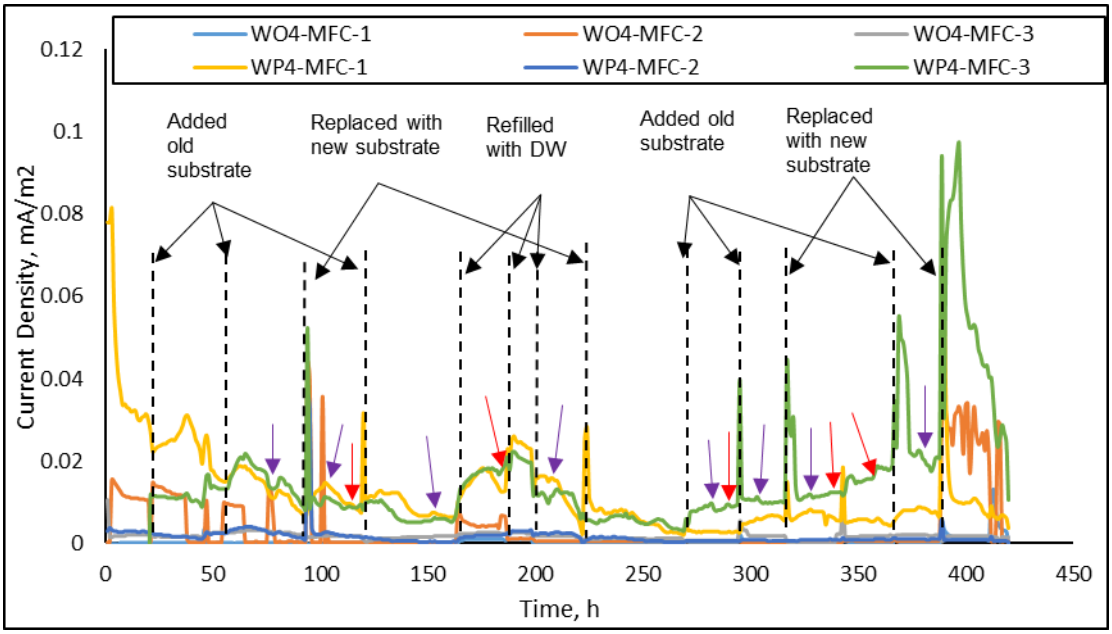


**Figure 3.11** Current density of 4 mm wall thickness oak and Scots pine containers according to the surface area of the anode.

#### *3.3.3.2. The WML-MFC with 2 mm and 3 mm thickness*

This section examines the performance of Wood-based Microbial Fuel Cells (WML-MFC) with reduced wall thicknesses of 2 mm and 3 mm under Closed Circuit (CC) conditions. The experiment spanned 1000 hours, with non-uniform Hydraulic Retention

Times (HRT) and daily refilling of containers to compensate for moisture diffusion-induced water loss. The resistors used were 820 kΩ for oak and 467 kΩ for Scots pine.

During this period, the highest Maximum Power Density (MPD) and Maximum Current Density (MCD) recorded for the 2 mm and 3 mm WML-MFCs were 5.14 $mW/m^2$ and 0.023 $mA/m^2$, and 4.7 $mW/m^2$ with 0.0029 $mA/m^2$, respectively (refer to Figures 3.12 to 3.17). Notably, the 3 mm Scots pine (WP3-MFC) outperformed the 3 mm oak (WO3-MFC) by approximately 500% in terms of current and power density. In contrast, the 2 mm oak (WO2-MFC) generated around 200% higher current and power density than the 2 mm Scots pine (WP2-MFC).

A unique observation was the occurrence of negative voltage in WP2-MFC, lasting over 300 hours (see Fig. 3.15). Additionally, the 2 mm WML-MFCs exhibited more significant voltage fluctuations with sharp peaks and rapid drops compared to the 3 mm models. These peaks and valleys were even more pronounced than in the 4 mm WML-MFCs, suggesting a correlation with wall thickness and material density.

The observed behavior indicates that lower-density container walls, such as those made from Scots pine, lead to increased oxygen intrusion, resulting in the Oxygen Reduction Reaction (ORR) occurring within the anode chamber. This phenomenon, coupled with enhanced hydrogen escape and greater water loss, underscores the challenges in using thinner-walled containers. Consequently, for containers with wall thicknesses less than 3 mm, it is advisable to use denser wood species or incorporate a Proton Exchange Membrane (PEM) into the system to mitigate these issues.

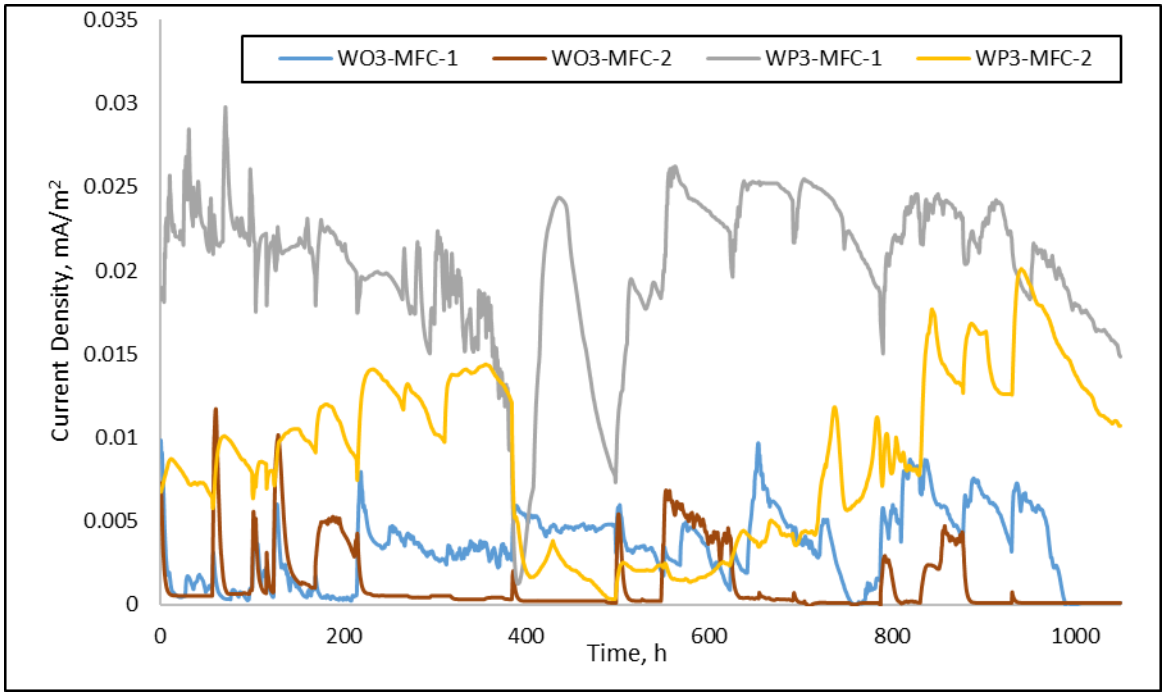


**Figure 3.12** Current density of 3 mm wall thickness oak and Scots pine containers according to the surface area of the anode.

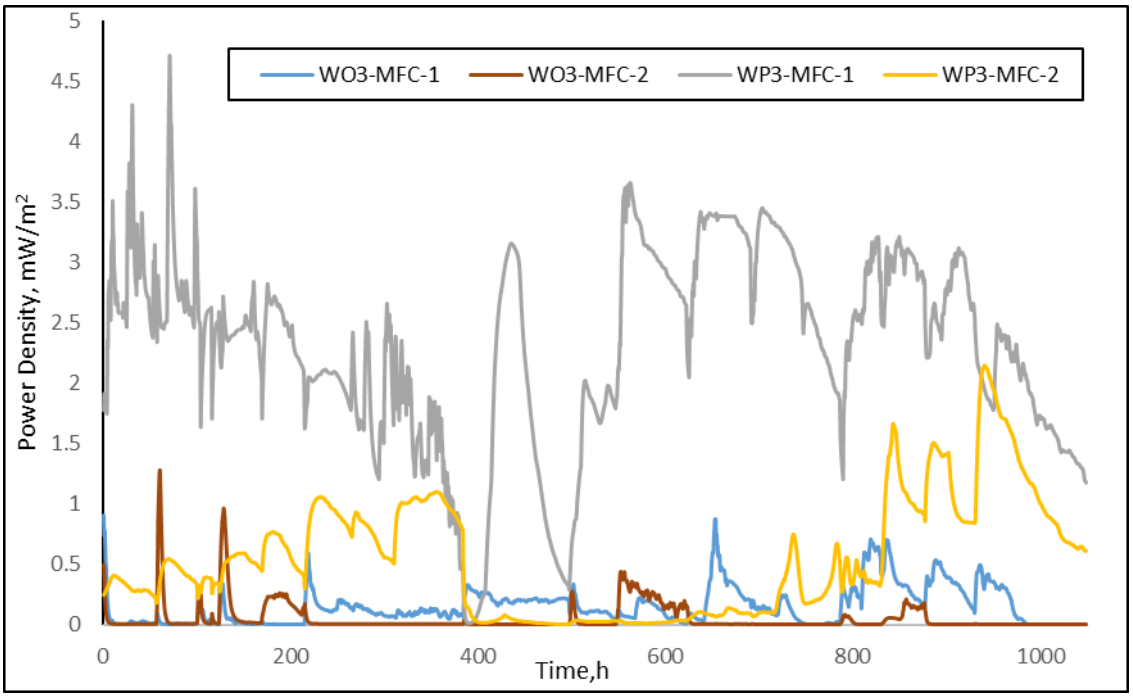


**Figure 3.13** Power density of 3 mm wall thickness oak containers according to the surface area of the anode.

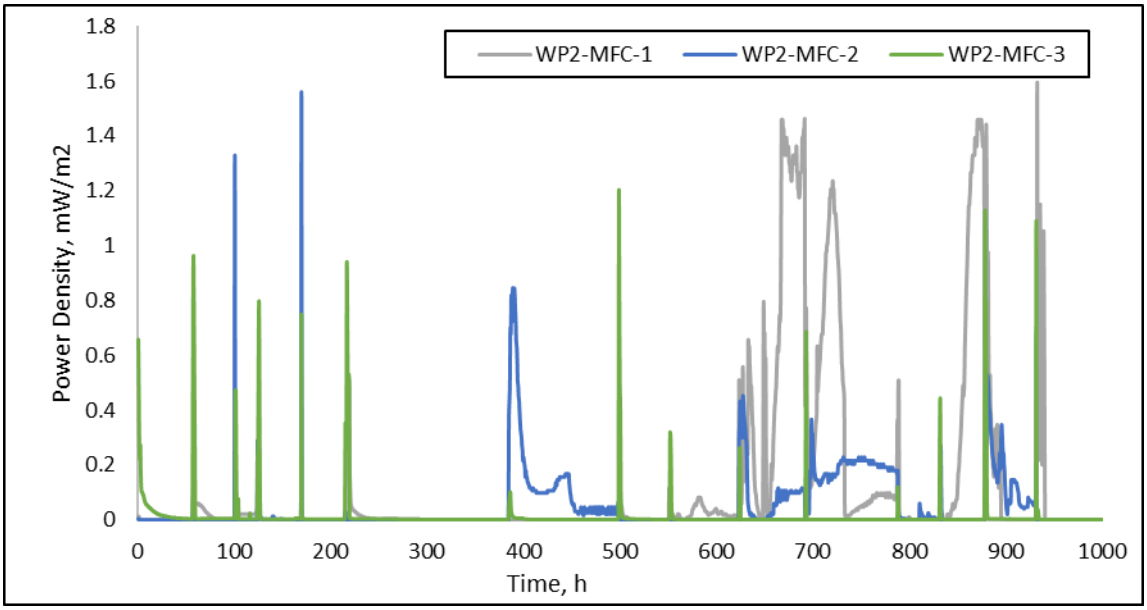


**Figure 3.14** Power density of 2 mm wall thickness Scots pine containers according to the surface area of the anode.

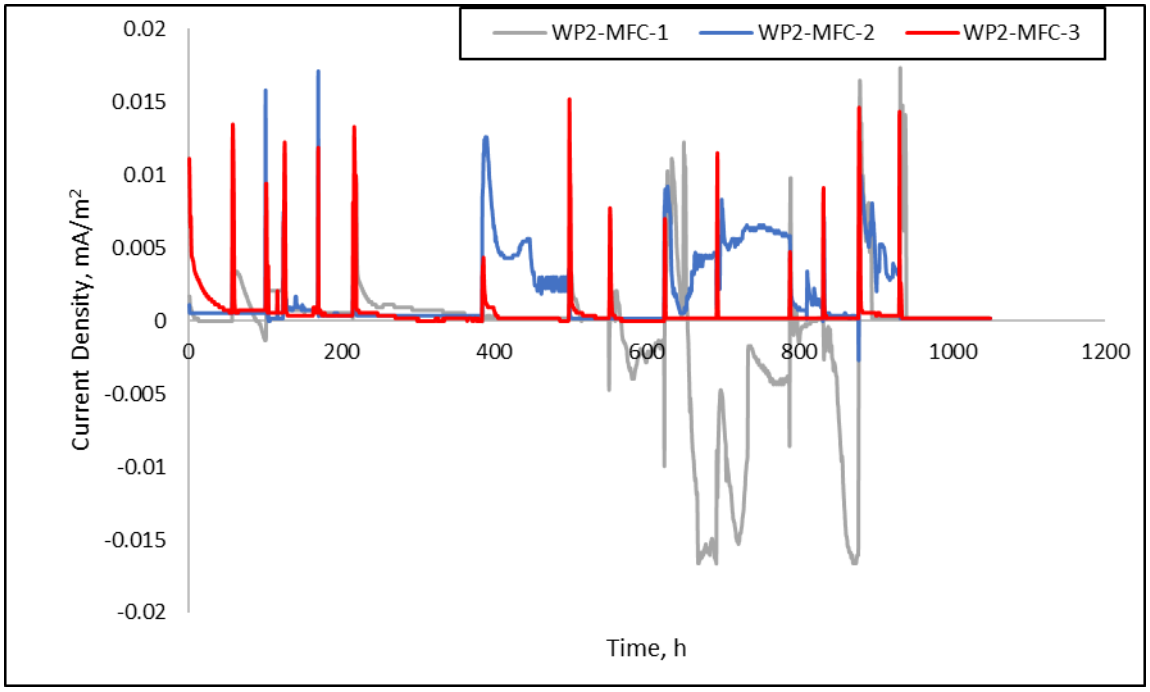


**Figure 3.15** Current density of 2 mm wall thickness Scots pine containers according to the surface area of the anode.

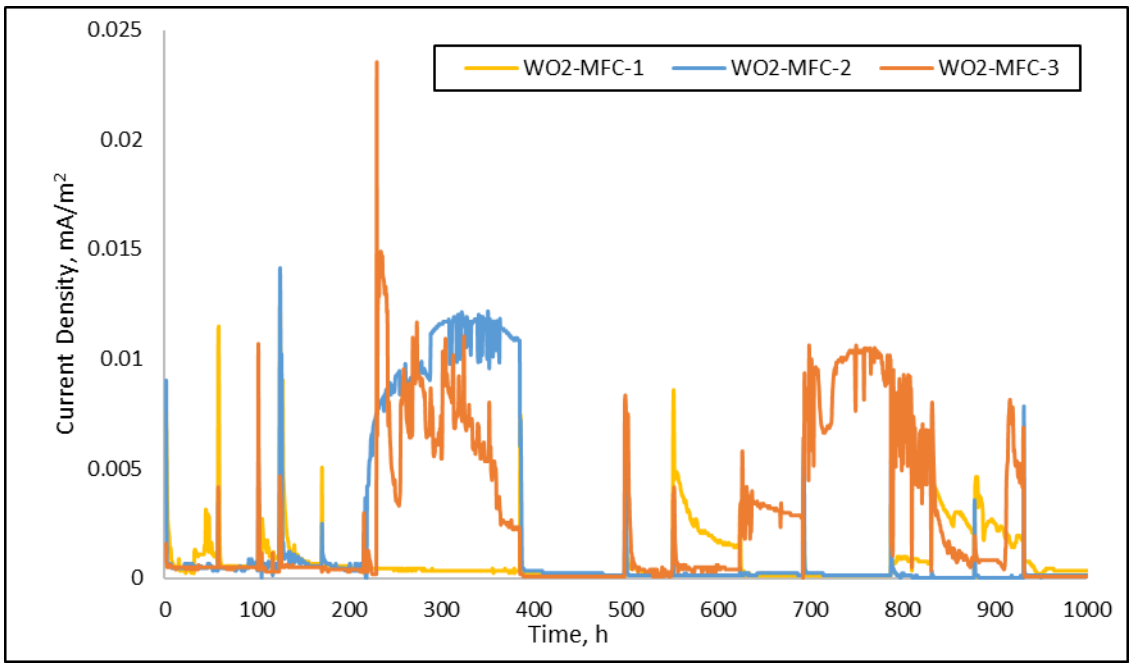


**Figure 3.16** Current density of 2 mm wall thickness oak containers according to the surface area of the anode.

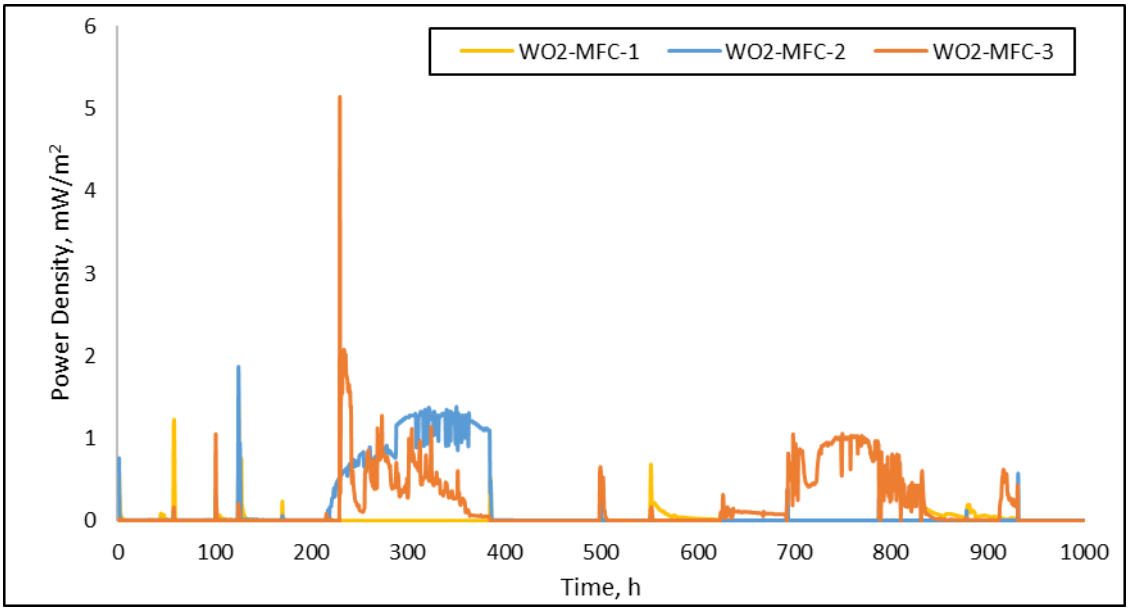


**Figure 3.17** Power density of 2 mm wall thickness oak containers according to the surface area of the anode.

These findings provide valuable insights into the impact of wall thickness and wood density on the performance of WML-MFCs. They highlight the need for careful

selection of materials and structural design to optimize bioelectricity generation and overall system efficiency.

### *3.3.4. Effluent condition and wastewater treatment performance of WML-MFC*

In this study, we assessed the wastewater treatment efficacy of Wood-based Microbial Fuel Cells (WML-MFC) by monitoring pH, conductivity, and Chemical Oxygen Demand (COD) of influent and effluent across different incubation periods in batch mode. Measurements were taken at various intervals after introducing new substrate and following each subsequent replacement.

**Conductivity and pH Changes:**

We observed a consistent increase in effluent conductivity across all container types. In the 4 mm wall thickness Scots pine containers, effluent conductivity nearly doubled that of the influent, while oak containers recorded increases between 27-100%. This rise can be attributed to influent concentration due to water loss through moisture diffusion and the release of wood extractives into the water. Similar trends were noted in 3 mm and 2 mm wall thickness containers, although the rise in conductivity was less pronounced.

Regarding pH, a divergence was noted based on the container wall thickness and wood type. In 4 mm oak and Scots pine containers, the pH tended to decrease. However, in 3 mm and 2 mm containers, we recorded an increase in pH from around 4 to approximately $5 \pm 0.8$. This suggests the wood walls' substantial impact on normalizing the pH of the influent around $5 \pm 0.4$, depending on its initial value.

**COD Reduction Efficiency:**

Focusing on 4 mm wall thickness WML-MFCs, which showed the best electrical performance, COD reduction was analyzed at different HRTs. In Scots pine containers, the COD reduction in effluent was 18% after 24 hours, increasing to 40% after 48 hours and reaching 48% in the 48-72 hour window. Conversely, oak containers demonstrated a slower COD reduction rate, with a 3% decrease after 24 hours, 22% after 48 hours, and 39% after 72 hours. These results indicate that Scots pine containers are more effective in water treatment within the first 48 hours.

However, after three days, the rate of water treatment slowed in all 4 mm containers. Contributing factors include the average daily water loss (Scots pine: 4.8

ml/day, Oak: 1.3 ml/day), leading to inactive anode regions due to air exposure, and galvanic corrosion of copper electrodes, which inhibits microbial growth. A continuous-fed WML-MFC system could mitigate these issues by reducing oxygen intrusion, preventing copper oxide accumulation, and maintaining continuous substrate contact with the anode.

In thinner wall containers (2 mm and 3 mm), there was an unexpected increase in COD of the effluent. This contrast with the 4 mm containers suggests that wall thickness is a critical factor in WML-MFC design, especially for water loss management and treatment efficiency, with Scots pine showing particular promise.

This comprehensive analysis underscores the importance of wall thickness and wood type in designing WML-MFCs for effective wastewater treatment. The findings highlight the need for strategic system design, including continuous feeding mechanisms, to address challenges like water loss and electrode exposure, which significantly impact treatment efficiency.

**Table 3.1** Influent and effluent conditions under different HRTs of one day to four days with 4 mm wall thickness WML-MFCs.

| The incubation period (or HRT), day | containers | Influent COD, mg/l | Effluent COD, mg/l | Influent pH | Effluent pH | Influent conductivity, μS/cm | Effluent conductivity, μS/cm |
|---|---|---|---|---|---|---|---|
| | WO4-MFC | | 4091 | 6.3 | 4.99 | 372 | 706 |
| 1 | WP4-MFC | 4240 | 3475 | 6.4 | 5.41 | 654 | 1202 |
| | WO4-MFC | | 3812 | 4.87 | 4.6 | 680 | 866 |
| 2 | WP4-MFC | 4941 | 2929 | 4.93 | 4.01 | 890 | 1306 |
| | WO4-MFC | | 400 | 6.73 | 5.75 | 429 | 809 |
| 3 | WP4-MFC | 664 | 340 | 6.88 | 5.92 | 688 | 1012 |

| | | | | | | | |
|---|---|---|---|---|---|---|---|
| | WO4-MFC | --- | --- | 5.43 | 5.2 | 460 | 662 |
| 4 | WP4-MFC | --- | --- | 6.36 | 5.38 | 538 | 1080 |

**Table 3.2** Influent and effluent conditions under different HRTs of one day to four days different with 3 mm wall thickness WML-MFCs.

| The incubation period (or HRT), day | containers | Influent pH | Effluent pH | Influent conductivity, μS/cm | Effluent conductivity, μS/cm |
|---|---|---|---|---|---|
| | WO3-MFC | 4.67 | 5.16 | 790 | 2370 |
| 1 | WP3-MFC | 4.67 | 5.16 | 790 | 2270 |
| | WO3-MFC | 4.67 | 5.05 | 790 | 2240 |
| 2 | WP3-MFC | 4.67 | 5.04 | 790 | 2330 |
| | WO3-MFC | 4.81 | 5.45 | 1090 | 1790 |
| 3 | WP3-MFC | 4.81 | 5.52 | 1090 | 1880 |
| | WO3-MFC | 4.67 | 5.2 | 790 | 2170 |
| 4 | WP3-MFC | 4.67 | 5.07 | 790 | 2370 |

**Table 3.3** Influent and effluent conditions under different HRTs from one day to four days with 2 mm wall thickness WML-MFCs.

| The incubation period (or HRT), day | containers | Influent pH | Effluent pH | Influent conductivity, μS/cm | Effluent conductivity, μS/cm |
|---|---|---|---|---|---|

| | | | | | |
|---|---|---|---|---|---|
| | WO2-MFC | 4.67 | 5.13 | 790 | 2360 |
| 1 | WP2-MFC | 4.67 | 5.24 | 790 | 3230 |
| | WO2-MFC | 4.67 | 5.04 | 790 | 2190 |
| 2 | WP2-MFC | 4.67 | 5.31 | 790 | 3030 |
| | WO2-MFC | 4.81 | 5.4 | 1090 | 1850 |
| 3 | WP2-MFC | 4.81 | 5.51 | 1090 | 1770 |
| | WO2-MFC | 4.67 | 5.2 | 790 | 2260 |
| 4 | WP2-MFC | 4.67 | 5.35 | 790 | 2750 |

### *3.3.5. Effect of HRT on the bioelectricity production*

HRT influence was assessed under four different HRTs (1, 2, 3, and 4 days). WP4-MFC-1 displayed the highest OCV of 0.551 V with HRT of 2 days with a high COD substrate, while WP4-MFC-3 showed the highest bioelectricity production with MPD and MCD of 35 $mW/m^2$ and 0.09 $mA/m^2$, respectively, with HRT of 2 days. The voltage increased with longer HRTs probably due to the longer contact time between biofilm and organic matter; under a stable condition of the substrate with no movement in the anolyte helps the bacteria to grow and create a denser network of biofilm (Li et al., 2013). In contrast, the quick and dramatic drop in voltage observed with WP2-MFCs and WO2-MFCs necessitates an HRT of less than a day, or better yet, a continuous-feeding system.

Over the course of three days, HRT was tested using distilled water to determine the relationship between the water level in the anode chamber and electrical production (to exclude the organic loading rate (OLR) impact). A one-day HRT was shown to increase the bioelectrical productivity of 4 mm wall thickness Scots pine WML-MFCs by 50% (Fig. 3.10, 3.11). This may be attributable to a combination of factors, but it is mostly focused on the level of the water as de-ionized water is used, firstly, keeping the containers full of anolyte helps the anode to stay fully immersed under the substrate for a longer period; water-loss in 4 mm wall thickness Scots pine and oak containers was around 40% and 10%, respectively, within 48 h (as indicated in Table 3.4). A larger percentage of water loss was seen in some containers of WO3-MFCs, WP3-MFCs, WO2-MFCs, and WP2-MFCs, respectively (Tables 3.5, 3.6). Also, having an anolyte in the container helps the wooden

walls of the containers become saturated with water, which restrains oxygen from intruding through the wood plate (Sorz and Hietz, 2006). Thirdly, Galvanic corrosion of copper within the anolyte inhibited microbial development due to the toxicity of copper oxide toward living cells, continuous influent (or de-ionized water) adding helps to dilute the copper dioxide (Kumar et al., 2021; Naz et al., 2020; Trevors and Cotter, 1990).

The bioelectricity and water treatment of WML-MFC were less effective when the HRT was more than two days due to the low water level in each container and escalating the galvanic corrosion of copper wire. However, from other research, other prototypes of MFCs demonstrated higher bioelectric outcomes and better water treatment performance with four days of HRT and more (Li et al., 2013; Sharma and Li, 2010). Because of the significant impact of the container wall thickness on the water loss ratio; a higher container wall thickness leads to less water loss. Eventually, this directly impacts bioelectric output and water treatment capability. This work was conducted briefly; further research would be necessary to understand HRT's effect on WML-MFC better and solve the challenges.

**Table 3.4** Water loss in batch-mode fed for 4 mm wall thickness WML-MFC containers.

| The incubation period (HRT), day | Water loss due to moisture diffusion through the wooden wall, ml | | | | | |
|---|---|---|---|---|---|---|
| | WP4-MFC-1 | WP4-MFC-2 | WP4-MFC-3 | WO4-MFC-1 | WO4-MFC-2 | WO4-MFC-3 |
| 1 | 4.9 | 4.3 | 5 | 1.5 | 1 | 1.2 |
| 2 | 10.7 | 9.8 | 8.8 | 3.3 | 4.3 | 4 |
| 3 | 15 | 14.4 | 12.9 | 5.9 | 5.8 | 5.6 |

**Table 3.5** Water loss in batch-mode fed for 3 mm wall thickness WML-MFC containers.

| The incubation period | Water loss due to moisture diffusion through the wooden wall, ml | | | | | |
|---|---|---|---|---|---|---|
| | WP3-MFC-1 | WP3-MFC-2 | WP3-MFC-3 | WO3-MFC-1 | WO3-MFC-2 | WO3-MFC-3 |

| (HRT), day | | | | | | |
|---|---|---|---|---|---|---|
| 1 | 3 | 3 | 4.5 | 2.2 | 2.1 | 4.5 |
| 2 | 9.2 | 9 | 7 | 4.5 | 3.2 | 6.8 |
| 3 | 13.6 | 16.2 | 13.2 | 6 | 4.6 | 8 |

**Table 3.6** Water loss in batch-mode fed for 2 mm wall thickness WML-MFC containers.

| The incubation period (HRT), day | Water loss due to moisture diffusion through the wooden wall, ml | | | | | |
|---|---|---|---|---|---|---|
| | WP2-MFC-1 | WP2-MFC-2 | WP2-MFC-3 | WO2-MFC-1 | WO2-MFC-2 | WO2-MFC-3 |
| 1 | 6 | 7 | 4 | 2 | 1.5 | 2 |
| 2 | 7 | 10 | 9 | 4.2 | 3 | 4.1 |
| 3 | 14.5 | 16.8 | 17.1 | 8.9 | 7 | 9.5 |

### *3.3.6. Effect of sugar quantity and culture density*

The anode chamber of the 4 mm wall thickness WML-MFCs was refilled with new substrate once they began operating with OC. Measurements typically involved five effluent replacement cycles and nine replenishment cycles. In each effluent replacement or refilling cycle, the anode chamber is filled with either newly seeded sludge substrate or substrate from prior days or distilled water. When the effluent was changed out for newly planted influent, the current and power rose due to the high sugar content and dense mixed culture. Substrates with less sugar produced lower current density and output power density than those produced by substrates with higher sugar contents (Fig. 3.11, 3.12). The CD curved short and dropped quickly after the containers were replenished with distilled water between 164 and 222 h because the culture density inside the anode was decreasing.

### *3.3.7. Cathode condition during the experiment*

A primary goal of this research was to assess the durability of the cathode electrode against microbial attack. After three months of operation, visual inspections showed no biofilm or microbial degradation on the cathodes of WML-MFCs (see Figures 3.18, 3.19). SEM analysis further confirmed these findings. Both control (unused) and used cathodes from oak and Scots pine WML-MFCs displayed similar clean, smooth carbon fiber surfaces. Some debris and wetness-induced remnants were noted, but no significant microbial damage. These results indicate that using wood as a separator and container in WML-MFCs could offer a cost-effective solution for maintaining cathode integrity while producing bioelectricity.

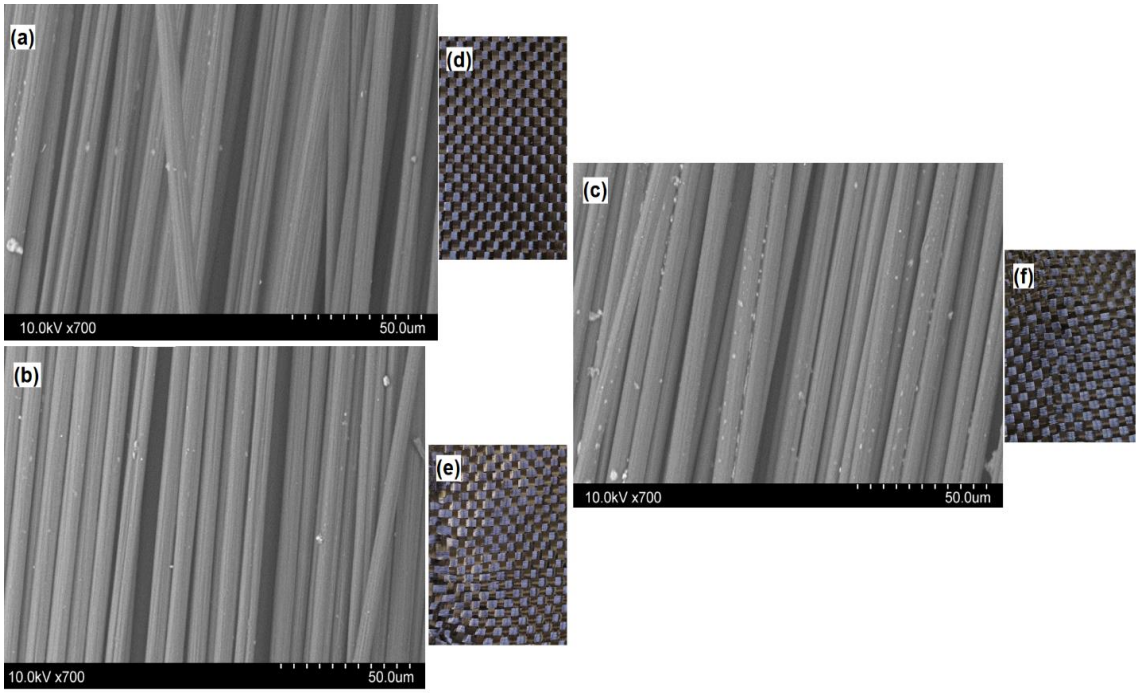


**Figure 3.18** SEM images of 4 mm wall thickness WML-MFC carbon cloths of the cathode electrode, (a) Control sample, (b) WO4-MFC, and (c) WP4-MFC. Digital photographs of the cathode electrode, (d) Control sample, (e) WO4-MFC, and (f) WP4-MFC.

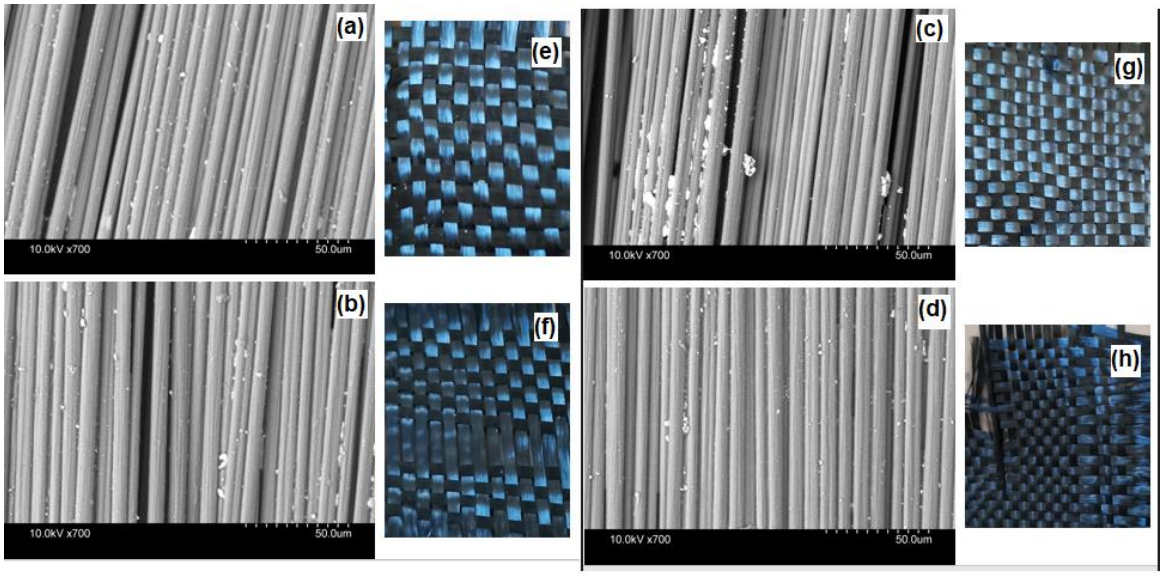


**Figure 3.19** SEM images of carbon cloths of the cathode electrode from, (a) WO2-MFC, (b) WP2-MFC, (c) WO3-MFC, and (d) WP3-MFC. Digital photographs of the cathode electrode from (e) WO2-MFC, (f) WP2-MFC, (g) WO3-MFC, and (h) WP3-MFC.

### *3.3.8. Mechanical properties and morphological structure of wood plates*

After three months of operation, the mechanical properties and morphological changes of the wooden walls in WML-MFCs were examined using Dynamic Mechanical Analysis (DMA) and Scanning Electron Microscopy (SEM). DMA revealed a significant mechanical loss in oak, while Scots pine exhibited only minor changes (Fig. 3.20). This difference may be attributed to variations in moisture diffusion and its effects on the mechanical properties of the wood. Chemical reactions occurring within the wood during moisture absorption and desorption also contribute to these changes.

SEM analysis showed that used oak samples developed surface cracks, whereas Scots pine maintained a smooth surface (Fig. 3.21, 3.22). These cracks could significantly affect the durability and strength of the wood, particularly in thinner walls. Furthermore, both oak and Scots pine showed debris accumulation on their surfaces, with oak absorbing more color from the wastewater, indicating the presence of copper oxide from the anode connection (Table 3.7). These findings suggest that Scots pine is more durable against microbial attack and the impacts of moisture diffusion. However, further long-term studies are needed to fully understand the effects on wood species durability.

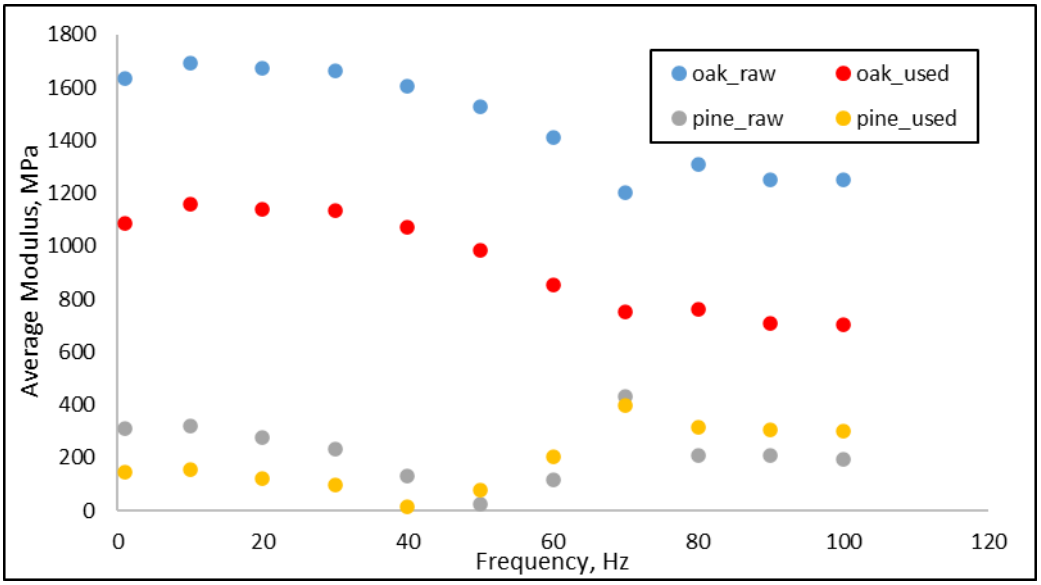


**Figure 3.20** Average elastic modulus versus frequency for 4 mm wall thickness oak and Scots pine at constant temperature (25 ℃) and humidity (14% RH). Blue dots are raw-oak before use in the samples. The red dots are oak after three months of continuous use. Grey dots are raw-Scots pine before use in the samples. Yellow dots are Scots pine after 3 months of continuous use.

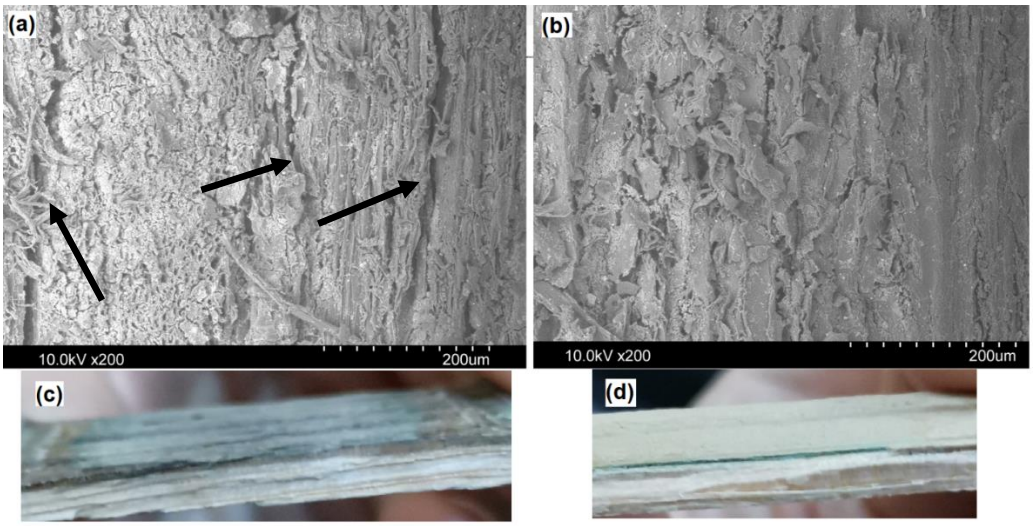


**Figure 3.21** SEM micrographs of the inner surface of 4 mm wall thickness WML-MFC after three months of use from (a) oak (b) Scots pine. Digital photographs from the container wall show the inner surface cross-section and the side view of (c) oak (d) Scots pine.

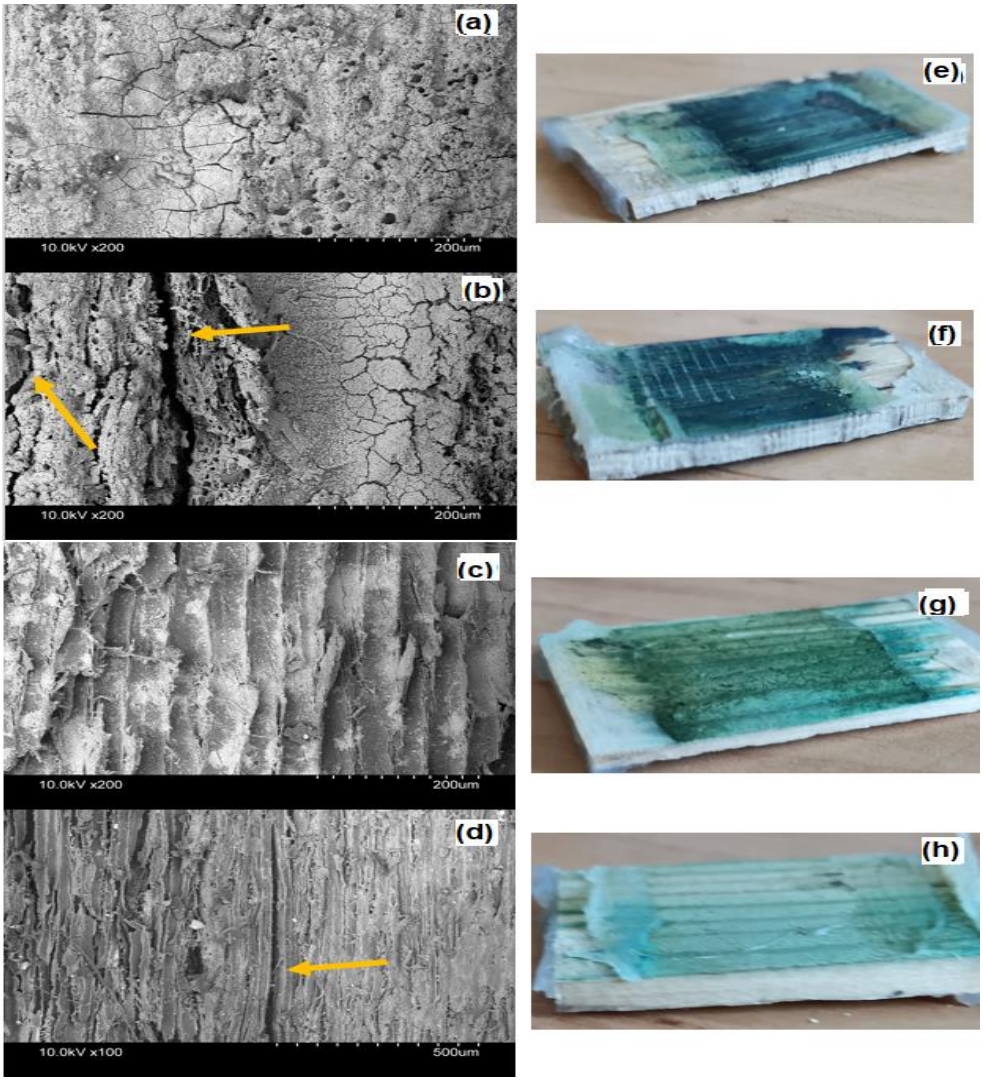


**Figure 3.22** SEM micrographs of the inner surface of WML-MFC after two months of use from (a) WO2-MFC, (b) WO3-MFC, (c) WP2-MFC and (d) WP3-MFC. Digital photographs from the container wall show the inner surface cross-section and the side view of (e) WO2-MFC (f) WO3-MFC, (g) WP2-MFC, and (h) WP3-MFC.

### *3.3.9. The EDX analysis of WML-MFCs*

Energy-Dispersive X-ray (EDX) analysis was conducted to investigate the elemental composition of the inner surfaces of WML-MFC containers made from oak and Scots pine. This analysis is crucial for understanding how these materials interact with the contents of the WML-MFC, particularly in terms of metal absorption from wastewater.

#### 3.3.9.1. Elemental Composition:

Both oak and Scots pine naturally contain Carbon (C) and Oxygen (O) in varying percentages, as highlighted in Figure 3.23 and detailed in Table 3.7. For instance, the 2

mm oak container showed 37.51% O and 27.83% C. Notably, 23.04% Copper (Cu) was detected, presumably absorbed from wastewater after the anode copper wire underwent galvanic corrosion. Traces of Fluorine, Aluminum, and Iron were also found, albeit in smaller quantities. Similar patterns were observed in oak containers of 3 mm and 4 mm wall thickness.

#### 3.3.9.2. Nitrogen Presence and Copper Absorption:

A unique finding was the presence of Nitrogen (2.47% and 3.80%) in the 4 mm wall thickness containers of oak and Scots pine, respectively, which was absent in thinner containers. This might be attributable to the higher percentage of domestic wastewater used in these containers.

Copper absorption varied across different containers and wood types. Oak with 3 mm wall thickness exhibited higher Cu absorption than its 2 mm counterpart. However, the 4 mm oak container showed the least Cu absorption compared to the 2 mm and 3 mm variants. In contrast, Scots pine absorbed less Cu than oak, by 21 – 39% compare to Oak containers. The highest Cu absorption in Scots pine was observed in the 3 mm container (18.41%).

#### 3.3.9.3. Other Chemical Elements:

Besides C and O, with Scots pine containers elements like Fluorine, Iron, Aluminium, Nitrogen, Mercury, and others wewre observed. The distinct elemental compositions of these containers indicate different interactions with the wastewater constituents.

There are no known studies to date that directly compare with these findings regarding the absorption of heavy metals from wastewater by oak and Scots pine of various wall thicknesses. However, these results underscore an additional advantage of WML-MFCs: the ability of wooden walls to absorb metals, including heavy metals, from wastewater. This absorption process may not only aid in wastewater treatment but also potentially inhibit the growth of fungal and bacterial colonies on the wooden walls, thereby enhancing the longevity and durability of these containers.

**Table 3.7** EDX of oak and Scots pine containers.

| Elements | WO2-MFC (wt.%) | WO3-MFC (wt.%) | WO4-MFC (wt.%) | WP2-MFC (wt.%) | WP3-MFC (wt.%) | WP4-MFC (wt.%) |
|---|---|---|---|---|---|---|
| Oxygen | 37.51 | 32.39 | 40.46 | 40.37 | 37.59 | 36.17 |
| Carbon | 27.83 | 21.64 | 39.72 | 37.38 | 37.09 | 33.89 |
| Copper | 23.04 | 23.57 | 13.14 | 14.90 | 18.41 | 12.42 |
| Fluorine | 0.36 | – | – | 0.23 | 0.03 | – |
| Iron | 6.93 | 8.67 | 4.61 | 2.08 | 1.50 | 3.56 |
| Aluminum | 0.24 | 0.07 | 0.08 | 0.20 | 0.58 | 1.22 |
| Nitrogen | – | 0.04 | 2.47 | – | – | 3.80 |
| Mercury | – | – | – | 0.06 | 0.30 | – |
| Others | 4.08 | 13.65 | 1.52 | 4.78 | 4.50 | 8.94 |

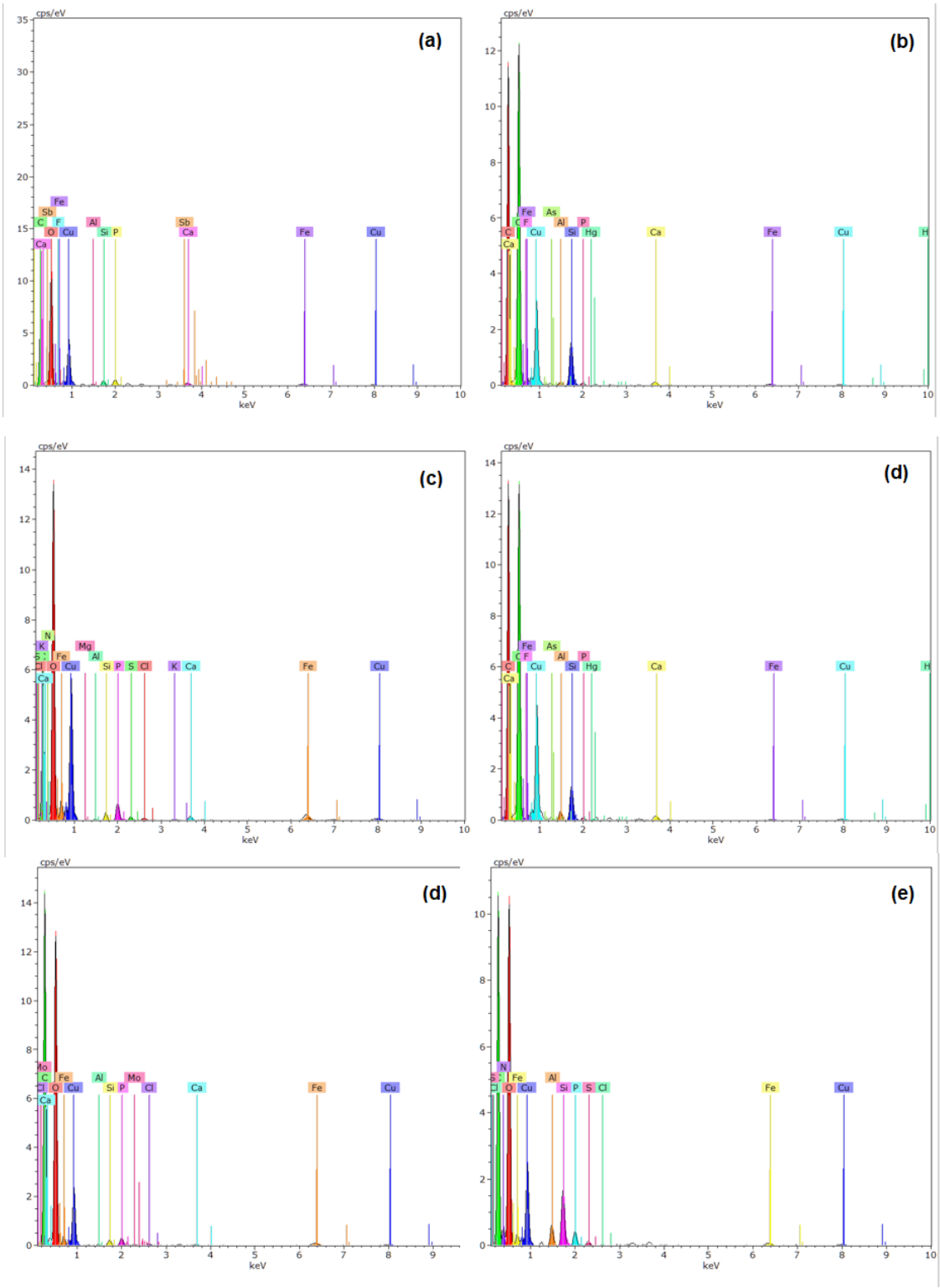


**Figure 3.23** EDX spectra of WML-MFCs after 3 months of use; (a) WO2-MFC, (b) WP2-MFC, (c) WO3-MFC, (d) WP3-MFC, (e) WO4-MFC, (f) WP4-MFC.

# CHAPTER IV

# CONCLUSIONS & FURTHER STUDY

# 4. CONCLUSIONS

## 4.1. Chapter Synopsis

This chapter proposes the main conclusions from the present research work, followed by the directions for further research. The findings were derived from studying wooden microbial fuel containers, using three different species as container and separator, and constructing the containers with different wall thicknesses. The underlying basis of the research is to develop and optimize the ML-MFC by protecting the cathode from deterioration and biofilm formation with a low-cost, sustainable, and eco-friendly solution.

## 4.2. Research conclusions and achievements

The present work has attempted to address the issue of cathode deterioration and biofilm formation in ML-MFCs by simultaneously using wood as a separator and container. Untreated wooden containers, carbon felt, and carbon cloth was chosen to check the capability and viability of this novel work. It is noteworthy that no chemical pretreatment was done to adjust the experimental parameters like conductivity, and pH. The WML-MFC container turned out to be a very promising biomaterial for the fabrication of ML-MFCs. For further understanding and development of WML-MFC, the effect of different wall thicknesses was tested depending on the bioelectric and water treatment capability. Comparing the wall thickness of 4 mm, 3 mm, and 2 mm, it was found that the electric production and water treatment capability were the greatest with the 4 mm wall thickness.

The study effort has been condensed into the following bullet points, which outline the accomplishments and implications.

1. The WML-MFC prototype showed the potential to provide full safety of the cathode from any biofouling, thus preventing cathode deterioration (**CT-CP4**) **(CT-PA)**.
2. The cost of building ML-MFC and its maintenance decrease enormously, saving the cathode from deterioration builds hope for commercializing ML-MFCs in the future. Further, a wooden membrane-less microbial fuel cell system is a cost-effective, and environment-friendly approach (**CT-BC2)**.
3. With Scots pine 4 mm containers, the highest COD reduced percentage was 48%, whereas, in the oak containers, it was 39% within a hydraulic retention time of 48 h. For this experiment, three wood species with 4 mm wall thickness were assessed (black locust, oak, and Scots pine). Black locust resulted in the lowest bioelectricity compared to the other species with the lowest stability on the pick of its highest OCV. The MPD (anode-based)

and OCV could reach 35 mW/m$^2$, 551 mV, and 4 mW/m$^2$, 269 mV (with 330 kΩ resistor) for Scots pine and oak, respectively. For black locust, the maximum OCV reached 51 mV, which could be sustained for 2 h maximum (**CT-JP1-submitted)**.

4. Water loss occurs due to moisture diffusion in wood. The amount of water loss is a function of the wall thickness as well as the wood species. The water loss is more at less wall thickness of WML-MFCs. This can be an issue, therefore it is important to feed the substrate to the system with continuous-feeding instead of patch-feeding **(CT-JP1-submitted) (CT-CP4).**

5. Wood, being an insulation material, can protect microbial activity against low ambient temperatures during winter; since low temperatures drastically affect the vitality of the microbial culture. Thus, WML-MFC can help in maintaining the performance efficiency even in cold weather (**CT-BC2)**.

6. The bioelectricity and water treatment of WML-MFC were most effective at HRT of 2 days with 4 mm wall thickness **(CT-JP1-submitted)**.

7. With 2 mm and 3 mm wall thickness still possible to have a successful WML-MFC which could be used for different purposes. The highest MPD and MCD, obtained with 2 mm and 3 mm wall thickness of WML-MFCs, were 5.14 mW/m$^2$ at 0.023 mA/m$^2$, and 4.7 mW/m$^2$ at 0.0029 mA/m$^2$, respectively during 1000 h of experimentation. Although these parameters (MPD and MCD) are less than those obtained for containers of 4 mm wall thickness, they manifest the viability of the idea **(CT-PA).**

8. For effective water treatment, 4 mm is the minimum wall thickness required to fabricate WML-MFC **(CT-PA)**.

9. The highest electric production is possible with 3 mm wall thickness of WML-MFC in case of utilizing the right resistor. The 3 mm wall thickness of WML-MFC yielded the maximum power density (without the water treatment) **(CT-PA) (CT-JP1-submitted)**.

10. Containers with a wall thickness of less than 3 mm must be fabricated from a dense wood species, or PEM must be included in the system. Compared to MWL-MFCs with a wall thickness of 3 mm Scots pine MWL-MFCs with a wall thickness of 2 mm exhibited negative voltage for more than 300 h, as well as highly sharp peaks and rapid decreases in voltage. In addition, the peaks and valleys of 3 mm MWL-MFCs were sharper than those of 4 mm MWL-MFCs **(CT-PA) (CT-JP1-submitted)**.

11. The wooden walls of the containers have a massive impact on the pH and normalise the pH of the influent around 5 ± 0.4; if the utilized influent's pH is less than 5,

it will rise to 5 ± 0.4; if the influent's pH is greater than 5, it will fall to 5 ± 0.4 **(CT-PA) (CT-JP1-submitted)**.

12. Wooden walls of WML-MFCs absorb metals and heavy metals from the effluent. This aids the water treatment process and improves the water's quality, and it also protects the wooden wall from rust and decay and provide a longer life for the WML-MFC containers **(CT-PA) (CT-CP4) (CT-JP1-submitted)**.

### 4.3. Research limitations

Through the experiment, several challenges were met, which can be improved to enhance the performance efficiency of WML-MFCs.

1. Batch-fed mode and manual filling of the containers resulted in high voltage fluctuations. Inside each WML-MFC, high air diffusion took place during the replacement of wastewater. It is possible to avoid this issue by building the container with four sides of plexiglass material and two sides only with wood.
2. Untreated wooden walls are vulnerable to oxygen intrusion, leading to the wastage of organic materials in the anolyte and shifting the dominant microbial culture. It would be interesting, to use PEM between the wood plate and cathode layer; this may help to reduce the oxygen intrusion. Moreover, with wood treatment, WML-MFC can become more compact and microbial-protective.
3. Untreated cathode led to low ORR. Free hydrogen may have escaped the cathode without going through the ORR process. The top and bottom parts of the WML-MFC container could be changed to plexiglass. This will help in building a continuous-fed WML-MFC and gain more control over the direction of hydrogen flow and obtain less leakage.
4. Securing the connections between the wooden plates of the container with a stronger adhesive. With some prototypes, leakage was observed, this comes to the lack of adhesive strength between the wood plates.
5. Wood is an anisotropic material. The profile of antibacterial compounds may change from one point to another, thus creating inherent differences between containers. The extraction of antibacterial compounds may improve the quality of the WML-MFC prototype.
6. Low conductivity of the substrate causes an increase in the internal resistance inside the WML-MFC containers and reduces bioelectric production of it.

7. The occurrence or increasing of copper oxide amount inside the substrate can be avoided by changing the copper wire to titanium, carbon rod or stainless steel or other microorganism-friendly metals for binding the carbon anode electrode.

### 4.4. Recommendations for further study

More research is required on the invented WML-MFC model for evaluating the continuous-fed mode, anode/cathode volume ratio, wooden wall thickness effect, using PEM around the container to block oxygen intrusion, different cathode and anode configurations, differently treated anode and cathode materials, other wood species can be tested with various substrates using different biocatalysts, different treatments of the wooden wall, and combining wood with plexiglass or any other material in the structure.

**REFERENCES**

Aaron, D., Tsouris, C., Hamilton, C.Y., Borole, A.P., 2010. Assessment of the Effects of Flow Rate and Ionic Strength on the Performance of an Air-Cathode Microbial Fuel Cell Using Electrochemical Impedance Spectroscopy. Energies 3, 592–606. https://doi.org/10.3390/en3040592

Adekunle, A., Gariepy, Y., Lyew, D., Raghavan, V., 2016. Energy recovery from cassava peels in a single-chamber microbial fuel cell. Energy Sources, Part A Recover. Util. Environ. Eff. 38, 2495–2502. https://doi.org/10.1080/15567036.2015.1086909

Ahn, Y., Logan, B.E., 2010. Effectiveness of domestic wastewater treatment using microbial fuel cells at ambient and mesophilic temperatures. Bioresour. Technol. 101, 469–475. https://doi.org/10.1016/j.biortech.2009.07.039

Ambrozkiewicz, B., Wolszczak, G.L. and P., 2020. Modelling of Electromagnetic Energy Harvester with Rotational Pendulum Using Mechanical Vibrations to Scavenge Electrical Energy 10, 671.

An, J., Kim, B., Jang, J.K., Lee, H.S., Chang, I.S., 2014. New architecture for modulization of membraneless and single-chambered microbial fuel cell using a bipolar plate-electrode assembly (BEA). Biosens. Bioelectron. 59, 28–34. https://doi.org/10.1016/j.bios.2014.02.063

Buitrón, G., Moreno-Andrade, I., 2014. Performance of a Single-Chamber Microbial Fuel Cell Degrading Phenol: Effect of Phenol Concentration and External Resistance. Appl. Biochem. Biotechnol. 174, 2471–2481. https://doi.org/10.1007/s12010-014-1195-5

Cai, T., Jiang, N., Zhen, G., Meng, L., Song, J., Chen, G., Liu, Y., Huang, M., 2020a. Simultaneous energy harvest and nitrogen removal using a supercapacitor microbial fuel cell. Environ. Pollut. 266, 115154. https://doi.org/10.1016/j.envpol.2020.115154

Cai, T., Meng, L., Chen, G., Xi, Y., Jiang, N., Song, J., Zheng, S., Liu, Y., Zhen, G., Huang, M., 2020b. Application of advanced anodes in microbial fuel cells for power generation: A review. Chemosphere 248, 125985. https://doi.org/10.1016/j.chemosphere.2020.125985

Call, T.P., Carey, T., Bombelli, P., Lea-Smith, D.J., Hooper, P., Howe, C.J., Torrisi, F.,

2017. Platinum-free, graphene based anodes and air cathodes for single chamber microbial fuel cells. J. Mater. Chem. A 5, 23872–23886. https://doi.org/10.1039/c7ta06895f

Capodaglio, A.G., Olsson, G., 2020. Energy issues in sustainable urban wastewater management: Use, demand reduction and recovery in the urban water cycle. Sustainability 12, 226. https://doi.org/10.3390/su12010266

Chan, K.K., Thung, W.E., Ong, S.A., Ho, L.N., Wong, Y.S., Yin, E.C.R., 2020. Simultaneous heavy metal reduction and voltage generation with synergy membrane-less microbial fuel cell. IOP Conf. Ser. Earth Environ. Sci. 463. https://doi.org/10.1088/1755-1315/463/1/012067

Cheng, S., Liu, H., Logan, B.E., 2006. Increased performance of single-chamber microbial fuel cells using an improved cathode structure. Electrochem. commun. 8, 489–494. https://doi.org/10.1016/j.elecom.2006.01.010

Cheng, S., Logan, B.E., 2011. Increasing power generation for scaling up single-chamber air cathode microbial fuel cells. Bioresour. Technol. 102, 4468–4473. https://doi.org/10.1016/j.biortech.2010.12.104

Cheng, S., Logan, B.E., 2007. Ammonia treatment of carbon cloth anodes to enhance power generation of microbial fuel cells. Electrochem. commun. 9, 492–496. https://doi.org/10.1016/j.elecom.2006.10.023

Clauwaert, P., Verstraete, W., 2009. Methanogenesis in membraneless microbial electrolysis cells. Appl. Microbiol. Biotechnol. 82, 829–836. https://doi.org/10.1007/s00253-008-1796-4

Darvishi, F., Hiligsmann, H.S., 2018. Microbial Fuels Technologies and Applications, Taylor & Francis Group. https://doi.org/10.1201/9781351246101

Dong, Y., Qu, Y., He, W., Du, Y., Liu, J., Han, X., Feng, Y., 2015. A 90-liter stackable baffled microbial fuel cell for brewery wastewater treatment based on energy self-sufficient mode. Bioresour. Technol. 195, 66–72. https://doi.org/10.1016/j.biortech.2015.06.026

Du, F., Xie, B., Dong, W., Jia, B., Dong, K., Liu, H., 2011. Continuous flowing membraneless microbial fuel cells with separated electrode chambers. Bioresour.

Technol. 102, 8914–8920. https://doi.org/10.1016/j.biortech.2011.07.056

Du, Y., Feng, Y., Teng, Q., Li, H., 2015. Effect of inorganic salt in the culture on microbial fuel cells performance. Int. J. Electrochem. Sci. 10, 1316–1325.

Ebrahimzadeh, P.R., 1998. Effect of impregnation on mechanosorption in wood and paper studied by dynamic mechanical analysis. Wood Sci. Technol. 32, 101–118.

ElAnzeery, H.M.G.E.M., ElBagouri, M.A.E.S., Guindi, R., 2012. Novel Radio Frequency Energy Harvesting model, in: 2012 IEEE International Power Engineering and Optimization Conference Melaka, Malaysia. pp. 209–213. https://doi.org/10.1109/PEOCO.2012.6230862

Erensoy, A., Çek, N., 2018. Alternative Biofuel Materials for Microbial Fuel Cells from Poplar Wood. ChemistrySelect 3, 11251–11257. https://doi.org/10.1002/slct.201802171

Fan, Y., Hu, H., Liu, H., 2007. Enhanced Coulombic efficiency and power density of air-cathode microbial fuel cells with an improved cell configuration. J. Power Sources 171, 348–354. https://doi.org/10.1016/j.jpowsour.2007.06.220

Feng, C., Wan, Q., Lv, Z., Yue, X., Chen, Y., Wei, C., 2011. One-step fabrication of membraneless microbial fuel cell cathode by electropolymerization of polypyrrole onto stainless steel mesh. Biosens. Bioelectron. 26, 3953–3957. https://doi.org/10.1016/j.bios.2011.02.046

Feng, Y., Wang, X., Logan, B.E., Lee, H., 2008. Brewery wastewater treatment using air-cathode microbial fuel cells. Appl. Microbiol. Biotechnol. 78, 873–880. https://doi.org/10.1007/s00253-008-1360-2

Feng, Y., Yang, Q., Wang, X., Logan, B.E., 2010. Treatment of carbon fiber brush anodes for improving power generation in air-cathode microbial fuel cells. J. Power Sources 195, 1841–1844. https://doi.org/10.1016/j.jpowsour.2009.10.030

Gadkari, S., Fontmorin, J.M., Yu, E., Sadhukhan, J., 2020. Influence of temperature and other system parameters on microbial fuel cell performance: Numerical and experimental investigation. Chem. Eng. J. 388, 124176. https://doi.org/10.1016/j.cej.2020.124176

Gálvez, A., Greenman, J., Ieropoulos, I., 2009. Landfill leachate treatment with microbial

fuel cells; scale-up through plurality. Bioresour. Technol. 100, 5085–5091. https://doi.org/10.1016/j.biortech.2009.05.061

Gartner, B.L., Moore, J.R., Gardiner, B.A., 2004. Gas in stems: Abundance and potential consequences for tree biomechanics. Tree Physiol. 24, 1239–1250. https://doi.org/10.1093/treephys/24.11.1239

Ge, Z., He, Z., 2016. Long-term performance of a 200 liter modularized microbial fuel cell system treating municipal wastewater: Treatment, energy, and cost. Environ. Sci. Water Res. Technol. 2, 274–281. https://doi.org/10.1039/c6ew00020g

Ghangrekar, M.M., Shinde, V.B., 2008. Simultaneous sewage treatment and electricity generation in membrane-less microbial fuel cell. Water Sci. Technol. 58, 37–43. https://doi.org/10.2166/wst.2008.339

Ghangrekar, M.M., Shinde, V.B., 2007. Performance of membrane-less microbial fuel cell treating wastewater and effect of electrode distance and area on electricity production. Bioresour. Technol. 98, 2879–2885. https://doi.org/10.1016/j.biortech.2006.09.050

Gil, G.C., Chang, I.S., Kim, B.H., Kim, M., Jang, J.K., Park, H.S., Kim, H.J., 2003. Operational parameters affecting the performance of a mediator-less microbial fuel cell. Biosens. Bioelectron. 18, 327–334. https://doi.org/10.1016/S0956-5663(02)00110-0

Guerrini, E., Grattieri, M., Faggianelli, A., Cristiani, P., Trasatti, S., 2015. PTFE effect on the electrocatalysis of the oxygen reduction reaction in membraneless microbial fuel cells. Bioelectrochemistry 106, 240–247. https://doi.org/10.1016/j.bioelechem.2015.05.008

Harshiny, M., Samsudeen, N., Kameswara, R.J., Matheswaran, M., 2017. Biosynthesized FeO nanoparticles coated carbon anode for improving the performance of microbial fuel cell. Int. J. Hydrogen Energy 42, 26488–26495. https://doi.org/10.1016/j.ijhydene.2017.07.084

Hassan, S.H.A., Gad El-Rab, S.M.F., Rahimnejad, M., Ghasemi, M., Joo, J.H., Sik-Ok, Y., Kim, I.S., Oh, S.E., 2014. Electricity generation from rice straw using a microbial fuel cell. Int. J. Hydrogen Energy 39, 9490–9496.

https://doi.org/10.1016/j.ijhydene.2014.03.259

Helseth, L.E., Guo, X.D., 2016. Hydrophobic polymer covered by a grating electrode for converting the mechanical energy of water droplets into electrical energy.

Hindatu, Y., Annuar, M.S.M., Gumel, A.M., 2017. Mini-review: Anode modification for improved performance of microbial fuel cell. Renew. Sustain. Energy Rev. 73, 236–248. https://doi.org/10.1016/j.rser.2017.01.138

Huang, L., Li, X., Ren, Y., Wang, X., 2016. In-situ modified carbon cloth with polyaniline/graphene as anode to enhance performance of microbial fuel cell. Int. J. Hydrogen Energy 41, 11369–11379. https://doi.org/10.1016/j.ijhydene.2016.05.048

Ivars-Barceló, F., Zuliani, A., Fallah, M., Mashkour, M., Rahimnejad, M., Luque, R., 2018. Novel applications of microbial fuel cells in sensors and biosensors. Appl. Sci. 8, 1184. https://doi.org/10.3390/app8071184

Jadhav, G.S., Ghangrekar, M.M., 2009. Performance of microbial fuel cell subjected to variation in pH, temperature, external load and substrate concentration. Bioresour. Technol. 100, 717–723. https://doi.org/10.1016/j.biortech.2008.07.041

Jang, J.K., Pham, T.H., Chang, I.S., Kang, K.H., Moon, H., Cho, K.S., Kim, B.H., 2004. Construction and operation of a novel mediator- and membrane-less microbial fuel cell. Process Biochem. 39, 1007–1012. https://doi.org/10.1016/S0032-9592(03)00203-6

Jia, Y., Feng, H., Shen, D., Zhou, Y., Chen, T., Wang, M., Chen, W., Ge, Z., Huang, L., Zheng, S., 2018. High-performance microbial fuel cell anodes obtained from sewage sludge mixed with fly ash. J. Hazard. Mater. 354, 27–32. https://doi.org/10.1016/j.jhazmat.2018.04.008

Jiang, D., Curtis, M., Troop, E., Scheible, K., McGrath, J., Hu, B., Suib, S., Raymond, D., Li, B., 2011. A pilot-scale study on utilizing multi-anode/cathode microbial fuel cells (MAC MFCs) to enhance the power production in wastewater treatment. Int. J. Hydrogen Energy 36, 876–884. https://doi.org/10.1016/j.ijhydene.2010.08.074

Jiang, D., Li, B., 2009. Novel electrode materials to enhance the bacterial adhesion and increase the power generation in microbial fuel cells (MFCs). Water Sci. Technol. 59, 557–563. https://doi.org/10.2166/wst.2009.007

Jiang, H.M., 2017. Combination of Microbial Fuel Cells with Microalgae Cultivation for Bioelectricity Generation and Domestic Wastewater Treatment. Environ. Eng. Sci. 34, 489–495. https://doi.org/10.1089/ees.2016.0279

Jiang, Q., Xing, D., Zhang, L., Sun, R., Zhang, J., Zhong, Y., Feng, Y., Ren, N., 2018. Interaction of bacteria and archaea in a microbial fuel cell with ITO anode. RSC Adv. 8, 28487–28495. https://doi.org/10.1039/c8ra01207e

Jiménez González, M.L., Benítez, C.H., Juarez, Z.A., Pérez, E.Z., Coutiño, V.Á.R., Robles, I., Godínez, L.A., Rodríguez-Valadez, F.J., 2020. Study of the effect of activated carbon cathode configuration on the performance of a membrane-less microbial fuel cell. Catalysts 10, 619. https://doi.org/10.3390/catal10060619

Jothinathan, D., Nasrin Fathima, A.H., Mylsamy, P., Benedict Bruno, L., Sivasankar, V., 2018. Microbial fuel cell research using animal waste: A feebly-explored area to others, in: Microbial Fuel Cell Technology for Bioelectricity. Springer, Cham, pp. 151–168. https://doi.org/10.1007/978-3-319-92904-0_8

Kaboorani, A., Blanchet, P., 2014. Determining the linear viscoelastic region of sugar maple wood by dynamic mechanical analysis. BioResources 9, 4392–4409. https://doi.org/10.15376/biores.9.3.4392-4409

Kamau, J.M., Mbui, D.N., Mwaniki, J.M., Mwaura, F.B., 2018. Utilization of rumen fluid in production of bio–energy from market waste using microbial fuel cells technology. ournal Appl. Biotechnol. Bioeng. 5, 227–231.

Karuppiah, T., Pugazhendi, A., Subramanian, S., Jamal, M.T., Jeyakumar, R.B., 2018. Deriving electricity from dye processing wastewater using single chamber microbial fuel cell with carbon brush anode and platinum nano coated air cathode. 3 Biotech 8, 437. https://doi.org/10.1007/s13205-018-1462-1

Khalili, H.B., Mohebbi-Kalhori, D., Afarani, M.S., 2017. Microbial fuel cell (MFC) using commercially available unglazed ceramic wares: Low-cost ceramic separators suitable for scale-up. Int. J. Hydrogen Energy 42, 8233–8241. https://doi.org/10.1016/j.ijhydene.2017.02.095

Khan, M.D., Khan, N., Sultana, S., Khan, M.Z., Sabir, S., Azam, A., 2018. Microbial Fuel Cell: Waste Minimization and Energy Generation, in: Oves Mohammad Khan,

Zain Mohammad, Iqbal, I. (Eds.), Modern Age Environmental Problems and Their Remediation. Springer, Cham, pp. 129–146. https://doi.org/10.1007/978-3-319-64501-8

Khater, D.Z., Amin, R.S., Fetohi, A.E., El-Khatib, K.M., Mahmoud, M., 2022. Bifunctional manganese oxide–silver nanocomposites anchored on graphitic mesoporous carbon to promote oxygen reduction and inhibit cathodic biofilm growth for long-term operation of microbial fuel cells fed with sewage. Sustain. Energy Fuels 6, 430–439. https://doi.org/10.1039/D1SE01479J

Kim, J., Kim, B., An, J., Lee, Y.S., Chang, I.S., 2016. Development of anode zone using dual-anode system to reduce organic matter crossover in membraneless microbial fuel cells. Bioresour. Technol. 213, 140–145. https://doi.org/10.1016/j.biortech.2016.03.012

Kodama, T., 2003. High-temperature solar chemistry for converting solar heat to chemical fuels. https://doi.org/10.1016/S0360-1285(03)00059-5

Komatsu, T., 1989. Day-night reversion in the horizontal distributions of dissolved oxygen content and pH in aSargassum forest. J. Oceanogr. Soc. Japan 45, 106–115. https://doi.org/10.1007/BF02108884

Kondaveeti, S., Moon, J.M., Min, B., 2017. Optimum spacing between electrodes in an air-cathode single chamber microbial fuel cell with a low-cost polypropylene separator. Bioprocess Biosyst. Eng. 40, 1851–1858. https://doi.org/10.1007/s00449-017-1838-3

Kumar, G.G., Sarathi, V.G.S., Nahm, K.S., 2013. Recent advances and challenges in the anode architecture and their modifications for the applications of microbial fuel cells. Biosens. Bioelectron. 43, 461–475. https://doi.org/10.1016/j.bios.2012.12.048

Kumar, V., Pandita, S., Singh Sidhu, G.P., Sharma, A., Khanna, K., Kaur, P., Bali, A.S., Setia, R., 2021. Copper bioavailability, uptake, toxicity and tolerance in plants: A comprehensive review. Chemosphere 262, 127810. https://doi.org/10.1016/j.chemosphere.2020.127810

Lee, D., Chang, J., Lai, J., 2015. Bioresource Technology Microalgae – microbial fuel cell : A mini review. Bioresour. Technol. 198, 891–895.

https://doi.org/10.1016/j.biortech.2015.09.061

Lee, Y., Nirmalakhandan, N., 2011. Electricity production in membrane-less microbial fuel cell fed with livestock organic solid waste. Bioresour. Technol. 102, 5831–5835. https://doi.org/10.1016/j.biortech.2011.02.090

Lepage, G., Albernaz, F.O., Perrier, G., Merlin, G., 2012. Characterization of a microbial fuel cell with reticulated carbon foam electrodes. Bioresour. Technol. 124, 199–207. https://doi.org/10.1016/j.biortech.2012.07.067

Li, W.W., Yu, H.Q., He, Z., 2014. Towards sustainable wastewater treatment by using microbial fuel cells-centered technologies. Energy Environ. Sci. 7, 911–924. https://doi.org/10.1039/c3ee43106a

Li, X., Zhu, N., Wang, Y., Li, P., Wu, P., Wu, J., 2013. Animal carcass wastewater treatment and bioelectricity generation in up-flow tubular microbial fuel cells: Effects of HRT and non-precious metallic catalyst. Bioresour. Technol. 128, 454–460. https://doi.org/10.1016/j.biortech.2012.10.053

Li, Z., Haynes, R., Sato, E., Shields, M.S., Fujita, Y., Sato, C., 2014. Microbial Community Analysis of a Single Chamber Microbial Fuel Cell Using Potato Wastewater. Water Environ. Res. 86, 324–330. https://doi.org/10.2175/106143013x13751480308641

Lin, C.C., Wei, C.H., Chen, C.I., Shieh, C.J., Liu, Y.C., 2013. Characteristics of the photosynthesis microbial fuel cell with a Spirulina platensis biofilm. Bioresour. Technol. 135, 640–643. https://doi.org/10.1016/j.biortech.2012.09.138

Liu, D., Fang, W., Li, J., Zhang, L., Yan, M., Tang, H., 2022. Three-dimensional hierarchical MoO2/MoC@NC-CC free-standing anode applied in microbial fuel cells. J. Mater. Chem. A 10, 4110–4119. https://doi.org/10.1039/D1TA09791A

Liu, H., Cheng, S., Logan, B.E., 2005. Production of electricity from acetate or butyrate using a single-chamber microbial fuel cell. Environ. Sci. Technol. 39, 658–662. https://doi.org/10.1021/es048927c

Liu, H., Logan, B.E., 2004. Electricity generation using an air-cathode single chamber microbial fuel cell in the presence and absence of a proton exchange membrane. Environ. Sci. Technol. 38, 4040–4046. https://doi.org/10.1021/es0499344

Liu, H., Ramnarayanan, R., Logan, B.E., 2004. Production of Electricity during Wastewater Treatment Using a Single Chamber Microbial Fuel Cell. Environ. Sci. Technol. 38, 2281–2285. https://doi.org/10.1021/es034923g

Liu, S.H., Lai, C.Y., Chang, P.H., Lin, C.W., Chen, Y.H., 2020. Enhancing copper recovery and electricity generation from wastewater using low-cost membrane-less microbial fuel cell with a carbonized clay cup as cathode. J. Clean. Prod. 247, 119118. https://doi.org/10.1016/j.jclepro.2019.119118

Logan, B.E., 2010. Scaling up microbial fuel cells and other bioelectrochemical systems. Appl. Microbiol. Biotechnol. 85, 1665–1671. https://doi.org/10.1007/s00253-009-2378-9

Logan, B.E., 2008. Microbial Fuel Cells. John Wiley & Sons. https://doi.org/10.1016/B978-0-444-53199-5.00098-1

Logroño, W., Pérez, M., Urquizo, G., Kadier, A., Echeverría, M., Recalde, C., Rákhely, G., 2017. Single chamber microbial fuel cell (SCMFC) with a cathodic microalgal biofilm: A preliminary assessment of the generation of bioelectricity and biodegradation of real dye textile wastewater. Chemosphere 176, 378–388. https://doi.org/10.1016/j.chemosphere.2017.02.099

Luo, H., Liu, G., Zhang, R., Jin, S., 2007. Characteristics of generating electricity with microbial fuel cell by different organics as fuel, in: Proceedings of ISES World Congress 2007(Vol. I–Vol. V). Springer Berlin Heidelberg, pp. 2449–2452. https://doi.org/10.1007/978-3-540-75997-3_496

Luo, H., Xu, G., Lu, Y., Liu, G., Zhang, R., Li, X., Zheng, X., Yu, M., 2017. Electricity generation in a microbial fuel cell using yogurt wastewater under alkaline conditions. RSC Adv. 7, 32826–32832. https://doi.org/10.1039/c7ra06131e

Malvankar, N.S., Tuominen, M.T., Lovley, D.R., 2012. Biofilm conductivity is a decisive variable for high-current-density Geobacter sulfurreducens microbial fuel cells. Energy Environ. Sci. 5, 5790–5797. https://doi.org/10.1039/c2ee03388g

Marashi, S.K.F., Kariminia, H.R., 2015. Performance of a single chamber microbial fuel cell at different organic loads and pH values using purified terephthalic acid wastewater. J. Environ. Heal. Sci. Eng. 13, 27. https://doi.org/10.1186/s40201-015-

0179-x

Min, B., Cheng, S., Logan, B.E., 2005. Electricity generation using membrane and salt bridge microbial fuel cells. Water Res. 39, 1675–1686. https://doi.org/10.1016/j.watres.2005.02.002

Min, B., Logan, B., 2004. Continuous Electricity Generation from Domestic Wastewaterand Organic Substrates in a Flat Plate Microbial Fuel Cell. Environ. Sci. Technol. 38, 5809–5814.

Mohamed, A., Zmuda, H.M., Ha, P.T., Coats, E.R., Beyenal, H., 2021. Large-scale switchable potentiostatically controlled/microbial fuel cell bioelectrochemical wastewater treatment system. Bioelectrochemistry 138, 107724. https://doi.org/10.1016/j.bioelechem.2020.107724

Mohanakrishna, G., Abu-Reesh, I.M., Al-Raoush, R.I., He, Z., 2018. Cylindrical graphite based microbial fuel cell for the treatment of industrial wastewaters and bioenergy generation. Bioresour. Technol. 247, 753–758. https://doi.org/10.1016/j.biortech.2017.09.174

Mousavi, S.M.S., Ayati, B., Ganjidoust, H., 2016. Phenol removal and bio-electricity generation using a single-chamber microbial fuel cell in saline and increased-temperature condition. Energy Sources, Part A Recover. Util. Environ. Eff. 38, 3300–3307. https://doi.org/10.1080/15567036.2016.1156196

Mtaita, T.A., 2003. CHAPTER 3 - Food, in: HAZELTINE, B., BULL, C.B.T.-F.G. to A.T. (Eds.), . Academic Press, San Diego, pp. 277–480. https://doi.org/10.1016/B978-012335185-2/50047-4

Nastro, R.A., 2014. Microbial fuel cells in waste treatment: Recent advances. Int. J. Performability Eng. 10, 367–376.

Nawaz, A., Raza, W., Gul, H., Durrani, A.K., Algethami, F.K., Sonne, C., Kim, K.H., 2020. Upscaling feasibility of a graphite-based truncated conical microbial fuel cell for bioelectrogenesis through organic wastewater treatment. J. Colloid Interface Sci. 570, 99–108. https://doi.org/10.1016/j.jcis.2020.02.099

Nayak, J.K., Amit, Ghosh, U.K., 2018. An innovative mixotrophic approach of distillery spent wash with sewage wastewater for biodegradation and bioelectricity generation

using microbial fuel cell. J. Water Process Eng. 23, 306–313. https://doi.org/10.1016/j.jwpe.2018.04.003

Naz, S., Gul, A., Zia, M., 2020. Toxicity of copper oxide nanoparticles: A review study. IET Nanobiotechnology 14, 1–13. https://doi.org/10.1049/iet-nbt.2019.0176

Palanisamy, G., Jung, H.Y., Sadhasivam, T., Kurkuri, M.D., Kim, S.C., Roh, S.H., 2019. A comprehensive review on microbial fuel cell technologies: Processes, utilization, and advanced developments in electrodes and membranes. J. Clean. Prod. 221, 598–621. https://doi.org/10.1016/j.jclepro.2019.02.172

Pallavi CK, Udayashankara TH, 2016. A Review on Microbial fuel Cells Employing Wastewaters as Substrates for Sustainable Energy Recovery and Wastewater Treatment. IOSR J. Environ. Sci. 10, 31–36. https://doi.org/10.9790/2402-1012023136

Pant, D., Van Bogaert, G., Diels, L., Vanbroekhoven, K., 2010. A review of the substrates used in microbial fuel cells (MFCs) for sustainable energy production. Bioresour. Technol. 101, 1533–1543. https://doi.org/10.1016/j.biortech.2009.10.017

Park, H. Il, Wu, C., Lin, L.S., 2012. Coal tar wastewater treatment and electricity production using a membrane-less tubular microbial fuel cell. Biotechnol. Bioprocess Eng. 17, 654–660. https://doi.org/10.1007/s12257-011-0374-2

Pauline, S., Boopathi, A., 2018. Treatment of slaughterhouse wastewater using microbial fuel cell. Int. J. Adv. Res. Ideas Innov. Technol. 4, 228–230.

Peng, X., Chu, X., Wang, S., Shan, K., Song, D., Zhou, Y., 2017. Bio-power performance enhancement in microbial fuel cell using Ni-ferrite decorated anode. RSC Adv. 7, 16027–16032. https://doi.org/10.1039/C7RA01253E

Prida, A., Boulet, J.C., Ducousso, A., Nepveu, G., Puech, J.L., 2006. Effect of species and ecological conditions on ellagitannin content in oak wood from an even-aged and mixed stand of Quercus robur L. and Quercus petraea Liebl. Ann. For. Sci. 63, 415–424. https://doi.org/10.1051/forest:2006021

Rabaey, K., Verstraete, W., 2005. Microbial fuel cells: Novel biotechnology for energy generation. Trends Biotechnol. 23, 291–298. https://doi.org/10.1016/j.tibtech.2005.04.008

Rahimnejad, M., Adhami, A., Darvari, S., Zirepour, A., Oh, S.E., 2015. Microbial fuel cell as new technology for bioelectricity generation: A review. Alexandria Eng. J. 54, 745–756. https://doi.org/10.1016/j.aej.2015.03.031

Rahimnejad, M., Najafpour, G.D., 2011. Microbial Fuel Cells: A New Source of Power, in: Biochemical Engineering and Biotechnology. Elsevier B.V, pp. 1–31.

Saba, B., Christy, A.D., Yu, Z., Co, A.C., 2017. Sustainable power generation from bacterio-algal microbial fuel cells (MFCs): An overview. Renew. Sustain. Energy Rev. 73, 75–84. https://doi.org/10.1016/j.rser.2017.01.115

Sándor, M., Mihály, B., 2006. Magyarország ipari fái - Wood species of Hungary. Szaktudás Kiadó Ház Zrt, Budapest.

Santoro, C., Arbizzani, C., Erable, B., Ieropoulos, I., 2017. Microbial fuel cells: From fundamentals to applications. A review. J. Power Sources 356, 225–244. https://doi.org/10.1016/j.jpowsour.2017.03.109

Santoro, C., Flores-Cadengo, C., Soavi, F., Kodali, M., Merino-Jimenez, I., Gajda, I., Greenman, J., Ieropoulos, I., Atanassov, P., 2018. Ceramic Microbial Fuel Cells Stack: Power generation in standard and supercapacitive mode. Sci. Rep. 8, 1–12. https://doi.org/10.1038/s41598-018-21404-y

Santoro, C., Ieropoulos, I., Greenman, J., Cristiani, P., Vadas, T., Mackay, A., Li, B., 2013. Current generation in membraneless single chamber microbial fuel cells (MFCs) treating urine. J. Power Sources 238, 190–196. https://doi.org/10.1016/j.jpowsour.2013.03.095

Santoro, C., Serov, A., Stariha, L., Kodali, M., Gordon, J., Babanova, S., Bretschger, O., Artyushkova, K., Atanassov, P., 2016. Iron based catalysts from novel low-cost organic precursors for enhanced oxygen reduction reaction in neutral media microbial fuel cells. Energy Environ. Sci. 9, 2346–2353. https://doi.org/10.1039/c6ee01145d

Sanz, M., Fernández De Simón, B., Esteruelas, E., Muñoz, Á.M., Cadahía, E., Hernández, T., Estrella, I., Pinto, E., 2011. Effect of Toasting Intensity at Cooperage on Phenolic Compounds in Acacia (Robinia pseudoacacia) Heartwood. J. Agric. Food Chem. 59, 3135–3145. https://doi.org/10.1021/jf1042932

Savizi, I.S.P., Kariminia, H.R., Bakhshian, S., 2012. Simultaneous decolorization and bioelectricity generation in a dual chamber microbial fuel cell using electropolymerized-enzymatic cathode. Environ. Sci. Technol. 46, 6584–6593. https://doi.org/10.1021/es300367h

Schlesing, W., Buhk, M., Osterhold, M., 2004. Dynamic mechanical analysis in coatings industry. Prog. Org. Coatings 49, 197–208. https://doi.org/10.1016/j.porgcoat.2003.09.009

Sharma, Y., Li, B., 2010. Optimizing energy harvest in wastewater treatment by combining anaerobic hydrogen producing biofermentor (HPB) and microbial fuel cell (MFC). Int. J. Hydrogen Energy 35, 3789–3797. https://doi.org/10.1016/j.ijhydene.2010.01.042

Simeon, M.I., Otache, M.Y., Ewemoje, T.A., Raji, A.O., 2019. Application of urine as fuel in a soil-based membrane-less single chamber microbial fuel cell. Agric. Eng. Int. CIGR J. 21, 115–121.

Slate, A.J., Whitehead, K.A., Brownson, D.A.C., Banks, C.E., 2019. Microbial fuel cells: An overview of current technology. Renew. Sustain. Energy Rev. 101, 60–81. https://doi.org/10.1016/j.rser.2018.09.044

Song, Y.E., Lee, S., Kim, M., Na, J.G., Lee, Jinwon, Lee, Jinwoo, Kim, J.R., 2020. Metal-free cathodic catalyst with nitrogen- and phosphorus-doped ordered mesoporous carbon (NPOMC) for microbial fuel cells. J. Power Sources 451, 227816. https://doi.org/10.1016/j.jpowsour.2020.227816

Sorz, J., Hietz, P., 2006. Gas diffusion through wood: Implications for oxygen supply. Trees - Struct. Funct. 20, 34–41. https://doi.org/10.1007/s00468-005-0010-x

Sun, N., Das, S., Frazier, C.E., 2007. Dynamic mechanical analysis of dry wood: Linear viscoelastic response region and effects of minor moisture changes. Holzforschung 61, 28–33. https://doi.org/10.1515/HF.2007.006

T. Aswin, S, S.B., Sikkandar, M.Y., 2017. Optimization of Microbial Fuel Cell for Treating Industrial Wastewater and Simultaneous Power Generation. Int. J. Chem. Sci. 15, 132–143.

Tahir, C.A., Pásztory, Z., Agarwal, C., Csóka, L., 2022. Electricity Generation and

Wastewater Treatment with Membrane-Less Microbial Fuel Cell, in: Inamuddin, M.I., A., R., P. (Eds.), Application of Microbes in Environmental and Microbial Biotechnology. Springer, Singapore, pp. 235–261. https://doi.org/10.1007/978-981-16-2225-0_8

Tee, P.F., Abdullah, M.O., Tan, I.A.W., Amin, M.A.M., Nolasco-Hipolito, C., Bujang, K., 2018. Bio-energy generation in an affordable, single-chamber microbial fuel cell integrated with adsorption hybrid system: effects of temperature and comparison study. Environ. Technol. (United Kingdom) 39, 1081–1088. https://doi.org/10.1080/09593330.2017.1320433

Thung, W.E., Ong, S.A., Ho, L.N., Wong, Y.S., Ridwan, F., Oon, Y.L., Oon, Y.S., Lehl, H.K., 2019. Enhancement of mass and charge transport in scaled-up microbial fuel cell by using innovative configuration of bioanode. Int. J. Environ. Sci. Technol. 16, 8175–8184. https://doi.org/10.1007/s13762-019-02390-8

Torres-Rivero, K., Bastos-Arrieta, J., Fiol, N., Florido, A., 2021. Chapter Ten - Metal and metal oxide nanoparticles: An integrated perspective of the green synthesis methods by natural products and waste valorization: applications and challenges, in: Verma, S.K., Das, A.K.B.T.-C.A.C. (Eds.), Biosynthesized Nanomaterials. Elsevier, pp. 433–469. https://doi.org/https://doi.org/10.1016/bs.coac.2020.12.001

Trevors, J.T., Cotter, C.M., 1990. Copper toxicity and uptake in microorganisms. J. Ind. Microbiol. 6, 77–84. https://doi.org/10.1007/BF01576426

Tugtas, A.E., Cavdar, P., Calli, B., 2011. Continuous flow membrane-less air cathode microbial fuel cell with spunbonded olefin diffusion layer. Bioresour. Technol. 102, 10425–10430. https://doi.org/10.1016/j.biortech.2011.08.082

Venkata Mohan, S., Mohanakrishna, G., Sarma, P.N., 2008. Effect of anodic metabolic function on bioelectricity generation and substrate degradation in single chambered microbial fuel cell. Environ. Sci. Technol. 42, 8088–8094. https://doi.org/10.1021/es8012529

Vicari, F., D'Angelo, A., Galia, A., Quatrini, P., Scialdone, O., 2016. A single-chamber membraneless microbial fuel cell exposed to air using Shewanella putrefaciens. J. Electroanal. Chem. 783, 268–273. https://doi.org/10.1016/j.jelechem.2016.11.010

Waller, M.G., Trabold, T.A., 2013. Review of Microbial Fuel cells for wastewater treatment: Large-Scale Applications, future Needs and current Research gaps, in: Nternational Conference on Fuel Cell Science, Engineering and Technology. American Society of Mechanical Engineers, p. V001T01A011. https://doi.org/10.1115/FuelCell2013-18185

Wang, H.Y., Su, J.Y., 2013. Membraneless microfluidic microbial fuel cell for rapid detection of electrochemical activity of microorganism. Bioresour. Technol. 145, 271–274. https://doi.org/10.1016/j.biortech.2013.01.014

Wang, P., Li, H., Du, Z., 2013. Deposition of iron on graphite felts by thermal decomposition of Fe(CO)5 for anodic modification of microbial fuel cells. Int. J. Electrochem. Sci. 8, 4712–4722.

Wang, R., Yan, M., Li, H., Zhang, L., Peng, B., Sun, J., Liu, D., Liu, S., 2018. FeS2 Nanoparticles Decorated Graphene as Microbial-Fuel-Cell Anode Achieving High Power Density. Adv. Mater. 30, 1800618. https://doi.org/10.1002/adma.201800618

Wang, W., Wang, X., Wang, Y., Jiang, B., Song, H., 2022. A spherical multishell hollow carbon-based catalyst with a controllable N-species content for the oxygen reduction reaction in air-breathing cathode microbial fuel cells. React. Chem. Eng. 7, 978–986. https://doi.org/10.1039/D1RE00528F

Wang, Z., Lee, T., Lim, B., Choi, C., Park, J., 2014. Microbial community structures differentiated in a single-chamber air-cathode microbial fuel cell fueled with rice straw hydrolysate. Biotechnol. Biofuels 7, 9. https://doi.org/10.1186/1754-6834-7-9

Wei, J., Liang, P., Huang, X., 2011. Recent progress in electrodes for microbial fuel cells. Bioresour. Technol. 102, 9335–9344. https://doi.org/10.1016/j.biortech.2011.07.019

Yamashita, T., Ishida, M., Asakawa, S., Kanamori, H., Sasaki, H., Ogino, A., Katayose, Y., Hatta, T., Yokoyama, H., 2016. Enhanced electrical power generation using flame-oxidized stainless steel anode in microbial fuel cells and the anodic community structure. Biotechnol. Biofuels 9, 1–10. https://doi.org/10.1186/s13068-016-0480-7

Yang, F., Ren, L., Pu, Y., Logan, B.E., 2013. Electricity generation from fermented primary sludge using single-chamber air-cathode microbial fuel cells. Bioresour.

Technol. 128, 784–787. https://doi.org/10.1016/j.biortech.2012.10.021

Yang, G., Sun, Y., Yuan, Z., Lü, P., Kong, X., Li, L., Chen, G., Lu, T., 2014. Application of surface-modified carbon powder in microbial fuel cells. Cuihua Xuebao/Chinese J. Catal. 35, 770–775. https://doi.org/10.1016/s1872-2067(14)60023-1

Yang, S., Jia, B., Liu, H., 2009. Effects of the Pt loading side and cathode-biofilm on the performance of a membrane-less and single-chamber microbial fuel cell. Bioresour. Technol. 100, 1197–1202. https://doi.org/10.1016/j.biortech.2008.08.005

Yang, W., Li, J., Zhang, L., Zhu, X., Liao, Q., 2017. A monolithic air cathode derived from bamboo for microbial fuel cells. RSC Adv. 7, 28469–28475. https://doi.org/10.1039/c7ra04571a

Yang, Y., Sun, G., Xu, M., 2011. Microbial fuel cells come of age. J. Chem. Technol. Biotechnol. 86, 625–632. https://doi.org/10.1002/jctb.2570

Yang, Y., Yan, L., Song, J., Xu, M., 2018. Optimizing the electrode surface area of sediment microbial fuel cells. RSC Adv. 8, 25319–25324. https://doi.org/10.1039/c8ra05069d

Ye, D., Zhang, P., Zhu, X., Yang, Y., Li, J., Fu, Q., Chen, R., Liao, Q., Zhang, B., 2018. Electricity generation of a laminar-flow microbial fuel cell without any additional power supply. RSC Adv. 8, 33637–33641. https://doi.org/10.1039/C8RA07340F

You, J., Fan, H., Winfiel, J., Ieropoulos, I.A., 2020. Complete Microbial Fuel Cell Fabrication Using Additive layer manufacturing. molecules 25, 3051.

You, S., Zhao, Q., Zhang, J., Jiang, J., Wan, C., Du, M., Zhao, S., 2007. A graphite-granule membrane-less tubular air-cathode microbial fuel cell for power generation under continuously operational conditions. J. Power Sources 173, 172–177. https://doi.org/10.1016/j.jpowsour.2007.07.063

Yuan, G.E., Deng, H., Ru, X., Zhang, X., 2018. Electricity generation from heavy metal-containing wheat grain hydrolysate using single-chamber microbial fuel cells: Performance and long-term stability. Int. J. Electrochem. Sci. 13, 8589–8601. https://doi.org/10.20964/2018.09.05

Yuan, Y., Zhao, B., Zhou, S., Zhong, S., Zhuang, L., 2011. Electrocatalytic activity of anodic biofilm responses to pH changes in microbial fuel cells. Bioresour. Technol.

102, 6887–6891. https://doi.org/10.1016/j.biortech.2011.04.008

Zeng, L., Zhao, S., Zhang, L., He, M., 2018. A facile synthesis of molybdenum carbide nanoparticles-modified carbonized cotton textile as an anode material for high-performance microbial fuel cells. RSC Adv. 8, 40490–40497. https://doi.org/10.1039/C8RA07502F

Zhang, X., Sun, H., Liang, P., Huang, X., Chen, X., Logan, B.E., Cecconet, D., Molognoni, D., Callegari, A., Capodaglio, A.G., Hosseini, M.G., Ahadzadeh, I., Zhang, L., Li, J., Zhu, X., Ye, D., Liao, Q., Li, X.M., Cheng, K.Y., Wong, J.W.C., 2013. A dual-chambered microbial fuel cell with Ti/nano-TiO 2/Pd nano-structure cathode. Chem. Eng. J. 220, 500–511. https://doi.org/10.1016/j.ijhydene.2017.07.231

Zhang, Y., Ye, J.S., 2015. Graphene-Based Microbial Fuel Cells, in: Yusoff, A.R. bin M. (Ed.), Graphene-Based Energy Devices. Wiley-VCH Verlag GmbH & Co. KGaA, pp. 339–354. https://doi.org/10.1002/9783527690312

Zhao, Y., Ma, Y., Li, T., Dong, Z., Wang, Y., 2018. Modification of carbon felt anodes using double-oxidant HNO3/H2O2 for application in microbial fuel cells. RSC Adv. 8, 2059–2064. https://doi.org/10.1039/c7ra12923h

Zhou, M., Chi, M., Wang, H., Jin, T., 2012. Anode modification by electrochemical oxidation: A new practical method to improve the performance of microbial fuel cells. Biochem. Eng. J. 60, 151–155. https://doi.org/10.1016/j.bej.2011.10.014

Zhuang, L., Zhou, S., Wang, Y., Liu, C., Geng, S., 2009. Membrane-less cloth cathode assembly (CCA) for scalable microbial fuel cells. Biosens. Bioelectron. 24, 3652–3656. https://doi.org/10.1016/j.bios.2009.05.032

## LIST OF PUBLICATIONS

***Patent Application:***

**CT-PA:** P2300280, A wooden membrane-less microbial fuel cell reactor configuration.

***Journal Publication:***

**CT-JP1:** Tahir, C.A., Agarwal, C.A., Pásztory, Z., Csóka, L., 2024. A novel membrane-less microbial fuel cell reactor using wood as container and separator to prevent air–cathode deterioration and biofouling. *Discover WATER*, 15–29. https://doi.org/10.1007/s43832-024-00085-x

***Book Chapters:***

**CT-BC2**: Tahir, C.A., Pásztory, Z., Agarwal, C., Csóka, L., 2022. Electricity Generation and Wastewater Treatment with Membrane-Less Microbial Fuel Cell, in: Inamuddin I., Ahmad M., Prasad R. (Eds.), Application of Microbes in Environmental and Microbial Biotechnology. *Springer, Singapore*, pp. 235–261. https://doi.org/10.1007/978-981-16-2225-0_8

**CT-BC1**: Tahir, C.A., Agarwal, C.A., Csóka, L., 2020. Advances in Green Ion-Batteries using Aqueous Electrolytes, in: Boddula, R., Inamuddin, I., Pothu, R., Asiri, A.M. (Eds.), Rechargeable Batteries: History, Progress, and Applications. *Scrivener Publishing LLC, Beverly (MA)*, pp. 379–402.

***Conference Proceedings:***

**CT-CP4**: Tahir, C.A., Hasan, K.M.F., 2022. Integrating wood into microbial fuel cell technology, in: Németh, R., Christian, H., Rademacher, P., Bak, M., Báder, M. (Eds.), 10TH HARDWOOD CONFERENCE PROCEEDINGS, Hardwood Conference Proceedings, ISSN 2631-004X ; 10. Soproni Egyetemi Kiadó, Sopron.

**CT-CP3**: Tahir, C.A., Nahit, A., 2020. SIMULATION AND OPTIMIZATION OF NATURAL GAS SWEETENING PLANT WITH HYSYS 8.0, in: Faitli, J. (Ed.), Proceedings of the Miskolc IPW- IV. Sustainable Raw Materials International Project Week. Institute of Raw Material Preparation and Process Engineering, University of Miskolc, Miskolc-Egyetemváros, pp. 247–255.

**CT-CP2**: Tahir, C.A., Levente, C., 2019. MEMBRANE-LESS MICROBIAL FUEL

CELL'S PRODUCTIVITY USING WASTEWATER AND SLAUGHTER-HOUSE WASTE, in: Rákhely, G., Hodúr, C. (Eds.), II. Sustainable Raw Materials Conference Book - International Project Week and Scientific Conference. University of Szeged, Szeged, pp. 98–101.

**CT-CP1**: Tahir, C.A., Csóka, L., 2019. Review of the recent development in rechargeable aqueous batteries, in: Czupy, I. (Ed.), III. RING – FENNTARTHATÓ NYERSANYAG-GAZDÁLKODÁS - III. SUSTAINABLE RAW MATERIALS KONFERENCIAKÖTET - PROCEEDINGS. Soproni Egyetem Kiadó, Sopron, pp. 178–180.

***Doctoral complex exam 2020:***

**CT-CE**: Chenar A. Tahir, "Optimization and configuration of membrane-less microbial fuel cell design", University of Sopron (Hungary), June **2020**

***Doctoral conference 2019:***

**CT-DC**: Chenar A. Tahir, "Membrane-less microbial fuel cell's Productivity with using wastewater", University of Sopron (Hungary), May **2019**